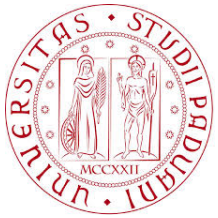

UNIVERSITÀ DEGLI STUDI DI PADOVA

Dipartimento di Fisica e Astronomia "Galileo Galilei"

Master Degree in Physics

Final Dissertation

Testing a specific Generalized Brans-Dicke model with the unified Effective Field Theory approach

Thesis supervisor
Prof. Sabino Matarrese

Thesis co-supervisor
Prof. Alessandra Silvestri

Candidate
Sofia Canevarolo

Academic Year 2019/2020

Contents

Abstract

One of the most intriguing puzzle of modern Cosmology resides in the late time accelerated expansion of our Universe. Our standard model of Cosmology, the ΛCDM model, based on the General Relativity theory of gravity, explains this phenomenon in terms of a cosmological constant added into the Einstein equations. Despite the successful agreement of the ΛCDM model with cosmological data, some issues and internal inconsistencies are still without a satisfactory explanation. This motivates the quest for alternative cosmological model and the necessity of probing gravity at cosmic scales. This Master Thesis is about studying a specific modified gravity model, dubbed as Generalized Brans-Dicke theory, employing the unified language offered by the Effective Field Theory approach to dark energy. Implementing the Generalized Brans-Dicke theory in the EFTCAMB cosmological code, we study the model from a phenomenological point of view. We focus in particular on stability criteria, cosmological perturbations and we perform a Monte Carlo Markov Chain likelihood analysis to estimate parameters using recent cosmological datasets.

Introduction

The standard model of Cosmology predicts that almost 70% of the total energy budget of our Universe is accounted by a still unknown form of energy, dubbed as dark energy, which is responsible for the late time accelerated expansion of our Universe. The discovery of this phenomenon was achieved in 1998 by two groups that were investigating Supernovae redshift [1]-[2]. Supernovae, known as standard candles of Cosmology because their absolute magnitude can be recovered, allowed to put constraints on the theoretical expectations of the amount of matter and dark energy. Thanks to this first discovery and to following measurements, today we know that our Universe indeed is mostly filled by dark energy. On the other hand, a fully satisfactory explanation of what is this dark energy, is still missing.

The theoretical landscape that tries to explain the phenomenon is really rich [19]. Our standard model of Cosmology explains it in terms of a cosmological constant, that might be interpreted as vacuum energy density. This leaves some unresolved issues that motivate the search of alternative models that go beyond the standard model. In particular, this is achieved introducing some new dynamical dark energy component in the Universe or trying to modify our underlying theory of gravity. Given the big variety of models present in the literature, it is then crucial to prepare the basis for a confrontation with cosmological data.

The Effective Field Theory (EFT) approach to dark energy [80] is a great candidate to help creating a bridge between experimental data and theoretical models. Indeed, it offers a unified language that gives the possibility to work in a model-independent framework using a parametrized action. With the EFT formalism, it is possible to study not only specific viable models but also perform agnostic tests of gravity. Indeed, most of the dark energy or modified gravity models of interest can be mapped into the EFT language.
Moreover, another key point, that makes the EFT approach appealing, is the possibility to study it through its implementation into the Einstein-Boltzmann solver CAMB [82]-[83] that allows to study observables of interest in Cosmology, such as expansion history, growth of structure, gravitational lensing and Cosmic Microwave Background, in the frame of dark energy and modified gravity models.

The purpose of this Thesis is to study and analyze a specific modified gravity model, called Generalized Brans-Dicke theory [89], using the Effective Field Theory approach to dark energy and the EFTCAMB cosmological code. The Generalized Brans-Dicke theory is realized adding a scalar degree of freedom which is non-minimally coupled to the metric and with a term in the action that describes a non-linear self-interaction of the scalar field. This model is interesting for our scope because it can provide deSitter solutions as late time attractor. Moreover, the presence of the non-linear self-interaction term is crucial to satisfy the necessity of recovering General Relativity in the regions of high density tested by solar system experiments.

The contents of this Thesis are organized as follows:
Chapter 1: I will start from a general description of the standard model of Cosmology, the ΛCDM model, in particular focusing on the background peculiarities. Moreover, I will introduce the discovery of the late time accelerated expansion of the Universe as well as other cosmological evidences of the dark energy existence. The interpretation of the cosmological constant in terms of vacuum energy will also be exposed.

Chapter 2: I will talk about cosmological perturbations in the frame of General Relativity and how to compare theoretical predictions and observations with the tool of the power spectrum. I will also briefly introduce some observables that will be studied in the following part of the Thesis.
Chapter 3: I will present some reasons that motivate the quest of models that go beyond the ΛCDM model. Some theorems that can be used as a guidance in this search will also be presented. Finally, I will introduce some remarkable theories of dark energy and modified gravity.
Chapter 4: I will discuss the viability conditions that have to be considered exploring new cosmological models. In particular, I will talk about screening mechanisms, instabilities and constraints coming from the recent observations of gravitational waves.
Chapter 5: I will introduce the Effective Field Theory approach to dark energy and its implementation in the EFTCAMB cosmological code.
Chapter 6: I will present my work of studying the Generalized Brans-Dicke model employing the EFT formalism and the EFTCAMB code. I will talk about how I implemented the model in the code and how I exploited the code to study the viability conditions for the model and to perform the cosmological perturbations analysis. Finally, I will conclude with a MCMC likelihood analysis to study the theory in view of cosmological data.
Conclusions: I will summarize and discuss the contents of this Thesis.
Appendices: I will study in more details some topics mentioned in the main chapters. The choice of the topics reflects also a personal interest. In particular, I will give more details about the first-order gravitational perturbations and about conformal transformations of the metric. Then, I will explain how $f(R)$ theories can be seen as subclass of Brans-Dicke theories and how to go from Jordan to Einstein frame, in the case of $f(R)$ theories but as an example that can be generalized to other models. Finally in the last appendix, I will further analyze the Chameleon mechanism and in particular I will look for an explicit solution in the case of a spherical object.

Chapter 1

Introduction to Cosmology

1.1 ΛCDM

Through decades of increasingly accurate measurements of different observables, modern cosmology has gradually led to the so called ΛCDM as the standard model of Cosmology. This model describes a homogeneous and isotropic background, which is expanding, and small inhomogeneities that grow, under gravitational instability, into the structure that we observe around us. The name of the model remembers two fundamental components of our Universe: the dark energy which corresponds to the cosmological constant Λ and drives the late accelerated expansion of the Universe and cold dark matter (CDM).
The dark matter is a still unknown component of the Universe, different from the ordinary baryonic matter, since it interacts only gravitationally with the other fluids. It was introduced in the model to explain observations such as the speed of rotation of the galaxies in our Universe, indeed if we take into account only the gravity generated by their observable matter, then it is not enough to hold them together. Similarly, for the galaxies in clusters. This makes cosmologists think that something we have yet to detect is giving these galaxies extra mass, and thus it generates the extra gravity they need to stay intact. This strange form of matter was therefore called dark matter and it was labeled to be cold to highlight the fact that it decoupled from the other components of the Universe when its velocity was much less than the speed of light i.e. when it was non-relativistic.

In this first Chapter we will focus mostly on the background peculiarities and on observational evidences in support of dark energy. Cosmological perturbations and observables of interest in Cosmology are instead discussed in the next Chapter.

The theory of gravity that rules the ΛCDM Universe is General Relativity. In the frame of General Relativity in fact, it is possible to obtain the equations that describe the Universe and its evolution. To do so, the basic foundation is the metric element, which carries the structure of the desired spacetime. An expanding, isotropic and homogeneous Universe is described by the Friedman-Lemaitre-Robertson-Walker (FLRW) metric:

$$ds^2 = dt^2 - a(t)^2\left(\frac{dr^2}{1-kr^2} + r^2(d\theta^2 + sin(\theta)^2 d\phi^2)\right), \tag{1.1}$$

where $a(t)$ is the scale factor and k the spatial curvature parameter. Assuming this geometry, we then need to decide how to fill our Universe or, in other words, how to write the stress energy tensor entering the equations. The perfect fluid approximation is usually employed:

$$T_{\mu\nu} = (P+\rho)u_\mu u_\nu + P g_{\mu\nu}, \tag{1.2}$$

where u_μ is the 4-velocity of the fluid while ρ and P respectively its energy density and pressure. This approximation is realistic for example in a case such that the mean free path between particle collisions is much smaller than the scales of physical interest [8]. Furthermore, the perfect fluid is compatible with the Cosmological principle that prohibits anisotropic pressure.

The equations that combine the geometrical structure with the energetic constituents, are the Einstein equations; for a ΛCDM model they can be obtained from the following action:

$$S = \int d^4x\sqrt{-g}\frac{M_{pl}^2}{2}(R - 2\Lambda) + \int d^4x\sqrt{-g}\mathcal{L}_M(g_{\mu\nu}, \psi_M). \tag{1.3}$$

Varying the action with respect to the metric and assuming:

$$T_{\mu\nu} = -\frac{2}{\sqrt{-g}}\frac{\delta(\sqrt{-g}\mathcal{L}_M)}{\delta g^{\mu\nu}}. \tag{1.4}$$

We can find the Friedman equations that are the Einstein equations specialised to a FLRW spacetime:

$$\begin{aligned} H^2 &= \frac{8\pi G}{3}\rho - \frac{k}{a^2} + \frac{\Lambda}{3}, \\ \frac{\ddot{a}}{a} &= -\frac{4\pi G}{3}(\rho + 3P) + \frac{\Lambda}{3}, \\ \dot{\rho} &= -3H(\rho + P). \end{aligned} \tag{1.5}$$

The dot denotes a derivative with respect to the cosmic time. The equations above are not independent; in particular, the last one is the continuity equation that can be found combining the first two.
All the main ingredients that we use to describe our Universe are contained inside these equations. The Hubble parameter $H = \frac{\dot{a}}{a}$ quantifies the expansion rate of the Universe. ρ and P are respectively the total energy density and the total isotropic pressure considering all the different fluid contributions. The cosmological constant Λ plays the role of dark energy, a still unknown form of energy that drives the late time cosmic expansion of the Universe. And finally G that is obviously the Newton constant of gravitation. It is worth to notice that the term proportional to the spatial curvature parameter k is negligible: from an observational point of view, its contribution to the total energy budget today is very low and its dependence to $\propto a^{-2}$ makes it safely negligible also in the past.

It is easy to show that we can represent the cosmological constant as a perfect fluid with an energy density equal to $\rho_\Lambda = \frac{\Lambda}{8\pi G}$ and $P_\Lambda = -\rho_\Lambda$. This allows us to reabsorb the cosmological constant in the Friedman equation, recovering the form:

$$\begin{aligned} H^2 &= \frac{8\pi G}{3}(\rho + \rho_\Lambda) - \frac{k}{a^2}, \\ \frac{\ddot{a}}{a} &= -\frac{4\pi G}{3}(\rho + \rho_\Lambda + 3P + 3P_\Lambda). \end{aligned} \tag{1.6}$$

The fluids that we consider can be classified by providing a relation between ρ and P. In other words, we need to specify an equation of state that characterises the fluid and we choose it to be of the form:

$$P = w\rho, \tag{1.7}$$

where w is characteristic of the specific fluid.
Considering the case in which w is a constant, it is worth to substitute the equation of state inside the continuity equation and integrate it:

$$\rho = \rho_0\left(\frac{a}{a_0}\right)^{-3(1+w)}. \tag{1.8}$$

This equation describes the evolution of the energy density for fluids such as dust and radiation. We can indeed opt for $w = 0$ for pressureless material, that is a good approximation for any form of non relativistic matter. On the opposite extreme, for relativistic radiation we usually use $w = \frac{1}{3}$, as is can be derived from considerations of statistical mechanics and kinetic theory of gases.

Furthermore, the cosmological constant can be properly described by a $w = -1$ equation of state. Given this, it is possible to recover the energy density evolution of the fluids of the ΛCDM model:

$$\rho \propto \begin{cases} a^{-3} \text{ for dust} \\ a^{-4} \text{ for radiation} \\ a^{0} \text{ for the cosmological constant} \end{cases} \tag{1.9}$$

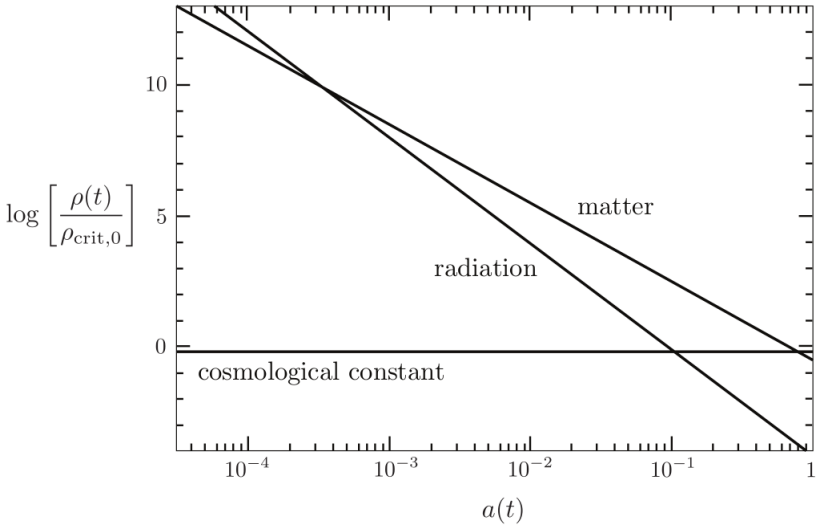

Figure 1.1: Energy densities evolution

As we anticipated, ΛCDM, in accordance with observations, is built to describe an Universe filled with radiation, matter and dark energy in terms of a cosmological constant. Defining the density parameter of a fluid as:

$$\Omega(t) = \frac{\rho(t)}{\rho_c(t)} = \frac{\rho(t) 8\pi G}{3H(t)^2}, \tag{1.10}$$

where ρ_c is the total energy density of a flat Universe. Similarly we can define a parameter density for the spatial curvature:

$$\Omega_k = -\frac{k}{a^2 H^2}. \tag{1.11}$$

A good reference for their density parameters at present is [9]:

$$\Omega_m^0 = 0.32, \qquad \Omega_r^0 = 9.4 \cdot 10^{-5}, \qquad \Omega_\Lambda^0 = 0.68, \tag{1.12}$$

while we have strong observational bounds on the spatial curvature $|\Omega_{0k}| < 0.01$, so less than 1% of the cosmic energy budget today.
In particular, the matter part can be divided between baryons and cold dark matter as:

$$\Omega_b^0 = 0.05, \qquad \Omega_c^0 = 0.27. \tag{1.13}$$

It is then clear that, with the evolution of $a(t)$, the main component of the Universe changes: as we can see in Figure 1.1, firstly the Universe goes from being radiation to matter dominated, this moment of the history of the Universe is known as matter-radiation equivalence. Writing the redsfhit parameter as:

$$1 + z = \frac{a_0}{a}, \tag{1.14}$$

where a_0 is the scale factor today, which is usually taken to be equal to 1. We can determine the redshift z_{eq} of the matter-radiation equivalence:

$$\rho_m(z_{eq}) = \rho_r(z_{eq}). \tag{1.15}$$

We therefore have:

$$\rho_r^0(1+z_{eq})^4 = \rho_m^0(1+z_{eq})^3. \tag{1.16}$$

With the density parameters (1.12):

$$1+z_{eq} = \frac{\rho_m^0}{\rho_r^0} = \frac{\Omega_m^0}{\Omega_r^0} \sim 3000. \tag{1.17}$$

Similarly we can find the moment in which a cosmological constant starts to dominate over the matter:

$$\rho_m(z_\Lambda) = \rho_\Lambda(z_\Lambda), \tag{1.18}$$

where z_Λ is the redshift of the equivalence matter-cosmological constant. Straightforwardly:

$$\rho_m^0(1+z_\Lambda)^3 = \rho_\Lambda^0 \Longrightarrow 1+z_\Lambda = \left(\frac{\Omega_\Lambda^0}{\Omega_m^0}\right)^{1/3}, \tag{1.19}$$

that, using again (1.12), gives $z_\Lambda \sim 0.3$.
Therefore, a cosmological constant should start to manifest only recently in our Universe history.

1.2 Dark energy

Historically, the cosmological constant was introduced by Einstein in the search for static solutions of Friedman equations. The idea was then rapidly rejected because of the discovery that such solutions were unstable and, above all, against cosmological observations. Indeed in the 1930's Hubble, looking at the galaxies redshift, realized that the Universe was not static but rather dynamic and expanding.
Nowadays, the cosmological constant has been reintroduced in the equations to describe a phenomenon discovered in the 1998: both Perlmutter et al. [Supernova Cosmology Project (SCP)] [1] and Riess et al. [High-redshift Supernova Search Team (HSST)] [2] independently reported the discovery of the accelerated expansion of the Universe from the observation of distant supernovae of Type Ia. The origin of Type Ia supernovae is the explosion of a white dwarf in a binary system, due to the fact that their mass exceeds a critical value known as Chandrasekhar mass by absorbing gas from the other star of the system.
It was at that time that the term "dark energy" appeared to label all the possible physical substances capable to explain the accelerated expansion of the Universe and some other open issues, such as the age of the Universe, as we will see in the next paragraph.
The equation of state of the dark energy is still unknown but, as we saw, in the ΛCDM frame, we assume $w_{DE} = w_\Lambda = -1$, which is consistent with all observations. This is not the only possibility, even if, thanks to data, we know that only small deviations from it are possible. In the most general case, we can assume w_{DE} to be a function of time so its continuity equation is:

$$\dot{\rho}_{DE} + 3H\rho_{DE}(1+w_{DE}(a)) = 0, \tag{1.20}$$

with the general solution:

$$\rho_{DE} = \frac{3H_0^2}{8\pi G}\Omega_{DE}^0\, exp\left[-3\int_1^a \frac{(1+w_{DE}(a))}{a}da\right]. \tag{1.21}$$

To see the direct link between the dark energy equation of state and the cosmological evolution, we can rewrite the first Friedmann equation in terms of the density parameters of the different fluids:

$$H(z) = H_0\left(\Omega_m^0(1+z)^3 + \Omega_r^0(1+z)^4 + \Omega_{DE}^0 exp\left[-3\int_1^a \frac{(1+w_{DE}(a))}{a}da\right]\right)^{\frac{1}{2}}, \tag{1.22}$$

where we used the approximation $\Omega_k^0 = 0$.
Then defining the quantity:

$$E(z) = \frac{H(z)}{H_0}, \tag{1.23}$$

we can rearrange the equation and differentiate it with respect to z in order to obtain a general expression for the equation of state of the dark energy:

$$w_{DE}(z) = \frac{(E(z)^2)'(1+z) - 3E(z)^2 - (1+z)^4\Omega_r^0}{3[E(z)^2 - \Omega_r^0(1+z)^4 - \Omega_m^0(1+z)^3]}, \tag{1.24}$$

where the prime denotes a derivative with respect to z. This relation is useful to place observational constraints on the equation of state of dark energy [10].
The request for dark energy to realize the accelerated expansion puts a strong constraint on the possible values of w_{DE}. Indeed exploiting the second Friedmann equation, it is easy to see:

$$\ddot{a} > 0 \Longleftrightarrow w < -\frac{1}{3}. \tag{1.25}$$

On the other hand, there is the so called "phantom" regime where $w_{DE} < -1$, here $\rho_{DE} + P_{DE} < 0$ meaning that ρ_{DE} increases with time, we will explore this better in Chapter 3.

Finally, it is important to keep always in mind the observational bounds on the equation of state of the dark energy. For example, the WMAP 5-years data combined with other observational data, gives $-1.097 < w_{DE} < -0.858$ at 95% confidence level [10].
If the dark energy is not a cosmological constant, then several parametrizations of its equation of state can be exploited to fit the data. Assuming to have a time-dependent w_{DE} we have for example:

- Chevallier-Polarski-Linde (CPL) parametrization [15]:

  $$w_{DE}(a) = w_0 + w_a(1-a), \tag{1.26}$$

  which is the first-order Taylor expansion of $w_{DE}(a)$ around a_0. w_0 and w_a are constants and they are respectively the value and the first derivative of w_{DE} today.

- Generalized Jassal-Bagla-Padmanabhan parametrization [16]:

  $$w_{DE}(a) = w_0 + (1-a)^{n-1}w_a, \tag{1.27}$$

  that for $n = 2$ reduces to the CPL parametrization. Again, w_0 and w_a are respectively the value and the first derivative of w_{DE} today.

- Turning point parametrization [17]:

  $$w_{DE}(a) = w_0 + w_a(a_t - a)^2, \tag{1.28}$$

  which is a second-order parabolic parametrization and it explores the possibility of a turning point in w_{DE}. Here, w_0 and w_a are the value and the first derivative of w_{DE} at the turning point a_t.

- Taylor expansion around $a = 0$ [18]:

  $$w_{DE}(a) = w_0 + w_a a + \frac{1}{2}w_2 a^2 + \frac{1}{6}w_3 a^3, \tag{1.29}$$

  where w_0, w_a, w_2 and w_3 are respectively the value, and the time derivatives of $w_{DE}(a)$ at $a = 0$.

1.2.1 Observational window on our Universe

In the following, it is interesting to highlight why a simpler "CDM" Universe is not enough.

Supernovae evidences

As already said, in 1998 supernovae Type Ia observations provided the first evidence of the accelerated expansion of the Universe.
The supernovae classification is made according to the absorption lines of chemical elements: Type I has a spectrum without an hydrogen line and, more in details, the spectrum of Type Ia contains in addition an absorption line of ionized silicon.
Supernovae Type Ia have a crucial feature that makes them particularly interesting for cosmological observations: they are named "standard candles" since their absolute magnitude at the peak of the brightness is almost constant and known to be around $M = -19$.
Defining the luminosity distance as:

$$d_L^2 = \frac{L}{4\pi F}, \tag{1.30}$$

where L is the intrinsic luminosity and F the observed flux of the supernovae. We can then use the distance modulus (valid for distance expressed in Megaparsec):

$$\mu = m - M = 5log_{10}(d_L) + 25, \tag{1.31}$$

that links m, the apparent luminosity, to M, the absolute one (that corresponds to the apparent luminosity of the source fixed at $d_L = 10pc$). It is immediately clear that knowing the absolute magnitude of the "standard candle" and measuring its apparent one, the luminosity distance of the supernova can be obtained observationally.
Today, Supernovae Type Ia have little statistical power compared to other other observables such as Baryonic Acoustic Oscillations (BAO) and Cosmic Microwave Background (CMB) power spectra (we will see better them in the next paragraphs). They remain useful in fixing the background cosmology at low redshifts where other kind of measurements, like BAO, are less precise [3]. Indeed as we see in Figure 1.2, they show an excellent agreement with Planck CMB power spectra, in combination with CMB lensing reconstruction.

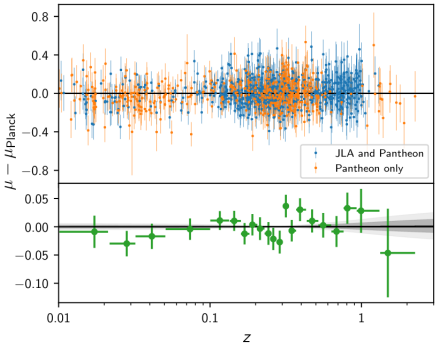

Figure 1.2: Distance modulus μ for supernovae in the Pantheon sample [50] with 1σ errors, compared to the Planck power spectra + lensing ΛCDM best fit. Supernovae that were also in the older Joint Lightcurve Analysis sample are shown in blue [51]. The lower panel shows the binned errors, with equal numbers of supernovae per redshift bin (except for the two highest redshift bins). Taken from [3].

To see how to extract information about dark energy from supernovae, we need to consider the measurement of the wavelength λ of their light; it is then possible to compute the redshift of the supernovae, for definition:

$$z = \frac{\lambda_0 - \lambda_e}{\lambda_e}, \tag{1.32}$$

where λ_0 is the observed wavelength while λ_e is the emitted one.
Combining the experimental information, it is consequently possible to estimate the observed dependence of the luminosity distance d_L on the redshift of the supernova.
The observational data can then be compared with theoretical prediction provided by (case $k = 0$):

$$d_L = r(1+z)a_0 = c(1+z)\int_0^z \frac{dz}{H(z)}, \tag{1.33}$$

which is found combining (1.30) with the theoretical prediction of the observed flux in an expanding Universe and computing the comoving radius for a light like geodesic. As we can see, (1.33) has a convenient dependence from the the Hubble parameter which is determined by the density parameters of all the components of our Universe, as in (1.22). For example, considering $\Omega_r^0 \sim 0$ and choosing the equation of state for the dark energy $w_{DE} = -1$, we can find the useful expression:

$$d_L = \frac{c(1+z)}{H_0} \int_0^z \frac{dz}{[(1-\Omega_{DE}^0)(1+z)^3 + \Omega_{DE}^0]^{1/2}}, \tag{1.34}$$

that can be evaluated numerically for different choices of Ω_{DE}^0.
Perlmutter et al.[1] showed that the cosmological constant is present in our Universe at the 99% confidence level.
Nowadays, many more accurate measurements were carried and, in the recent Planck 2018 release [3], the density parameter at present of dark energy is constrained to be $\Omega_\Lambda^0 = 0.6889 \pm 0.0056$, from Planck CMB power spectra, in combination with CMB lensing reconstruction and BAO.

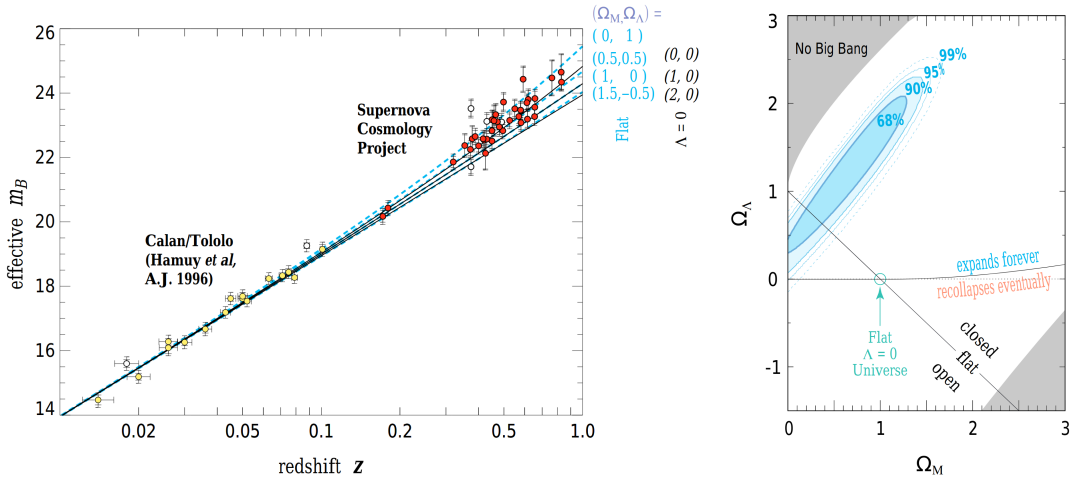

Figure 1.3: From Permutter et al. [1]. On the left, Hubble diagram of the the effective apparent luminosity m_B versus the redshift z for 42 high-redshift Type Ia supernovae from the Supernova Cosmology Project, and 18 low-redshift Type Ia supernovae from the Calán/Tololo Supernova Survey. The solid curves are the theoretical predictions for a range of cosmological models with zero cosmological constant. The dashed curves are for a range of flat cosmological models. On the right, best-fit confidence regions in the $\Omega_\Lambda - \Omega_m$ plane. The $68\%, 90\%, 95\%, 99\%$ statistical confidence regions are shown.

Age of the Universe

Another key evidence of the existence of an additional component, apart from the standard radiation and matter, was provided by the estimation of the age of the Universe. The age of the Universe can be indeed calculated from:

$$t_0 = \int_0^{t_0} dt = \int_0^{a_0} \frac{da}{H(a)a} = \int_0^{\infty} \frac{dz}{H(z)(1+z)}, \tag{1.35}$$

where, again, we are able to establish a dependence from the Hubble parameter which, in turn, depends on the density parameters of the Universe components (1.22). Considering again a flat Universe with $\Omega_r^0 \sim 0$ and $w_{DE} = -1$:

$$t_0 = \int_0^{\infty} \frac{dz}{H_0[(1-\Omega_{DE}^0)(1+z)^3 + \Omega_{DE}^0]^{1/2}(1+z)}, \tag{1.36}$$

it can be analytically integrated:

$$t_0 = \frac{H_0^{-1}}{3\sqrt{\Omega^0_{DE}}} ln\left(\frac{1+\sqrt{\Omega^0_{DE}}}{1-\sqrt{\Omega^0_{DE}}}\right), \tag{1.37}$$

for the the limit $\Omega^0_{DE} \to 0$ (Einstein-DeSitter Universe) becomes:

$$t_0 = \frac{2}{3H_0}, \tag{1.38}$$

that for $H_0 \sim 70\ km/Mpc \cdot s$, it is equal to $\sim 9.3\ Gyrs$. Oppositely, in the limit $\Omega^0_{DE} \to 1$ we have $t_0 \to \infty$. Thus, t_0 gets higher for increasing Ω^0_{DE}.
In an Einstein-DeSitter Universe a paradox was found: the theoretical prediction of the cosmic age was lower than the age of the oldest stars of our galaxy. This problem can be circumvented by including a dark energy component in our Universe, roughly assuming $\Omega^0_m \sim 0.3$, it is possible to find the better range of $\sim 12 - 16\ Gyrs$. Today, the value confirmed by the last Planck data release from CMB power spectra, in combination with CMB lensing reconstruction and BAO is $13.787 \pm 0.020\ Gyrs$ [3] so the dark energy is decisive to solve the age of the Universe issue.

Cosmic Microwave Background

The Cosmic Microwave Background (CMB) is the radiation coming from the last scattering surface, a space-like surface corresponding to the instant when the Universe became transparent to radiation. Previously, photons were tightly coupled through Thomson and Coulomb scatterings with matter in the so called photon-baryon fluid. As the Universe expanded, the temperature decreases, photons lose energy and they become no longer able to ionize hydrogen, that starts to form during the recombination epoch at $z \sim 1100$. In other words, the last scattering surface is the edge of our observable Universe. When the photons starts to stream freely, the properties of the plasma on this surface were directly imprinted in the spectrum of the CMB radiation that we can still observe today. The primary observables in the CMB radiation are the temperature fluctuations whose ratio, with respect to the mean temperature, is of the order of 10^{-5}. These fluctuations are extremely rich of physical information about our Universe, and they can be efficiently described by the temperature power spectrum, as described in the following. Indeed, we can expand the distribution of T measured on the sky as a sum over spherical harmonics:

$$\Theta(\theta,\phi) = \frac{\Delta T}{T}(\theta,\phi) = \sum_{l=0}^{\infty}\sum_{m=-l}^{+l} a_{lm} Y_{lm}(\theta,\phi), \tag{1.39}$$

with:

$$Y_{lm}(\theta,\phi) = (-1)^m \sqrt{\frac{2l+1}{4\pi}\frac{(l-m)!}{(l+m)!}} P_l^m(cos\theta) e^{im\phi}. \tag{1.40}$$

With P_l^m the associated Legendre polynomial. Using the orthonormality properties of the spherical harmonics, we can obtain the coefficients:

$$a_{lm} = \int \Theta(\theta,\phi) Y^*_{lm}(\theta,\phi) d\Omega. \tag{1.41}$$

In the usual convention, the angular power spectrum is defined as:

$$\langle a_{lm} a^*_{l'm'} \rangle = \delta_{ll'}\delta_{mm'} C_l. \tag{1.42}$$

The angular size θ in the sky is linked to the l multipole of the spherical harmonics thorough $\theta = \pi/l$.
From the theory point of view, the complete spectrum of temperature anisotropies can be derived solving the Einstein and Bolzmann equations. This is quite challenging since the equations for photons are coupled to the other matter components and it can be better achieved with the help of a cosmological code, like CAMB, as we will see in the following part of this Thesis.

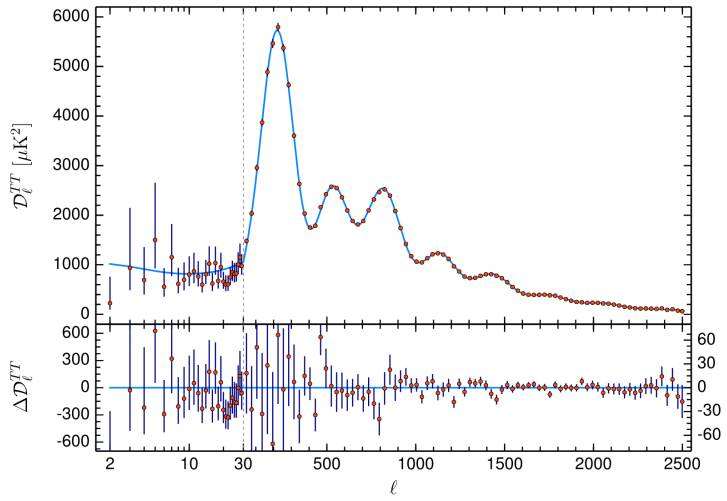

Figure 1.4: Planck 2018 [3] temperature power spectrum, $D_l^{TT} = l(l+1)C_l^{TT}/2\pi$. The base-$\Lambda CDM$ theoretical spectrum best fit is plotted in light blue in the upper panel. Residuals with respect to this model are shown in the lower panel.

The CMB spectrum can be used as a "standard ruler" (in comparison to the "standard candle" in the supernovae observation), that means using an object of known dimensions to extract the angular diameter distance:

$$d_A = \frac{D}{\Delta\theta}, \tag{1.43}$$

where D is the size of the object, known in the case of a "standard ruler", while $\Delta\theta$ is its measured angular size. Assuming to have all the object at the same comoving distance r, in a FLRW metric we have $D = a(t)r\Delta\theta$. Then the angular diameter distance becomes:

$$d_A = a(t)r = c\frac{a}{a_0}\int_0^z \frac{dz}{H(z)} = \frac{c}{(1+z)}\int_0^z \frac{dz}{H(z)} = \frac{d_L}{(1+z)^2}, \tag{1.44}$$

where, like before, we have found a dependence from the Hubble parameter which, in turns, depends on the density parameters of the all the fluids.

The acoustic peaks in the CMB power spectrum are the snapshot at the surface of last scattering of damped oscillations of the photon-baryon plasma under the competing effects of gravity and radiation pressure. For overdense regions of space smaller than the Hubble horizon indeed, matter contracted under self-gravity, heating up inside of them. On the contrary, radiation pressure worked to damp out inhomogeneity. At the last scattering surface, the oscillations were freezed out and encoded in the CMB power spectrum as maximum anisotropy (peaks), at specific scales. The acoustic peaks in the power spectrum of CMB temperature fluctuations are considered a good "standard ruler", therefore, for example, an effect we can look for, as a clue of dark energy existence, is the change of the position in the acoustic peaks due to modifications in the angular diameter distance.
In particular, the first peak is the peak corresponding to the scale that had the time to oscillate only once before recombination. Thus its angular scale θ_{peak} is expected to correspond to the scale of the sound horizon θ_s, which is defined as the distance that the sound could travel before recombination. This means that:

$$l_{peak} = \frac{\pi}{\theta_{peak}} = \frac{\pi}{\theta_s} = \frac{\pi}{r_s} d_A^{(c)}(z_{ric}), \tag{1.45}$$

where $d_A^{(c)}(z_{ric})$ is the comoving angular diameter distance at recombination and r_s is the comoving

sound horizon that can be independently computed. Indeed, the latter is:

$$r_s = \int_0^{t_s} \frac{c_s dt}{a(t)}, \tag{1.46}$$

where $t = 0$ is the Big Bang time and t_s the recombination time. Then we need the speed of sound of the photon-baryon fluid:

$$c_s = \sqrt{\frac{\delta P}{\delta \rho}} = \sqrt{\frac{\delta P_r}{\delta \rho_r + \delta \rho_b}} = \sqrt{\frac{\delta \rho_r}{3(\delta \rho_r + \delta \rho_b)}} = \frac{1}{\sqrt{3(1+R)}}, \tag{1.47}$$

with:

$$R = \frac{\delta \rho_b}{\delta \rho_r} = \frac{3\rho_b}{4\rho_r} = \frac{3\Omega_b}{4\Omega_r}, \tag{1.48}$$

where in the second equality we exploited the continuity equations for the baryon and radiation fluid: $\dot{\rho} + 3H(\rho + P) = 0$ that can be rewritten as $\frac{\delta \rho}{\rho(1+w)} = -3H\delta t$. Finally, the sound horizon can be expressed as:

$$r_s = \frac{c}{\sqrt{3}} \int_{z_s}^{\infty} \frac{dz}{H(z)\sqrt{1 + \frac{3\Omega_b(z)}{4\Omega_r(z)}}} \tag{1.49}$$

and it can be computed knowing the expansion history of the Universe at early time, with the dark energy component still subdominant. From Planck 2018 [3] measurements of CMB power spectra, in combination with CMB lensing reconstruction, we have $r_s = 144.43 \pm 0.26\ Mpc$.
Coming back, the multipole l of the peak can be directly read from the CMB power spectrum, for the first peak we have $l \sim 220$. Finally we can compare the resulting angular diameter distance from the theoretical one computed through (1.44).

The most important result of this reasoning is the possibility to strongly constrain the geometry of the Universe to be flat. Furthermore, the CMB acoustic peaks provide valuable information to constrain essentially all the cosmological parameters, since a modification of them translates directly in a modification of the temperature power spectrum, as we can see in Figure 1.5.

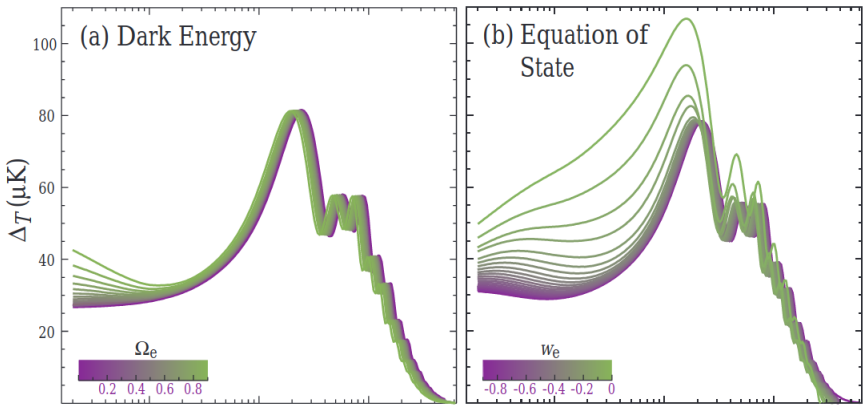

Figure 1.5: Sensitivity of the CMB temperature power spectrum to the energy density of the dark energy today in units of the critical density in a ΛCDM model and to the equation of state parameter of the dark energy [4].

Finally, another important clue of the dark energy existence can be read at low multipoles, where the power spectrum is dominated by the Integrated Sachs-Wolfe effect. This scales have entered the horizon only recently so they did not undergo oscillations before recombination. The CMB photons travels from the surface of last scattering to us, passing through the fluctuations that were previously frozen. In a matter dominated Universe, the metric perturbations are constant. In this frame, photons travelling through them would be blueshifted and then redshifted equally

while entering and climbing out the potential well, so their net energy should remain constant. However, in a dark energy dominated Universe, the metric perturbations are no longer constant and they become a further source of anisotropy for the CMB photons.
The Integrated Sachs-Wolfe effect signal is $\sim 10\%$ of the total CMB signal [5] and it is usually investigated thought its correlation with the distribution of matter around us.

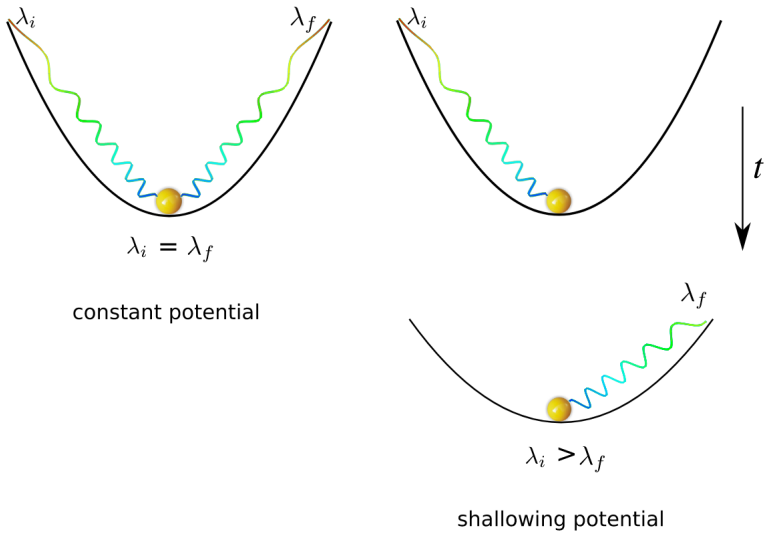

Figure 1.6: Schematic representation of the Integrated Sachs-Wolfe effect (ISW). On the left, a photon travelling a constant potential well with no changing in its energy. On the right, a photon travelling a time dependent potential with an energy change. Taken from [5].

Baryonic acoustic oscillations

Another dark energy probe is provided by the Baryonic Acoustic Oscillation (BAO), that refers to the imprint left by the acoustic oscillation of the photon-baryon plasma in the late time clusterings of matter and galaxies. Similarly to the CMB acoustic peaks, the standard ruler is the acoustic length scale at recombination, r_s as in (1.49), that can be computed with a good level of accuracy. At recombination the sound waves froze, photons started to stream freely and the baryon part of the waves was left in a spherical shell centered around the perturbation. Dark matter, which is uncoupled by baryons and photons, did not undergo the oscillations and it remained concentrated inside the potential wells. Both dark matter and baryons overdensities became the seeds of gravitational instability that forms today structure of galaxies and matter. We therefore expect to find galaxies both at the center of primordial potential wells and at the radius of the shell induced by baryons.
As previously done for the acoustic peaks, knowing the comoving sound horizon r_s at which the clusterings of galaxies formed, the angular diameter distance (1.44) can be computed at a given redshift and used to constrain the expansion history of the Universe. In particular, it is possible to check the comoving distance Δr between two galaxies both along our line of sight and perpendicular to it. In the latter case, for galaxies seen under an angle $\Delta\theta$, we have that $\Delta\theta = \frac{\Delta r}{d_A^{(com)}(z)}$. While for galaxies with redshift difference of Δz, we can consider an average Hubble rate and obtain: $\Delta r = \frac{\Delta z}{H}$. Combining the two information, it is possible to obtain an effective distance in function of the redshift defined as [11]:

$$D_V(z) = \left[(1+z)^2 d_A^2(z) \frac{cz}{H(z)}\right]^{1/3}, \tag{1.50}$$

that can be constrained by the observational data.

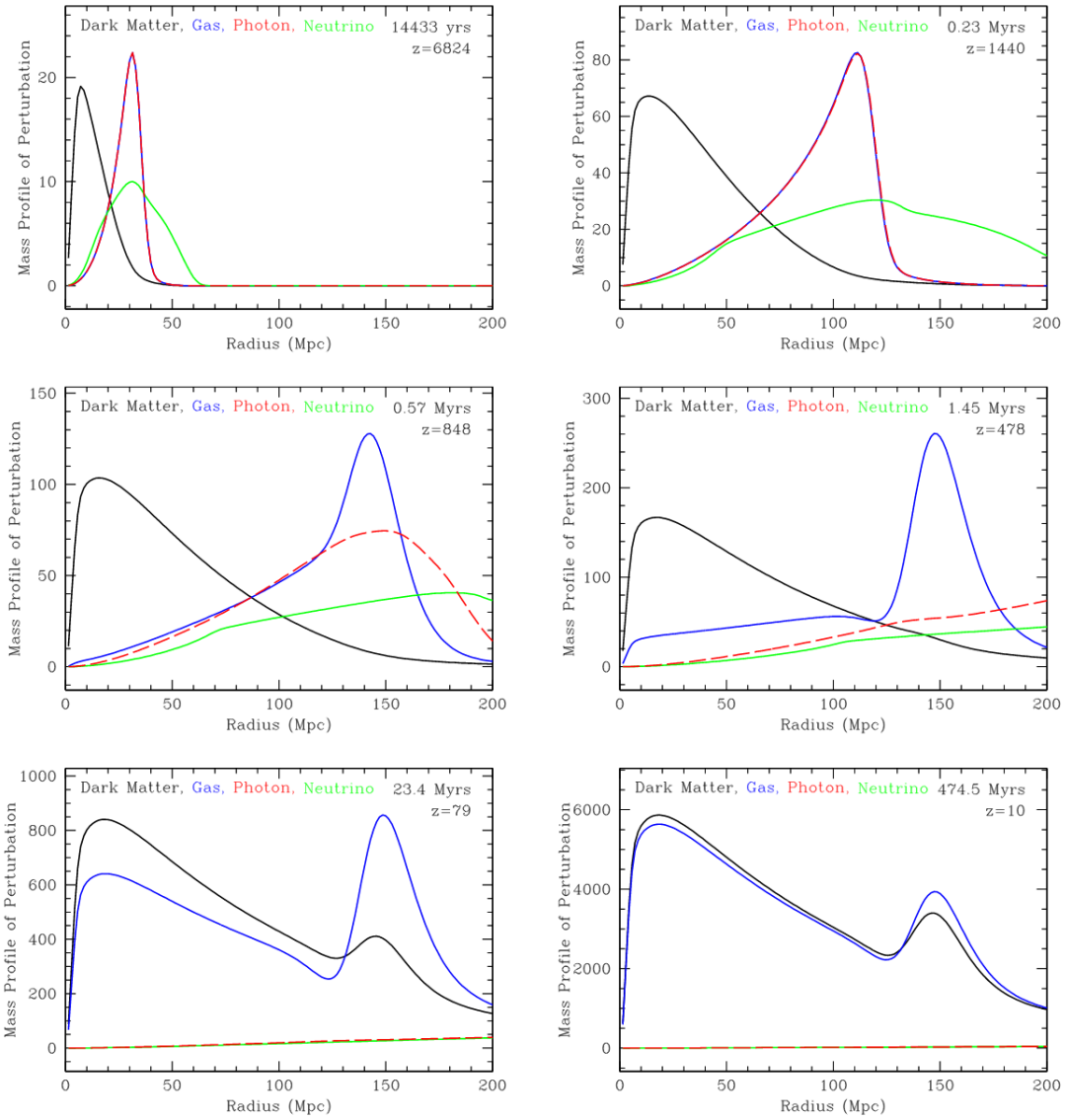

Figure 1.7: Simulation of the generation of the acoustic peak via linear-theory response to a point-like overdensity at the origin, [6]. Each figure show the mass profile of the perturbations of dark matter (black), baryons (blue), photons (red), and neutrinos (green) at different redshifts. From left to right: photons and baryons were tightly coupled and they oscillated in an acoustic wave, after recombination they decoupled and baryons were left to form a shell at specific scales. Galaxy formation is favored near the origin and at this specific scale.

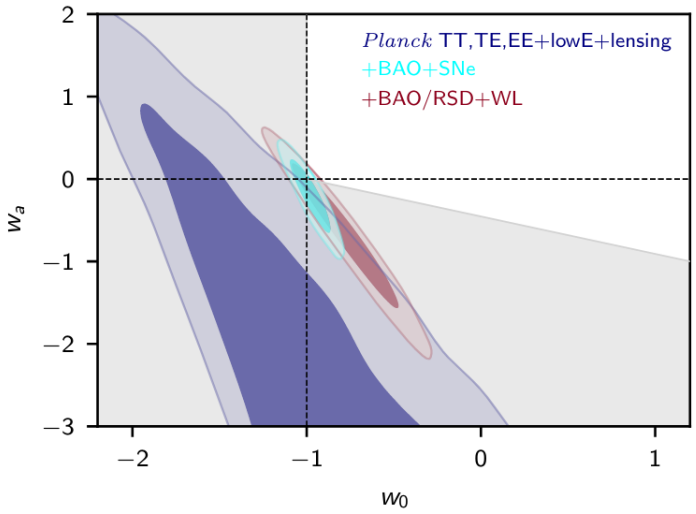

Figure 1.8: Marginalized posterior distributions of the (w_0, w_a) parameters of (1.26) for different data combinations [3]. The dashed lines indicate the point corresponding to ΛCDM.

Weak lensing

The gravitational bending of light can also be checked to find evidence of dark energy. The phenomenon that we observe more often is the weak gravitational lensing which distorts the shape, size and brightness of galaxies. As opposed to the strong gravitational lensing effect that causes the production of multiple images of the same object due to the deflection of light of massive structures.
Theoretically, the deformation of light due to gravitational lensing is described by two functions: the convergence κ and the complex shear $\gamma = \gamma_1 + i\gamma_2$; they are both contained inside the so called distortion matrix which is used to map the source plane to the image plane that we observe:

$$\delta x_i^S = A_{ij}\delta x_j^I, \tag{1.51}$$

where δx is the displacement vector in the two planes and A is the distortion matrix:

$$A = \begin{pmatrix} 1-\kappa-\gamma_1 & -\gamma_2 \\ -\gamma_2 & 1-\kappa+\gamma_1 \end{pmatrix}. \tag{1.52}$$

The convergence describes the isotropic magnification of the source while the shear quantify the distortion of the shape of the object i.e. how a circular source is transformed into an elliptical one. As previously for the CMB temperature, it is possible to build shear and convergence power spectra, taking the Fourier transform of the two-points correlation function between galaxies. In the limit of weak distortion the power spectra of the shear and convergence coincides. In particular, the weak lensing tomography is used and it consists in slicing the shear signal in redshift bins. For example, considering a galaxy in the redshift bin i and another one in the bin j, it is possible to write the tomography cross-power spectrum at a given multipole l as [14]:

$$P_{ij}^{\kappa}(l) = \int_0^{\infty} dz \frac{W_i(z)W_j(z)}{d_A^{(c)}(z)^2 H(z)} P_\delta\left(\frac{l}{d_A^{(c)}(z)}, z\right), \tag{1.53}$$

where $W(z)$ is a weight function that estimates the efficiency of the lensing, $d_A^{(c)}(z)$ the comoving angular diameter distance and P_δ is the mass density power spectrum. Experimentally, a large number of galaxies are required to measure the cosmic shear signal [12], which is related to the ellipticity of the observed galaxies.
The important feature, as we can see from (1.53), is that the shear power spectrum is dependent on the dark energy via the expansion history.
Nowadays, cosmic shear measurements are available from several collaborations, including the Dark Energy Survey (DES) [52] and KiDS [53]-[54].

1.2.2 Vacuum Energy

Coming back to the ΛCDM frame, the obvious questions that we then need to answer is what the cosmological constant Λ is physically.
Modern field theory associates this term with the vacuum energy density. This possibility is offered by a characteristic feature of General Relativity: the fact that the source of gravity is the entire stress-energy tensor and, as a consequence, the normalization of the energy is not arbitrary. In non gravitational physics on the contrary, only differences in energy from one state to another matter: for example, the shift of the potential energy of a particle by a constant term will not affect its motion [13].
In General Relativity therefore, we have to consider the existence of the vacuum energy that is the energy density of the empty spacetime. Clearly, we have to require the energy density not to introduce any preferred directions: this means that the corresponding stress-energy tensor needs to be Lorentz invariant in locally inertial coordinates. In Minkowski spacetime this implies the form:

$$T_{\mu\nu}^{(vac)} = -\rho_{(vac)}\eta_{\mu\nu}, \tag{1.54}$$

where $\eta_{\mu\nu}$ is the flat metric. It can be straightforwardly generalized to curved spacetime as:

$$T_{\mu\nu}^{(vac)} = -\rho_{(vac)}g_{\mu\nu}. \tag{1.55}$$

Comparing this expression with the perfect fluid stress-energy tensor (1.2) we can easily see that the vacuum energy density can behave as a perfect fluid with the equation of state:

$$\rho_{(vac)} = -P_{(vac)}, \tag{1.56}$$

that is exactly the equation of state of the cosmological constant present in the ΛCDM model, meaning that, as we saw, the energy density can be expressed as:

$$\rho_{(vac)} = \rho_\Lambda = \frac{\Lambda}{8\pi G}. \tag{1.57}$$

In this framework therefore, the terms "cosmological constant" and "vacuum energy" are interchangeable.
So it is feasible to introduce a cosmological constant representing the vacuum energy in the equations; however this doesn't help us in computing its expectation value, that should be a constant of nature. To estimate its value, an important contribution that we first need to take into account is the zero-point energy or the vacuum state energy of the quantum fields in our model.
Classically, the zero-point energy of a particle is the state in which the particle is motionless and at the minimum of the potential. Considering a one-dimensional harmonic oscillator potential $V(x) = \frac{\omega^2 x^2}{2}$, the minimum of the potential is clearly at $x = 0$ where therefore we have a null energy.
On the other hand, in quantum mechanics the uncertainty principle is established and it is possible to show that the minimum energy state of an harmonic oscillator is $E_0 = \frac{\omega\hbar}{2}$. So quantum fluctuations change the zero-point energy to a non zero value and, in presence of gravity, the addition of a constant to the potential is not negligible.
In quantum field theory, we can decompose a field in an infinite number of harmonic oscillators in Fourier space, each with a frequency $\omega = \sqrt{k^2 + m^2}$ where m is the mass associated to the field and k the module of the wave number of the mode. So we should add all the modes contribution to find the total vacuum energy density. To avoid an infinite result, an ultraviolet cutoff k_{max} up to which we trust our theory is chosen:

$$\rho_{vac} = \int_0^{k_{max}} \frac{d^3k}{(2\pi)^3} \frac{\hbar\sqrt{k^2 + m^2}}{2}, \tag{1.58}$$

the integral is dominated by high k modes ($k >> m$):

$$\rho_{vac} = \int_0^{k_{max}} \frac{4\pi\hbar k^3 dk}{2(2\pi)^3} \sim \hbar k_{max}^4, \tag{1.59}$$

where in the last passage we neglect the numerical factors. If we trust our quantum field theory up to the Planck mass energy scale, we find (in natural units):

$$\rho_{vac} \sim (M_{pl})^4 \sim (10^{18} GeV)^4, \tag{1.60}$$

which is 120 order of magnitude more than the observed value of the cosmological constant. This is the famous "cosmological constant problem", as we will see in the Chapter 3.

Chapter 2

Cosmological perturbations

Until now, we have treated our Universe as perfectly homogeneous and isotropic; this is not completely the case, indeed, to explain both the formation and evolution of large scale structures and the CMB power spectra, we have to introduce inhomogeneities.
For relatively small perturbations, we can exploit perturbation theory. In particular, Newtonian gravity is still a good approximation of General Relativity on scales well inside the Hubble radius and for non relativistic matter. On the other hand, when these conditions do not hold, we can expand the Einstein equations order-by-order in perturbations. In full generality, we will directly discuss perturbation theory within General Relativity. For more details about the Newtonian approach, see [9].

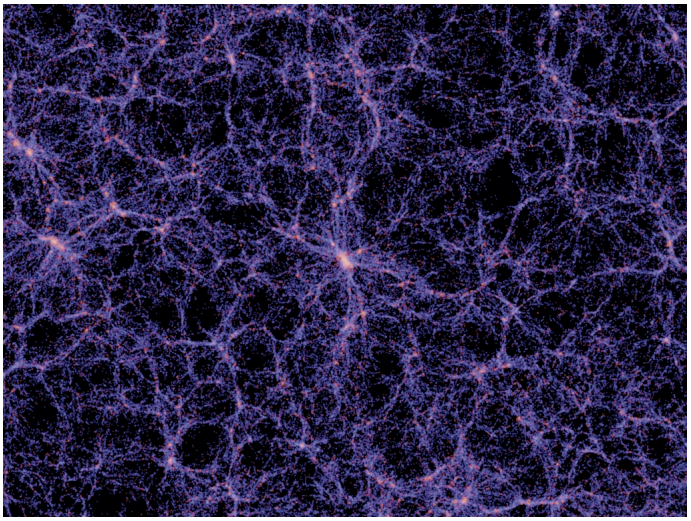

Figure 2.1: The galaxy distribution in the Millennium Simulation Project on very large scales (the width of the figure is $\sim 400 Mpc/h$). Taken from [55].

2.1 Relativistic perturbation theory

Einstein equations link together fields and the background geometry therefore, in the frame of perturbation theory, this implies not only the need of considering perturbations of the fields involved, but also of the background metric.

2.1.1 The gauge issue

Before perturbing Einstein equations, we need to address an important subtlety: General Relativity is invariant under diffeomorphisms, meaning that two solutions of Einstein's equations, related by

a diffeomorphism, are equivalent; this translates to the fact that perturbations are not uniquely defined but they depend on the so called gauge choice. Indeed, considering a generic tensor T, the perturbation of the physical quantity represented by the tensor is:

$$\delta T = T - T_0, \tag{2.1}$$

where T_0 is the tensor in the unperturbed background while T is the same tensor in the physical, and thus perturbed, spacetime. To quantify the difference of the tensor on the two space-time we need to provide a map that realises a one-to-one correspondence between points on the two spacetime; this map is called gauge choice. This choice is arbitrary and it will affect the value of the tensor perturbations. A gauge transformation corresponds to keep fixed the coordinates on the background spacetime and to vary the corresponding points on the physical one.
As we will see, two solutions are available to solve the gauge issue: to fix the gauge and and keep track of all the perturbations defined in that gauge, or to work with gauge-invariant quantities, that is to define particular combinations of the perturbations themselves which do not transform under gauge transformations.

By varying the one-to-one map between physical and background spacetime, the gauge transformations entail the necessity of comparing tensors at different points in the background space-time. However, the tensors comparisons is meaningful only if we evaluate them at the same spacetime point. Therefore, following [56], to compare a tensor field at point P and Q, we need to provide a transport law from P to Q. As we will see, this gives us two tensors at the same point P, one the transported of the other, that can be directly compared. To build the transport law, we can consider a manifold $\mathscr{M}$ covered by a coordinate system x^μ and we suppose to have on it a vector field defined as $\xi^\mu = \frac{dx^\mu}{d\lambda}$, where λ is the parameter of the congruence of curves generated by ξ. We take the point P to lie on one of this curves at $\lambda = 0$. Then a point Q, at a parametric distance λ from P, will be, at first order in λ:

$$\tilde{x}^\mu(\lambda) = x^\mu + \lambda\xi^\mu + ..., \tag{2.2}$$

where $\tilde{x}^\mu$ corresponds to the point Q and x^μ to P, in the same coordinate system. This is usually called "active coordinate transformations". It is now possible to introduce a new coordinate system y^μ on $\mathscr{M}$, defined as:

$$\begin{aligned} y^\mu(Q) := x^\mu(P) &= x^\mu(Q) - \lambda\xi^\mu(x(P)) + ... \\ &\simeq x^\mu(Q) - \lambda\xi^\mu(x(Q)) + ..., \end{aligned} \tag{2.3}$$

where in the second line we have substituted (2.2) and expanded keeping always the first order in λ. This is instead the so called "passive coordinate transformation", that consists in the relabelling of the point's name.
We can now exploit them to find a transport law to compare tensor fields. We can indeed consider a tensor field Z, with components Z^μ in the x^μ coordinates system. Similarly as before, we can then define another tensor field $\tilde{Z}$, with component $\tilde{Z}^\mu$ in the x^μ coordinates system, such that:

$$\tilde{Z}^\mu(x(P)) = Z'^\mu(y(Q)), \tag{2.4}$$

thus, such that, the new field in the x^μ coordinates at point P, is equal to the old field in a new coordinate system y^μ in the point Q. Applying an ordinary, passive coordinates transformation, we obtain:

$$\begin{aligned} \tilde{Z}^\mu(x(P)) = Z'^\mu(y(Q)) &= \frac{\partial y^\mu}{\partial x^\nu} Z^\nu(x(Q)) \\ &= \left(\delta^\mu_\nu - \lambda\frac{\partial \xi^\mu}{\partial x^\nu}\right) Z^\nu(x(P) + \lambda\xi(x(P))), \end{aligned} \tag{2.5}$$

where we have exploited (2.3) to compute the jacobian of the change of coordinate and to rewrite Z in the same point P as $\tilde{Z}$. Finally, expanding about the point $x(P)$, up to the first order in λ:

$$\tilde{Z}^\mu(x(P)) = Z^\mu(x(P)) + \lambda\mathscr{L}_\xi Z^\mu(x(P)) + o(\lambda^2), \tag{2.6}$$

where $\mathscr{L}_\xi Z^\mu(x(P))$ is the Lie derivative of Z^μ in the point $x(P)$ along the vector field ξ^μ:

$$\mathscr{L}_\xi Z^\mu = Z^\mu_{,\nu}\xi^\nu - \xi^\mu_{,\nu} Z^\nu, \tag{2.7}$$

where $_{,\mu} = \partial_\mu$. Thus, the Lie derivative allows to compare a field and its transformed at the same point. This is exactly what is needed, when we want to see how a tensor field, and in particular its perturbation with respect to the background space-time, changes under a gauge transformation:

$$\delta\tilde{T} = \delta T + \lambda \mathcal{L}_\xi T_0, \tag{2.8}$$

where $\delta\tilde{T}$ and δT are the differences between the tensor T_0 in the background spacetime and, respectively, the tensors $\tilde{T}$ and T in the physical spacetime connected to T_0 with two different one-to-one maps, i.e. two different gauge transformations.
In general, the Lie derivative of tensor with rank (p,q) is a new tensor with the same rank. For example, we have [56]:

- for a scalar: $\mathcal{L}_\xi S = S_{,\lambda}\xi^\lambda$,
- for a covariant vector: $\mathcal{L}_\xi Z_\mu = Z_{\mu,\lambda}\xi^\lambda + Z_\lambda \xi^\lambda_{,\mu}$,
- (0,2)-tensor: $\mathcal{L}_\xi T_{\mu\nu} = T_{\mu\nu,\lambda}\xi^\lambda + \xi^\lambda + \xi^\lambda_{,\mu} T_{\lambda\nu} + \xi^\lambda_{,\nu} T_{\mu\lambda}$.

2.1.2 $g_{\mu\nu}$ and $T_{\mu\nu}$ perturbations

Considering as the background space-time the FLRW metric, rewritten using the conformal time $d\tau = \frac{dt}{a(t)}$, we can now introduce the perturbations of the metric tensor, which are conventionally written as [56]:

$$\begin{aligned} g_{00} &= -a^2(\tau)\left[1 + 2\sum_{r=1}^{\infty}\frac{\Psi^{(r)}}{r!}\right], \\ g_{i0} = g_{0i} &= a^2(\tau)\sum_{r=1}^{\infty}\frac{\omega_i^{(r)}}{r!}, \\ g_{ij} &= a^2(\tau)\left[\left(1 - 2\sum_{r=1}^{\infty}\frac{\Phi^{(r)}}{r!}\right)\delta_{ij} + \sum_{r=1}^{\infty}\frac{\chi_{ij}^{(r)}}{r!}\right], \end{aligned} \tag{2.9}$$

where the index r is the order of perturbations that we want to consider and $\chi_i^{i\,(r)} = 0$. As we have already done for the Lie derivative, in this work we will stop at first order in perturbation.
It is then possible to decompose the metric perturbations with respect to their behaviour under local rotation of the spatial coordinates on hypersurfaces of constant time [57]. According to this, we have:

- scalar perturbations
- vector perturbations
- tensor perturbations

Indeed for example, the shift functions ω_i can be decomposed according to the Helmholtz theorem as:

$$\omega_i = \partial_i \omega^{\parallel} + \omega_i^{\perp}, \tag{2.10}$$

where $\omega_i^{\perp}$ is a divergence-free vector, i.e. $\partial^i \omega_i^{\perp} = 0$, and $\omega^{\parallel}$ is a proper scalar function. Similarly the traceless part of the metric can be decomposed as:

$$\chi_{ij} = D_{ij}\chi^{\parallel} + \partial_i \chi_j^{\perp} + \partial_j \chi_i^{\perp} + \chi_{ij}^{T}, \tag{2.11}$$

with $D_{ij} = \partial_i\partial_j - \frac{1}{3}\delta_{ij}\nabla^2$, $\chi^{\parallel}$ a proper scalar function, $\chi_i^{\perp}$ a divergence-free vector and χ_{ij}^{T} a traceless, transverse and symmetric tensor. Therefore, this decomposition allows to identify the three different kinds of perturbations that, at linear order, evolve independently and so it is possible to analyze them separately.

Clearly, due to the structure of Einstein equations, metric perturbations will directly translate in perturbations of the stress-energy tensor, which in turns will bring a back-reaction to the metric

and so on. It is therefore necessary to see how we can perturb also the right hand side of Einstein equations.
Considering the stress-energy tensor of a perfect fluid, it is possible to rewrite it in a more general version, adding the anisotropic stress-energy tensor:

$$T_{\mu\nu} = \rho u_\mu u_\nu + P h_{\mu\nu} + \pi_{\mu\nu}, \tag{2.12}$$

where indeed $\pi_{\mu\nu}$ is the anisotropic stress-energy tensor and $h_{\mu\nu} = g_{\mu\nu} + u_\mu u_\nu$. Thus, we need to perturb the quantities in (2.12):

- The energy density:

$$\rho(\vec{x}, \tau) = \rho^{(0)}(\tau) + \sum_{r=1}^{\infty} \frac{\delta\rho^{(r)}(\vec{x}, \tau)}{r!}, \tag{2.13}$$

  where $\rho^{(0)}$ indicates the energy density in the FLRW background.

- The pressure :

$$P(\vec{x}, \tau) = P^{(0)}(\tau) + \sum_{r=1}^{\infty} \frac{\delta P^{(r)}(\vec{x}, \tau)}{r!}. \tag{2.14}$$

  Being $P = P(\rho, S)$, where S is the entropy, in general it is true:

$$\delta P = \left(\frac{\partial P}{\partial \rho}\right)_S \delta\rho + \left(\frac{\partial P}{\partial S}\right)_\rho \delta S = c_s^2 \delta\rho + \delta P_{non-adiab}, \tag{2.15}$$

  where c_s^2 is the adiabatic speed of sound of the perturbation of the fluid and $\delta P_{non-adiab}$ is the non adiabatic perturbation.

- The four-velocity of the fluid:

$$u^\mu = \frac{1}{a}\left(\delta_0^\mu + \sum_{r=1}^{\infty} \frac{v^{\mu\ (r)}}{r!}\right), \tag{2.16}$$

  where v^i is called the peculiar velocity of the fluid.

As we said, these perturbations are not uniquely defined but instead they transform under a gauge transformation as in (2.8). To circumvent the problem, it is possible to fix the gauge, that means to choose the vector field ξ^μ along with we compute the Lie derivative of the perturbation. Indeed, according to Helmholtz theorem, we can decompose ξ^μ as:

$$\xi^\mu = (\xi^0, \xi^i) = (\alpha, \partial^i\beta + d^i), \tag{2.17}$$

thus to fix the gauge, we need to fix the two scalar functions α and β and the divergence-free vector d^i.
In this work, we will explore better the Poisson gauge and the synchronous gauge, the latter is used to treat perturbations in the Effective Field Theory approach to dark energy, as we will see better in Chapter 5.

Poisson gauge

The Poisson gauge is obtained by imposing the following conditions:

$$\omega^{\parallel} = 0, \qquad \chi^{\parallel} = 0, \qquad \chi_i^{\perp} = 0. \tag{2.18}$$

In this gauge, it is possible to find an analog to the Poisson formula for the Ψ and Φ perturbations. A particular subclass of the Poisson gauge is obtained by neglecting vector and tensor perturbations. This dynamical choice leads to the so called Newtonian or longitudinal gauge, which is a simple gauge with perturbed line element [62]:

$$ds^2 = a(\tau)(-(1+2\Psi)d\tau^2 + (1-2\Phi)\delta_{ij}dx^i dx^j). \tag{2.19}$$

An advantage of working in the Newtonian gauge is the fact that the metric tensor remains diagonal and computations are easier.

Synchronous gauge

The synchronous gauge consists in choosing $\Psi = 0$. This means that the component g_{00} of the metric tensor remains unchanged. Clearly, this does not fix completely the gauge, and, indeed, we also choose to set $\omega_i^{\perp} = \omega^{\parallel} = 0$ which leaves unchanged also the component g_{0i} of the metric tensor. Thus the perturbed metric element in the synchronous gauge is usually written as [62]:

$$ds^2 = a(\tau)(-d\tau^2 + (\delta_{ij} + h_{ij})dx^i dx^j), \tag{2.20}$$

where in $h_{ij} = \frac{h}{3}\delta_{ij} + D_{ij}h^{\parallel} + \partial_i h_j^{\perp} + \partial_j h_i^{\perp} + h_{ij}^T$ are contained all the perturbations of g_{ij} metric component.

Gauge-invariant quantities

As we said, a different approach to the gauge problem can be to work with the so called gauge-invariant quantities, which are quantities built in such a way that they do not transform under a gauge transformation. An example of scalar gauge-invariant quantities are the Bardeen potentials, that are defined as:

$$\begin{cases} \Psi_A = \Psi + (\omega^{\parallel})' + \mathcal{H}\omega^{\parallel} - \frac{1}{2}((\chi^{\parallel})'' + \mathcal{H}(\chi^{\parallel})') \\ \Phi_H = -\Phi - \frac{1}{6}\nabla^2\chi^{\parallel} + \mathcal{H}\omega^{\parallel} - \frac{1}{2}(\chi^{\parallel})'' \end{cases} \tag{2.21}$$

where $\mathcal{H} = \frac{1}{a}\frac{da}{d\tau}$. It is straightforward to check that the Bardeen potentials are invariant under (2.8). Then, it is possible to rewrite the perturbed Einstein equation using (2.21) remaining therefore in a gauge-invariant framework. More details of the calculations are in [57].

2.1.3 Perturbed Einstein equations

As we said, scalar, vector and tensor perturbations evolve independently at linear order. Therefore, it is easier to perturb Einstein equation separately for each kind of perturbations. In this work, we will focus on the evolution of scalar perturbation. Indeed, at linear order and for scalar perturbation, the perturbed metric can be written as:

$$g_{\mu\nu} = g_{\mu\nu}^{(0)} + \delta g_{\mu\nu} = a^2(\tau)\begin{pmatrix} -(1+2\Psi) & \partial_i\omega^{\parallel} \\ \partial_i\omega^{\parallel} & (1-2\Phi)\delta_{ij} + D_{ij}\chi^{\parallel} \end{pmatrix}, \tag{2.22}$$

where the apex (0) denotes the unperturbed quantity. The perturbed Einstein equation will be:

$$G_{\mu\nu}^{(0)} + \delta G_{\mu\nu} = 8\pi G(T_{\mu\nu}^{(0)} + \delta T_{\mu\nu}), \tag{2.23}$$

where the Einstein tensor is $G_{\mu\nu} = R_{\mu\nu} - \frac{1}{2}g_{\mu\nu}R$. To obtain the perturbed equations, we need to compute all the perturbed tensor necessary to obtain (2.23). These calculations are quite lengthy, for more details see Appendix A. For completeness, we write here the results which are the equations of motion for the scalar perturbations. From the $(0-0)$ component:

$$3\left(\frac{a'}{a}\right)\left(\hat{\Phi}' + \frac{a'}{a}\Psi\right) - \nabla^2\left(\hat{\Phi} + \frac{a'}{a}\sigma\right) = -4\pi G a^2\delta\rho, \tag{2.24}$$

with the shear perturbation is:

$$\sigma = \frac{1}{2}(\chi^{\parallel})' - \omega^{\parallel} \tag{2.25}$$

and

$$\hat{\Phi} = \Phi + \frac{1}{6}\nabla^2\chi^{\parallel}. \tag{2.26}$$

The $(0-i)$ first-order equation is:

$$\hat{\Phi}' + \frac{a'}{a}\Psi = -4\pi G a^2(\rho^{(0)} + P^{(0)})(v^{\parallel} + \omega^{\parallel}). \tag{2.27}$$

Clearly, both (2.24) and (2.27) are not dynamical equations and they are respectively referred to as energy and momentum constraint.
Then, defining the perturbed spatial stress-energy tensor as:

$$T^i_j = P^{(0)}((1+\Pi_L)\delta^i_j + \Pi^i_{jT}), \tag{2.28}$$

where $\Pi_L = \frac{\delta P}{P^{(0)}}$ and Π^i_{jT} is the traceless part related to the anisotropic stress-energy tensor $\pi_{\mu\nu}$.
It is possible to find from the trace part of the spatial perturbed Einstein equations:

$$\hat{\Phi}'' + 2\frac{a'}{a}\hat{\Phi}' + \frac{a'}{a}\Psi' + \left(2\left(\frac{a'}{a}\right)' + \left(\frac{a'}{a}\right)^2\right)\Psi = 4\pi G a^2(\Pi_L + \frac{2}{3}\nabla^2\Pi_T)P^{(0)}, \tag{2.29}$$

while from the traceless part:

$$\sigma' + 2\left(\frac{a'}{a}\right)\sigma + \hat{\Phi} - \Psi = 8\pi G a^2 \Pi_T P^{(0)}. \tag{2.30}$$

In particular, it is interesting to rewrite the last equation in the Newtonian gauge where $\sigma = 0$ and $\hat{\Phi} = \Phi$:

$$\Phi - \Psi = 8\pi G a^2 \Pi_T P^{(0)}, \tag{2.31}$$

which, in the case of $\Pi_T = 0$, gives $\Phi = \Psi$. This is a typical ΛCDM prediction that is not always verified in theories that goes beyond ΛCDM.

2.2 Observables of interest

Einstein equation describes the interactions of the fluids perturbations with the metric one. This is not enough, indeed, during the Universe history, the fluid components are coupled to each other: for example, photons interacts both with gravity and with free electrons through Compton scattering. Electrons, in turn, strongly interacts with protons and both of them interact with gravity. Neutrinos and dark matter affect and are affected by gravity. To systematically deal with all these couplings, the Boltzmann equation for each species of the Universe needs also to be solved. This is quite a challenging task that, as we will see, can be achieved exploiting the computational power of suitable codes, known as Einstein-Boltzmann solvers.
Once achieved this task, theoretical prediction and observations can be compared through the tool of power spectrum. From the theory point of view, the power spectrum is, non trivially, computed solving the Einstein-Boltzmann equations. Indeed, the ΛCDM model provides a complete explanation for the production and evolution of photons anisotropies and matter inhomogeneities. Thus, power spectra are a crucial tool to validate or rule out cosmological models. Here we will briefly see some of these observables that, later in this work, we will compute with the cosmological code CAMB [65].

2.2.1 About Boltzmann equation

Here, we briefly mention the basic notions concerning the Boltzmann equation, which can be written in the general compact form:

$$\mathbb{L}[f(x^\mu, p^\mu)] = \mathbb{C}[f(x^\mu, p^\mu)], \tag{2.32}$$

where $\mathbb{L}$ and $\mathbb{C}$ are respectively the Liouville and the Collision operators. f is the phase space distribution function of a certain species of particles which depends on the point x^μ and on the momentum vector $p^\mu = \frac{dx^\mu}{d\lambda}$, where λ parametrized the particle path.
The Liouville operator is the total derivative along the trajectory of a particle in the phase space. In the relativistic case, the operator takes into account also the role of gravity; its expression is:

$$\mathbb{L}[f(x^\mu, p^\mu)] = \frac{dx^\mu}{d\lambda}\frac{\partial f}{\partial x^\mu} + \frac{dp^\mu}{d\lambda}\frac{\partial f}{\partial p^\mu} = \left(p^\mu \frac{\partial}{\partial x^\mu} - \Gamma^\mu_{\rho\sigma} p^\rho p^\sigma \frac{\partial}{\partial p^\mu}\right) f, \tag{2.33}$$

it is possible to evaluate this expression on a FLRW spacetime, where the phase space distribution function can depend only from the time and the modulus of the 4-momentum in order to respect the requirements of homogeneity and isotropy. Indeed, it is straightforward to show that in this framework the Boltzmann equation takes the form:

$$E\frac{\partial f}{\partial t} - Hp^2\frac{\partial f}{\partial E} = \mathbb{C}[f(t,p)], \tag{2.34}$$

where $p^2 = g_{ij}p^i p^j$. Exploiting the definition of the number density:

$$n(t) = \frac{g}{(2\pi)^3}\int d^3p f(t,p) \tag{2.35}$$

and after some algebras [63], (2.34) can be easily rewritten as:

$$\dot{n}(t) + 3Hn(t) = \frac{g}{(2\pi)^3}\int \frac{d^3p}{E}\mathbb{C}[f(t,p)], \tag{2.36}$$

where it is immediately clear that, in absence of collisions i.e. $\mathbb{C} = 0$, the number density goes as $n \propto a^{-3}$, thus it is only suppressed by the expansion of the Universe. The term on the right hand side can be better understood considering a scattering process of the kind $1+2 \longleftrightarrow 3+4$. Indeed, focusing on the evolution of the particle of specie 1, the right hand side of equation (2.36) can be expressed as:

$$\frac{g_1}{(2\pi)^3}\int \frac{d^3p_1}{E_1}\mathbb{C}[f(t,p)] = \int d\Pi_1 d\Pi_2 d\Pi_3 d\Pi_4 (2\pi)^4\delta^{(4)}(p_1+p_2-p_3-p_4)$$
$$[|M_{3+4\to1+2}|^2 f_3 f_4(1\pm f_1)(1\pm f_2) - |M_{1+2\to3+4}|^2 f_1 f_2(1\pm f_3)(1\pm f_4)], \tag{2.37}$$

where $d\Pi_i = \frac{g_i d^3p_i}{(2\pi)^3 2E_i}$, $|M_{3+4\to1+2}|$ and $|M_{1+2\to3+4}|$ are the amplitudes of the processes that create and destroy the particle 1. The factors $(1\pm f_i)$ are the so called Fermi blocking term (-) and Bose enhancement factor (+) that describes the tendency of production of the particle i.

As we have already underlined the FLRW is not our physical Universe but only its background metric, in full generality the Bolzmann equation needs to be solved in a perturbed Universe such as the one defined in (2.9). Indeed, for example, choosing to work in the Newtonian gauge (2.19) and repeating the computations for this metric, it is possible to separate the unperturbed Bolzmann equation from the first-order one which links together the metric perturbations to the perturbations of the phase space distribution of a certain species.
For example, considering the photon distribution function, it is possible to expand it around the Bose-Einstein distribution function which corresponds to the zero order approximation. This leads to consider the function [63]:

$$f(\vec{x},p,\hat{p},t) = \left[exp\left(\frac{p}{T(t)(1+\Theta(\vec{x},\hat{p},t))}\right) - 1\right]^{-1}, \tag{2.38}$$

which is indeed the usual Bose-Einstein distribution function where we added the term $\Theta = \frac{\delta T}{T}$ that describes temperature perturbations that depend on the position $\vec{x}$ and on the direction of motion $\hat{p}$ of the particle, thus breaking the homogeneity and isotropy of the FLRW Universe. As usual, for a small perturbations Θ, the photon distribution function can be expanded around the Bose-Einstein function $f^{(0)}$ as:

$$f \simeq f^{(0)} - p\frac{\partial f^{(0)}}{\partial p}\Theta, \tag{2.39}$$

this is the very first step to find the equation that describes the photon distribution perturbation; as we said indeed the procedure consists in repeating the computation we have summarized for the FLRW metric in a perturbed metric and accounting for the interactions between species. In the case of photons the collision term is dominated by the contribution of the Compton scattering between photons and free electrons. It is worth to highlight that a useful decomposition of the

temperature perturbations is realized defining the the lth multipole moment of the temperature field as:

$$\Theta_l = \frac{1}{(-i)^l}\int_{-1}^{1}\frac{d\mu}{2}P_l(\mu)\Theta(\mu), \tag{2.40}$$

where $\mu = \frac{\vec{k}\cdot\hat{p}}{k}$, it is the cosine of the angle between the wavenumber $\vec{k}$ of the temperature perturbations and the photon direction of propagation $\hat{p}$. P_l is the Legendre polynomials of multipole l. As a consequence of the structures of the Legendre polynomials, the higher moments describe the small scale structure of the temperature field that can now be expressed as a whole hierarchy of moments $\Theta_l(\vec{x},t)$.
Similar computations need to be done for all the other fluids in the Universe, such as baryons, dark matter and neutrinos. The result is a set of Boltzmann equations involving the perturbed quantities of the distributions functions and the metric perturbations. Together with the perturbed Einstein equations that we have already presented in the previous section, they constitute the so called Einstein-Boltzmann equations. The initial conditions of this equations need to be search in the inflationary paradigm when the seeds of all the perturbations were established from quantum fluctuations of the inflaton field.
Solving the Einstein-Boltzmann equations is quite a challenging task and nowadays there are many cosmological codes that perform such calculations. The ultimate goal is clearly to compare theory and observations. This is realized computing the power spectra of the perturbations today which are the most important cosmological observables.

2.2.2 Power spectra

To describe observables of interest in cosmology, such CMB temperature or polarization fluctuations and large-scale structure, the more appropriate tool is the power spectrum. We have already discuss about it in the case of CMB temperature anisotropies power spectrum; now we will present the topic from a more general point of view. Indeed, the power spectrum is a suitable tool to describe quantities such as the perturbations with respect to the mean density of galaxies or the mean CMB temperature through a stochastic field that is Gaussian distributed around zero. Its Fourier transform is:

$$\delta(\vec{x},t) = \frac{1}{(2\pi)^3}\int d^3k e^{i\vec{k}\cdot\vec{x}}\delta_k(t). \tag{2.41}$$

Then the most important statistic is the so called two-point correlation function:

$$\xi(\vec{r}) = \langle\delta(\vec{x}+\vec{r},t)\delta(\vec{x},t)\rangle, \tag{2.42}$$

where $\langle ...\rangle$ denotes an ensemble average, thus interpreting the observed field as one of the infinite possible realizations of a random process.

Then, the power spectrum is nothing else than the Fourier transform of the two-point correlation function. Indeed, the power spectrum definition is:

$$\langle\delta_k(t)\delta_{k'}(t)\rangle = (2\pi)^3 P(|\vec{k}|)\delta^{(3)}(\vec{k}+\vec{k}'). \tag{2.43}$$

This can be easily seen exploiting the power spectrum definition:

$$\begin{aligned}\langle\delta(\vec{x}+\vec{r},t)\delta(\vec{x},t)\rangle &= \frac{1}{(2\pi)^6}\int d^3k\int d^3k' e^{i\vec{k}\cdot\vec{x}+i\vec{k}'\cdot(\vec{x}+\vec{r})}\langle\delta_k(t)\delta_{k'}(t)\rangle \\ &= \frac{1}{(2\pi)^3}\int d^3k e^{i\vec{k}\cdot\vec{r}}P(|\vec{k}|).\end{aligned} \tag{2.44}$$

Finally, computing the variance as $\sigma^2 = \xi(0)$, we find:

$$\langle\delta^2(\vec{x},t)\rangle = \frac{1}{(2\pi)^3}\int d^3k P(|\vec{k}|) = \int\frac{dk}{k}\Delta(k), \tag{2.45}$$

where:

$$\Delta(k) = \frac{k^3}{2\pi^2}P(|\vec{k}|). \tag{2.46}$$

(2.46) is the adimensional power spectrum, often used in Cosmology.
It is worth to notice that, from an observational point of view, the power spectrum definition brings an obstacle: clearly, the ensemble average is experimentally not feasible because only one possible realization of the considered random process can be observed i.e. we have access only to our own observable Universe. Assuming to have statistical homogeneity and isotropy of the process, the issue can be solved by performing a volume average instead of an ensemble average, taking the $V \to \infty$ limit for the volume. A field that allows to do so, is said to be ergodic.

More on CMB power spectra

In Chapter 1 we have already introduced the Cosmic Microwave Background and its angular power spectrum. It is worth to highlight that, from a theoretical point of view, the CMB power spectrum can be uniquely recovered solving the Bolzmann-Einstein equations and choosing the cosmological model. In particular, it is possible to derive the solution for the Θ_l multipoles, defined in (2.40), at present time, that in Fourier space is [63]:

$$\begin{aligned}\Theta_l(k,\tau_0) \simeq &[\Theta_0(k,\tau_s)+\Psi(k,\tau_s)]j_l[k(\tau_0-\tau_s)] \\ &+3\Theta_1(k,\tau_s)\left(j_{l-1}[k(\tau_0-\tau_s)]-\frac{l(l+1)j_l[k(\tau_0-\tau_s)]}{k(\tau_0-\tau_s)}\right) \\ &+\int_0^{\tau_0} d\tau e^{-\tau_D}[\dot{\Psi}(k,\tau)+\dot{\Phi}(k,\tau)]j_l[k(\tau_0-\tau)],\end{aligned} \tag{2.47}$$

where τ_D is the photon optical depth that is small if the photons travel freely and very large when the mean free path of the photon is small. $j_l[k\tau]$ are the spherical Bessel functions that estimate the contribution to the anisotropy due to a plane wave of wavenumber k on a scale l^{-1}. The three addends on the different lines are respectively identified as the Sachs-Wolfe, the Doppler and the Integrated Sachs-Wolfe term. The first term requires to know the temperature monopole Θ_0 and the gravitational potential Ψ at recombination; this is due to the fact that, to reach us, photons at the surface of last scattering had to climb out potential wells that redshifted their frequency. The Doppler term, which required the temperature dipole at the surface of last scattering, accounts for anisotropies produced by the Doppler effect due to the relative velocity that we have with respect to the surface of last scattering. Finally the Integrated Sachs-Wolfe effect account for the time dependence of the gravitational potential and indeed, unlike the first two terms that describe only effects produced at the surface of last scattering, the last term takes into account all the photon history until us.
The angular temperature power spectrum of the CMB can be found expanding over spherical harmonics as already done in (1.39) and performing a Fourier transform to exploit the result of the Boltzmann equation. Exploiting (1.42), the angular power spectrum can be then expressed as [63]:

$$C_l = \frac{2}{\pi}\int_0^\infty dk k^2 P(k)\left|\frac{\Theta_l(k)}{\delta(k)}\right|^2, \tag{2.48}$$

where $\delta(k)$ is the matter overdensity and $P(k)$ the matter power spectrum that we will explore better in the next paragraph. Thus, computing the Θ_l from (2.47) and solving the Boltzmann equation for non-relativistic matter, the CMB temperature anisotropies spectrum can be predicted.

It is worth to notice that the temperature field is not the only observable provided by the CMB radiation. Indeed, in more recent years, it was found that the CMB photons are polarized at a level of 5% of the temperature anisotropies. An often used geometrical decomposition of the polarization field consists in splitting the polarization pattern into two parts called E- and B-modes. Being only a fraction of the amplitude of the temperature anisotropies, polarization anisotropies took longer to be detected. Nowadays, the Planck satellite realized an accurate CMB polarization map [60], and it measured polarization power spectrum of E-modes and cross power spectrum of temperature and E-modes. The B-modes are still undetected and they are particularly relevant because of their link to primordial gravitational waves produced during inflation.
The polarization is the consequence of scattering processes that took place directly at the surface

of last scattering thus it provide a complementary probe to uncover more properties of the Universe at early stages [64]-[65] .

CMB lensing power spectrum

We have already discussed about the basis of weak lensing and its role to provide dark energy evidences. Here, we will focus in particular on CMB photons lensing effect and its power spectrum. Indeed, CMB photons travel almost the entire Universe before we detect them, thus, both temperature and polarization power spectra are affected by gravitational lensing due to inhomogeneities of the Universe.
Several effects can be read from the CMB pattern: the dominant effect consists in a smooth of the acoustic peaks, followed by the changing of E-modes polarization into B-modes one. CMB lensing is described also by higher-order statistics such as by 4-point correlation function [58], that, nowadays, can be measured with high precision in observations, such as Planck ones [59]. Therefore, observations of the lensed sky allows us to gain a lot of information about large scale-structure and and the Universe geometry between us and the recombination epoch.
Theoretically, the lensing deflection angle is written as the gradient of a lensing potential $\alpha = \vec{\nabla}\psi(\hat{n})$, that in turn is defined as [61]:

$$\psi(\hat{n}) = -2\int_0^{r_*} dr\left(\frac{r_* - r}{r r_*}\right)\Psi_W(r\hat{n}), \tag{2.49}$$

where r_* is the comoving distance at the surface of last scattering and Ψ_W is the Weyl potential which probes the matter distribution. Indeed, in the Newtonian gauge, the Weyl potential reduce to a simple function of the scalar metric perturbation Ψ and Φ defined in (2.9).

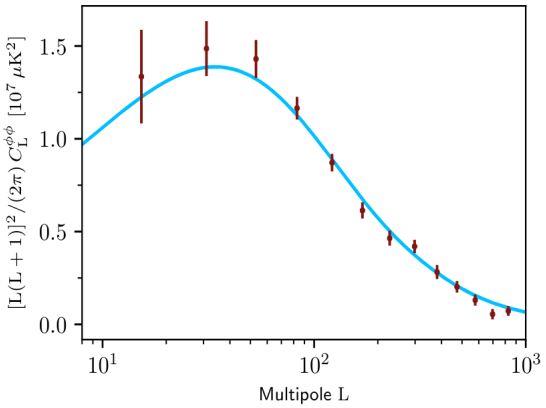

Figure 2.2: CMB lensing-potential power spectrum, measured by Planck. Taken from [60].

Matter power spectrum

The same physical mechanism that produced the CMB acoustic oscillations, that is the play between pressure and gravity, is also responsible for the non-relativistic matter power spectrum. Indeed, as we said, matter contracted in initially overdense regions starting the process of gravitational instability: as time evolves enough matter will fall in the region to form structures.
Knowing the evolution of the perturbations in the Universe history, it is therefore clear that it is possible to build a power spectrum that describes the distribution of the matter around us. Indeed, from the Fourier transform of the perturbed Einstein equations in Newtonian gauge, at late time (considering a Universe filled only by non-relativistic matter) and at large scales, we can write [63]:

$$\Phi = -\frac{4\pi G\rho_m a^2\delta}{k^2}, \tag{2.50}$$

where δ is the non-relativistic matter overdensity. Exploiting the definition of matter density parameter, we can extrapolate a useful expression for the matter overdensity:

$$\delta(\vec{k}, a) = -\frac{k^2 \Phi(\vec{k}, a) a}{(3/2)\Omega_m H_0^2}, \tag{2.51}$$

that allows to link the matter overdensity at late time and the gravitational potential Φ at each length scales. The gravitational potential at late time can be directly derived from its primordial expression, set during inflation, through the transfer function that describes its evolution during the horizon crossing and the radiation-matter equivalence and through the growth function which describes the scale independent evolution at late time. As a consequence, the matter power spectrum today can be recovered from the power spectrum of the gravitational potential during inflation [63].
On large scales, the power spectrum is almost proportional to the wavenumber k while on small scales it becomes a decreasing function of it, since small scale modes enter the horizon before matter-radiation equality and they are more suppressed. Furthermore, it is worth to notice that, below a certain scale, the linear perturbations theory is not valid anymore and non-linearities cannot be ignored.

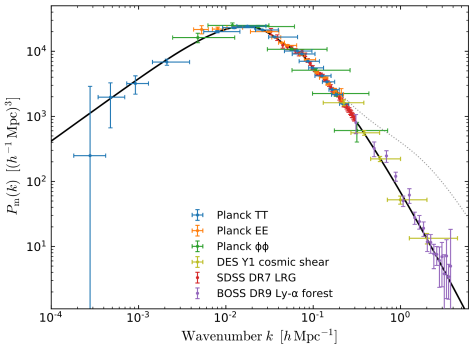

Figure 2.3: Linear-theory matter power spectrum (at z=0) from different cosmological probes. The black line is the ΛCDM prediction while the dotted line shows the impact of non-linearities. Taken from [60].

Chapter 3

Beyond ΛCDM

3.1 Cosmological constant issues

As we started to observe in Chapter 1, the ΛCDM model presents still some open issues such as the "cosmological constant problem" and the "coincidence problem". These may be seen as clues of the need of going beyond the model. However, from the theory point of view, this might be a challenging task since, as we saw, we already have strong observational constraints in favour of the ΛCDM model.

Cosmological constant problem

The "Cosmological constant problem" refers to the disagreement about the expected value of Λ from the theoretical and observational point of view.
Indeed, from observation, we expect the cosmological constant today to be of the order of H_0 (in natural units) [10]:

$$\Lambda^{(obs)} \sim H_0^2 \sim (2.13 \cdot h \cdot 10^{-42} GeV)^2, \tag{3.1}$$

that in terms of energy density means:

$$\rho_\Lambda^{(obs)} = \frac{\Lambda}{8\pi G} \sim 10^{-123} M_{pl}^4. \tag{3.2}$$

As we anticipated, if we compute the expected value of the cosmological constant as the vacuum energy and we decide to trust quantum field theory up to the Planck mass energy scale, we find a value about 120 times grater than the observed one.
A possible solution of the problem might consist in choosing, as cut off, some other energy scales known in particle physics. For example, a more conservative choice is to take $k_{max} \sim 1\, TeV$ that corresponds to the weak energy scales; up to these energies indeed, the Standard Model has been extremely well tested [20]. Plugging this value in (1.59), we can find the theoretical expectation:

$$\rho_{vac}^{(th)} \sim (1\ TeV)^4 \sim 10^{-60} M_{pl}^4, \tag{3.3}$$

which is still over than 60 order of magnitude different from the observed value.
It is straightforward to see that an appropriate scale for the cut-off would be $k_{max} \sim 10^{-3}\ eV$ which is not explainable in the framework of existing particle physics theory.

It is important to notice that some other contributions can come from the physics beyond the cut-off scale, meaning that the bare value of the cosmological constant Λ_0 is given by the sum of the energy density both below but also above, for example, the Planck mass scale [22]. It means that:

$$\Lambda_0 + M_{pl}^4 \sim \Lambda^{(obs)} \tag{3.4}$$

but this would require to adjust Λ_0 of almost 120 order of magnitude in order to restore the observed value. Therefore, Λ_0 should be fine-tuned with unimaginable precision. Given this, the "Cosmological constant problem" is also known as "Fine-tuning problem".

Coincidence problem

Another unlikely peculiarity of the dark energy is the fact that its density parameter today is of the same order of magnitude of the matter one. As we saw in Chapter 1 indeed, the Universe goes from being matter dominated to dark energy dominated only very recently in its history. From (1.19) we calculated that the matter-dark energy equivalence took place at $z_\Lambda \simeq 0.3$.

This is not a specific ΛCDM problem since the value of the density parameters today are constrained by observational data. Indeed, all alternative cosmological models are required to reproduce similar cosmological parameters at present, showing consequently a z_Λ really close to zero. What is required to solve the problem is a mechanism that naturally explains the coincidence.

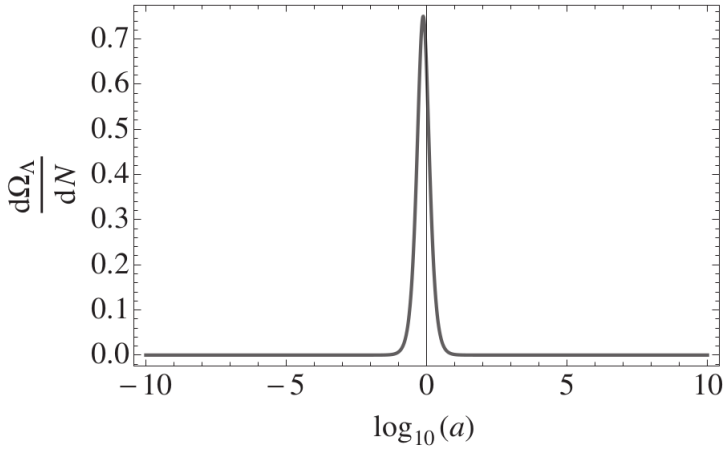

Figure 3.1: $\frac{d\Omega_\Lambda}{dN}$ as a function of $log_{10}(a)$ with $N = ln(a)$, assuming flat space with $\Omega_{DE} = 0.7$. Taken from [10].

3.1.1 The anthropic principle

A possible solution of the two questions above might be the argument provided by the anthropic principle. The anthropic principle was first formulated by Carter in 1973 and its basic idea is the requirement for physical theories to take into account the existence of life on Earth.
Indeed, according to Barrow and Tipler formulations, the values of physical and cosmological constants are not equally probable but they should assume values that allow the existence of places in the Universe where the carbon-based life can evolve; furthermore the Universe needs to be old enough for life to already exists [10].
A deeper study of this possibility was carried by Weinberg; in 1987 he was able to put the following bounds on the vacuum energy density [10]:

$$-10^{-123} M_{pl}^4 \lesssim \rho_\Lambda \lesssim 3 \cdot 10^{-121} M_{pl}^4, \tag{3.5}$$

where the upper bound is due to the requirement that the cosmological constant energy density did not dominate over the matter one for $z \gtrsim o(1)$ to allow the formation of large scale structure, while the lower bound prevents the cosmological constant to lead the collapse of the Universe if it became dominant before the present epoch.
Furthermore, Weinberg, explained that for this idea to make sense, it is necessary to allow multiple realizations of the Universe with different values of the cosmological constant. A nice argument that he carried in favour of his idea was an analogy with the radii of the planets in our solar system [43]. Indeed, Newton's theory of gravity failed to constrain these radii which were then explained in terms of historical accidents. The radius of the Earth can be constrained by an anthropic explanation: if it was not in the narrow range of distance from the sun to allow the existence of liquid water on the surface, then we would not be here. According to Weinberg, this would not be a satisfying explanation if the Earth was the only planet in the Universe. In such a case the

Earth's radius would be quite an amazing coincidence. The anthropic explanation works much better knowing that in our Universe there is a huge number of planets, each at a different radius from its star.
Similarly an anthropic explanation of the value of the cosmological constant is more plausible if its value varies among a different members of an ensemble constrained by the fact that it should be suitable for the evolution of intelligent life.
Recently, these anthropic ideas have been adopted in the context of String Theory; in this frame indeed, the possibility is to have meta-stable deSitter vacua, each with a different value of the cosmological constant [20]. The problems in this construction do not miss and, even if all the needed ingredients can be established, it may nevertheless be difficult to proof that the anthropic explanation is the correct one, since String Theory is not yet testable with observations.
Thus, having this possible path to address the cosmological constant problem, the theoretical landscape is anyhow in search of other possible explanations for the cosmic acceleration, as we will see in the next paragraphs.

3.2 Cosmological tensions

In addition to the issues linked to the cosmological constant, within the ΛCDM model some other unresolved observational puzzles are known and currently under investigation.
In fact, the standard model of Cosmology shows a discrepancy, usually dubbed as "tension", on the value of the Hubble constant measured with different probes. In particular, the tension resides in the measurements obtained with high-redshift, model-dependent experiments and local observations which make use of the cosmic distance ladder method. The former, provided by Planck 2018 data of anisotropies of the CMB, measures the value of $H_0 = 67.36 \pm 0.54\ km/s/Mpc$ [3], obtained assuming a flat ΛCDM Universe, while the latter returns a value of $H_0 = 73.5 \pm 1.4\ km/s/Mpc$ using Supernovae typeIa calibrated on Cepheid variable stars by the SH0ES collaboration [97]. The 4.2σ tension between these two measurements of the Hubble constant makes a statistical fluctuation an unlikely explanation.
Moreover, another controversial issue within the ΛCDM model results in the tension showed by the derived cosmological parameter:

$$S_8 = \sigma_8 \sqrt{\frac{\Omega_m}{0.3}}, \tag{3.6}$$

where σ_8 is defined as the amplitude of the linear matter power spectrum at scale of $8h^{-1}Mpc$. A tension within the ΛCDM model exists on the value of S_8 probed on small scales by Weak Lensing experiments and on large scale CMB measurements. In particular, the tension was fixed at 3.2σ level from the combination of KiDS dataset and DES 1 Year release in comparison to Planck 2018 data [98].
The root causes of both these tensions are still unknown and they are being investigated; the explanation can be that these inconsistencies are just a statistical fluke or that they are due to systematic errors in the experiments. Clearly, the most intriguing scenario would be that they are signals of new physics beyond the standard model of Cosmology, in this sense therefore they offer a good motivation in the quest of alternative cosmological models that go beyond ΛCDM.

3.3 Looking beyond ΛCDM

Although experimental data provide a great amount of evidence of the accelerating expansion of the Universe, this does not directly mean that the source of the expansion is a cosmological constant. Nowadays, the theoretical scenario is crowded of alternative theories to the cosmological constant, that, as seen above, presents still some unsolved issues.
Therefore, from now on we will assume the cosmological constant to be zero, or at least unable to account for the late accelerated expansion of the Universe, and we will explore which other possible source may be in our Universe. Obviously, this last statement should be explained in the framework of a new theory.

At this point, we have two main paths to follow: to postulate a new dynamical component, with the role of dark energy and its observed peculiarities, or to question about the theoretical background that describes how the fluids in the Universe interact with the underlying spacetime, that means to replace General Relativity with a Modified Gravity model. These two options are conceptually quite different: the former consists in predicting a still unobserved component of the Universe thanks to the consequences that we can already observe, while the latter, more drastic, changes the theory of gravity ruling our Universe. However, it is important to highlight that this division is not really fundamental within General Relativity: indeed, with a change of frame, it is possible to reabsorb in $T_{\mu\nu}$ all the gravity modifications that are conventionally operated to the left hand side of the Einstein's equation. On the other hand, within quantum field theory, the equivalence between the two classes of models is not so direct given that Dark Energy/Modified Gravity models can be distinguished by the different fields content.

As we will see with the Lovelock's theorem, Einstein theory of gravity is remarkably robust. In four dimensions, it is the only local theory of gravity having in its action just the degrees of freedom carried by the metric tensor and returning second-order equations of motion. Furthermore, Ostrogradsky theorem shows that a theory with higher than second-order equations of motion brings to an unstable system. As a consequence, the most common way to introduce new physics in the gravitational sector consists in introducing new degrees of freedom, such as Lorentz scalar fields. On the other side, a dynamical form of Dark Energy might also be a feasible solution: the cosmic acceleration indeed can be caused by the potential energy of a field. As in the inflationary paradigm, this scenario naturally leads to a slow-rolling cosmological scalar field.

Finally, it is worth to notice that, since General Relativity has been tested to high precision in the solar system and astrophysically, it is natural for Modified Gravity models to focus on the cosmological scales. Indeed, a good candidate Dark Energy/Modified Gravity (DE/MG) model should provide a so called screening mechanism, that suppresses deviations from General Relativity, allowing the new degrees of freedom to not manifest in local tests of gravity.

Lovelock's theorem

Going to the modified gravity field, it is important to know the limits that we have in the construction of new gravity models. Lovelock's Theorem, for example, puts stringent constraints on the theories that can be built from the metric tensor alone. Indeed, assuming to have only the gravitational field involved in the gravitational action:

$$S = \int d^4x \ \mathcal{L}(g_{\mu\nu}) \tag{3.7}$$

and being $E^{\mu\nu}$ the Euler-Lagrange equations of the considered theory:

$$E^{\mu\nu} = 0, \tag{3.8}$$

that can be obtained extrimising (3.7) with respect to the metric tensor.
The Lovelock's theorem states [19]:

The only possible second-order Euler-Lagrange expression obtainable in four dimensions from the scalar density Lagrangian (3.7) is:

$$E^{\mu\nu} = \alpha\sqrt{-g}\left[R^{\mu\nu} - \frac{1}{2}g^{\mu\nu}R\right] + \lambda\sqrt{-g}g^{\mu\nu}, \tag{3.9}$$

with α and λ constants, $R^{\mu\nu}$ the Ricci tensor and R the Ricci scalar.

This result, achieved by Lovelock in the 1971, was part of a wider work that consists in the generalization of Einstein General Relativity to higher dimensions, known as Lovelock Theory of Gravity. The crucial result that Lovelock found was that, in four dimensions and under the assumptions of his theorem, only Einstein equations, with or without a cosmological constant, are

allowed. This does not mean that we cannot further generalized the Einstein-Hilbert action to another one built from $g_{\mu\nu}$ and that restores the Einstein equations.
Indeed, in four-dimensions Lovelock found the most general scalar density Lagrangian:

$$\mathscr{L} = \alpha\sqrt{-g}R - 2\lambda\sqrt{-g} + \beta\epsilon^{\mu\nu\rho\lambda}R^{\alpha\beta}_{\ \ \mu\nu}R_{\alpha\beta\rho\lambda} + \gamma\sqrt{-g}(R^2 - 4R^{\mu}_{\ \nu}R^{\nu}_{\ \mu} + R^{\mu\nu}_{\ \ \rho\lambda}R^{\rho\lambda}_{\ \ \mu\nu}), \tag{3.10}$$

where β and γ are constants. It is possible to demonstrate that the third and fourth terms in (3.10) do not contribute to the final Euler-Lagrange equations of motion in four dimensions [19]. This means that we obtained again the Einstein equations.

The direct consequence of the Lovelock's theorem is that, to obtain a theory of gravity with equations of motion that differ from the Einstein ones, we need to renounce at some of the assumptions. So the possibilities for a modified gravity theory are:

- Admit additional fields in the gravitational action other than the metric tensor.
- Build a spacetime with more than four dimensions.
- Accept equations of motion with higher than second-order derivatives of the metric.
- Build a non-local theory.

Ostrogradsky's theorem

Ostrogradsky's theorem excludes the possibility of having a theory with equations of motion containing higher than second-order derivatives with respect to time. Indeed, considering a non-degenerate Lagrangian with higher orders derivatives we will see that the corresponding Hamiltonian is unbounded and therefore unstable. Following [20], we will show the demonstration in the context of classical mechanics of a single particle, knowing that the result can be generalized to field theory.
Considering the non-degenerate Lagrangian of the form:

$$\mathscr{L}(q; \dot{q}; ...; q^{(N)}), \tag{3.11}$$

where $q(t)$ is the particle position and its derivative with respect to time. Being the equation of motion of the form:

$$\sum_{i=0}^{N}\left(-\frac{d}{dt}\right)^{i}\frac{\partial\mathscr{L}}{\partial q^{(i)}} = 0, \tag{3.12}$$

it means that in the equation we will have terms up to $q^{(2N)}$, solvable with $2N$ initial conditions. Being a non-degenerate Lagrangian, we can, for example, express $q^{(2N)}$ as a function of all the other $2N-1$ coordinates.
Following Ostrogradsky, we can define the $(2N)$ canonical coordinates as:

$$Q_a = q^{(a-1)}, \quad P_a = \frac{\delta\mathscr{L}}{\delta q^{(a)}} = \sum_{i=a}^{N}\left(-\frac{d}{dt}\right)^{i-a}\frac{\partial\mathscr{L}}{\partial q^{(i)}}. \tag{3.13}$$

Exploiting the non degeneracy, we can solve for $q^{(N)}$ in terms of the coordinates Q_a and the N-th momentum P_N:

$$q^{(N)} = Q_{N+1} = F(Q_1, ..., Q_N, P_N). \tag{3.14}$$

Then, taking the Legendre transform, we can find the Hamiltonian of the system as:

$$\mathscr{H} = \sum_{a=1}^{N} P_a \cdot q^{(a)} - \mathscr{L} = P_1Q_2 + P_2Q_3 + ... + P_{N-1}Q_N + P_NF(Q_1, ..., Q_N, P_N) - \mathscr{L}(Q_1, ..., Q_N, F), \tag{3.15}$$

therefore the Hamiltonian is linear with respect to $P_1, .., P_{N-1}$, only P_N might show another dependence. It is straightforward to check that only for an usual Lagrangian of the form $\mathscr{L}(q, \dot{q})$, the corresponding Hamiltonian can be not pathological.

As a final comment, we should check that the Hamiltonian (3.15) expressed in terms of the Ostrogradsky coordinate corresponds to the ordinary Hamiltonian, that posses the properties of physical energy. To do so, we can consider the Hamilton equations for our system:

$$\dot{Q}_a = \frac{\partial \mathscr{H}}{\partial P_a}, \quad \dot{P}_a = -\frac{\partial \mathscr{H}}{\partial Q_a} \tag{3.16}$$

and we can apply them to Hamiltonian (3.15). Considering $a = 0, .., N-1$, the trivial result is:

$$\dot{Q}_a = Q_{a+1} \longrightarrow Q_{a+1} = q^{(a)}, \tag{3.17}$$

which is nothing more the definition in (3.13). Similarly, for $a = N$:

$$\dot{Q}_N = F + P_N \frac{\partial F}{\partial P_N} - \frac{\partial \mathscr{L}}{\partial F}\frac{\partial F}{\partial P_N} = F = Q_{N+1}, \tag{3.18}$$

where we have exploited the definition of P_N.
On the other hand, for $a = 2, ..., N$:

$$\dot{P}_a = -\left(P_{a-1} + P_N \frac{\partial F}{\partial Q_a} - \frac{\partial \mathscr{L}}{\partial Q_a} - \frac{\partial \mathscr{L}}{\partial F}\frac{\partial F}{\partial Q_a}\right) = -P_{a-1} + \frac{\partial \mathscr{L}}{\partial Q_a}, \tag{3.19}$$

where again we have used the P_N definition. It is easy to check that this result is the time derivative of the definition of P_a. Finally for $a = 1$:

$$\dot{P}_1 = -\left(P_N \frac{\partial F}{\partial Q_1} - \frac{\partial \mathscr{L}}{\partial F}\frac{\partial F}{\partial Q_1} - \frac{\partial \mathscr{L}}{\partial Q_1}\right) = \frac{\partial \mathscr{L}}{\partial Q_1} = \frac{\partial \mathscr{L}}{\partial q}, \tag{3.20}$$

that, applying the definition of P_1 and deriving it, becomes:

$$-\sum_{i=1}^{N}\left(-\frac{d}{dt}\right)^i \frac{\partial \mathscr{L}}{\partial q^{(i)}} = \frac{\partial \mathscr{L}}{\partial q}, \tag{3.21}$$

which is the Euler-Lagrange equation (3.12). Hence, it is clear that the Hamiltonian (3.15) generates the time evolution of the Ostrogradisky coordinates (3.13).

Summarizing, Ostrogradsky's result implies that the Hamiltonian of a non-degenerate higher derivative theory is unbounded below, and therefore it generates instability, known as Ostrogradsky instability.
It is worth to underline that an important postulate of the Ostrogradsky theorem is that the Lagrangian is non-degenerate. If this is not the case, a healthy second-order system can be obtained from a set of higher derivative equations of motion.

3.4 Dark energy/Modified gravity models

Nowadays, the theoretical landscape that tries to explain late time cosmic acceleration is very rich [19], as shown is Figure 3.2. The main alternatives to the ΛCDM model are the DE/MG vast classes of models, although the backreaction models might represent another possibility .
The backreaction class is a group of models that try to explain the cosmic acceleration through the gravitational backreaction of cosmological fluctuations. Indeed, as it is known, Einstein equation are second-order differential equations, so perturbations in the stress energy tensor contribute to the change in the underlying geometry, which, in turn, translates back to the stress energy tensor. It is possible to show that in the context of an inflationary background, an effective cosmological constant can be realized, leading to a Universe completely dominated by it in the asymptotic future [25]. In this work, we will not focus on these models.
On the other hand, in the frame of a dynamical dark energy model, the most simple choice might be to introduce a new scalar degree of freedom but extra vectors, tensors, or even higher rank fields might also be considered. In general, the new degrees of freedom can be either minimally coupled

or non-minimally coupled to gravity. Quintessence is the simplest example of a minimally coupled scalar field that represents a dynamical dark energy component.
Finally, in the modified gravity branch, some possibilities that have been explored are theories that break Lorentz-invariance, that give mass to the Graviton or higher dimensions scenario. Instead, remaining in the frame of a massless Graviton theory, scalar-tensor theories are the simplest kind of modified gravity models; they rely on a scalar field to extend Einstein gravity. Examples of this type are Brans-Dicke and $f(R)$ theories; in particular, the specific Generalized Brans-Dicke theory that we will explore in details in the Chapter 6.
Many more different models can be found in [19].

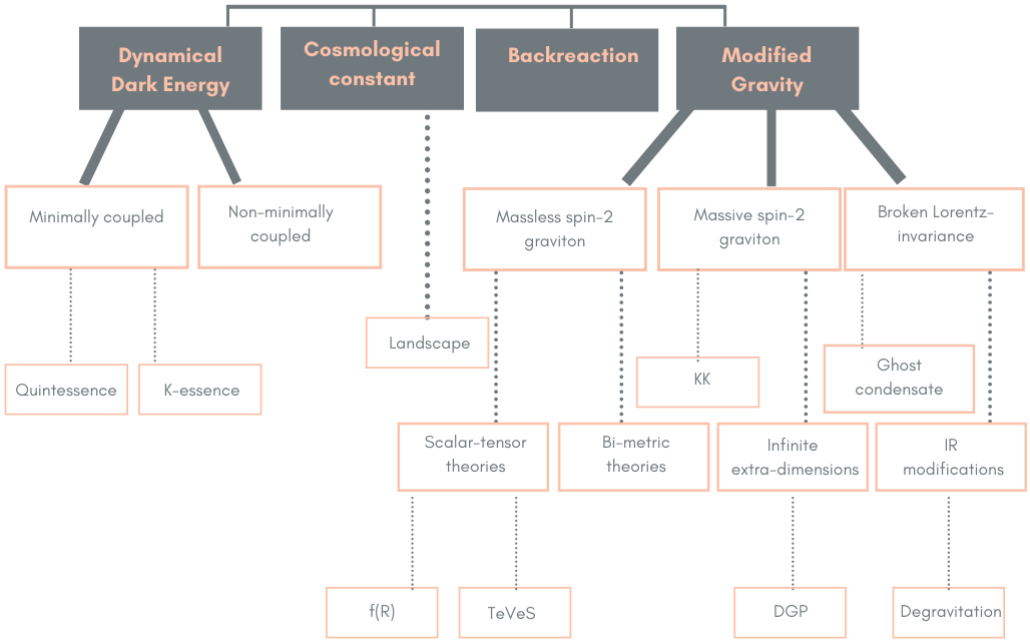

Figure 3.2: Theoretical Landscape of late time cosmic acceleration models.

3.4.1 Quintessence

As anticipated, Quintessence is probably one of the simplest dynamical dark energy model; the idea is really close to the one of the inflationary paradigm: it consists in adding to the action a canonical scalar field ϕ with a potential $V(\phi)$; ϕ interacts with the other fields through Einstein gravity. This means that the action of Quintessence is:

$$S = \int d^4x\sqrt{-g}\left(\frac{M_{pl}^2}{2}R + \mathcal{L}_\phi\right) + S_M, \tag{3.22}$$

where S_M is the part of the action that gathers all the other field contents. The canonical Lagrangian of the scalar field is:

$$\mathcal{L}_\phi = -\frac{1}{2}g^{\mu\nu}\partial_\mu\phi\partial_\nu\phi - V(\phi), \tag{3.23}$$

varying the action and exploiting the definition (1.4), we can obtain the stress-energy tensor for the field:

$$T^\phi_{\mu\nu} = \partial_\mu\phi\partial_\nu\phi + g_{\mu\nu}\left[-\frac{1}{2}g^{\alpha\beta}\partial_\alpha\phi\partial_\beta\phi - V(\phi)\right]. \tag{3.24}$$

Assuming the stress-energy tensor of the perfect fluid (1.2), it is easy to find the associated pressure and energy density:

$$\begin{aligned} T^0_0 &= -\frac{\dot{\phi}^2}{2} - V(\phi) = -\rho_\phi, \\ T^i_j &= \left[\frac{\dot{\phi}^2}{2} - V(\phi)\right]\delta^i_j = P_\phi \delta^i_j, \end{aligned} \tag{3.25}$$

where we have assumed a spatially constant field. It is now straightforward to find the equation of state parameter:

$$w_\phi = \frac{P_\phi}{\rho_\phi} = \frac{\dot{\phi}^2 - 2V(\phi)}{\dot{\phi}^2 + 2V(\phi)}, \tag{3.26}$$

to realize cosmic acceleration we need $w_\phi < -\frac{1}{3}$ thus the necessary requirement for the kinetic energy of the scalar field is to be sufficiently smaller compared to its potential. In other words, the potential needs to be sufficiently flat. In particular, to obtain $w_\phi \simeq -1$, as constrained by observation, we need to impose $\dot{\phi}^2 \ll V(\phi)$, which is equivalent to the slow-roll inflationary case. However, unlike inflation, we do not need to require the late time cosmic acceleration to end. In the inflationary theory, the accelerated expansion is realized if the following slow-roll parameters are small:

$$\begin{aligned} \epsilon &= \frac{M^2_{pl}}{16\pi}\left(\frac{1}{V}\frac{\partial V}{\partial \phi}\right)^2, \\ \eta_V &= \frac{M^2_{pl}}{8\pi}\frac{1}{V}\frac{\partial^2 V}{\partial \phi^2}, \end{aligned} \tag{3.27}$$

thus requiring $\epsilon \ll 1$ and $|\eta_V| \ll 1$. However, dark energy acceleration takes place while the density parameters of the other fluids are not completely negligible. Indeed, still nowadays the dark matter component has $\Omega^0_c \sim 0,27$ of the total energy density. Thus for dark energy cosmic acceleration, a better expression of the first slow-roll parameter is:

$$\epsilon = -\frac{\dot{H}}{H^2}. \tag{3.28}$$

The first definition of (3.27) can be found from (3.28) by deriving with respect to time the first Friedman equation and taking as the only source of energy density that of the Quintessence field. During inflation the energy density is dominated by the inflaton field and the two expression are equivalent. On the other hand for late time acceleration, we need to account for both dark energy and dark matter contributions [26].
Indeed, in full generality, the Friedman equations (1.6) for a flat Universe became:

$$\begin{aligned} H^2 &= \frac{8\pi G}{3}\left(\rho_M + \rho_r + \frac{\dot{\phi}^2}{2} + V(\phi)\right), \\ \frac{\ddot{a}}{a} &= -\frac{4\pi G}{3}(\rho_M + \rho_r + 3P_M + 3P_r + 2(\dot{\phi}^2 - V(\phi))), \end{aligned} \tag{3.29}$$

supposing to have a Universe filled by matter, radiation and the Quintessence scalar field. Thus for example, during the matter domination epoch we need that the matter density dominates over that of Quintessence: $\rho_M \gg \rho_\phi$. Similarly, during the radiation dominated epoch, the condition $\rho_r \gg \rho_\phi$ should be established. To do so for example, it is possible to require that ρ_ϕ tracks the evolution of ρ_M so that the dark energy manifests only at late time. Indeed, tracker solutions can bring to the scenario in which the Quintessence energy density approaches a fixed fraction of that of the other fluids, almost regardless to the initial conditions. This is also seen as a possible explanation of the cosmological constant coincidence problem. The tracking behaviour can be realized by the form of the potential $V(\phi)$ [10].
Furthermore, the equation of motion of the field can be obtained by varying the action with respect to the field:

$$\Box\phi = \frac{\partial V(\phi)}{\partial \phi}, \tag{3.30}$$

which is the usual Klein-Gordon equation for the scalar field. In a FLRW metric and again, considering a spatially constant field:

$$\ddot{\phi} + 3H\dot{\phi} = -V_{,\phi} \tag{3.31}$$

where $V_{,\phi} = \frac{\partial V(\phi)}{\partial \phi}$.
Two famous and well studied potentials for the Quintessence scalar field are [5]:

- Inverse power law potential:
$$V(\phi) = M^4 \left(\frac{\phi}{M_{pl}} \right)^{-n}. \tag{3.32}$$
- Exponential potential:
$$V(\phi) = M^4 exp\left(-\alpha \frac{\phi}{M_{pl}} \right), \tag{3.33}$$

where M is a mass scale and α a dimensionless parameter. The former potential does not have a minimum so the field rolls down the potential to infinity. They are both interesting because they can display the already mentioned tracker solutions, promising to solve the coincidence problem. On the other hand, the fine-tuning problem is not easily solved: to explain the tiny observed energy scale that accounts for the late time cosmic acceleration, the scalar potential and in particular its free parameters should have to be fine-tuned too. Indeed, as already explained, the field potential needs to satisfy the slow-rolls conditions, in particular the condition $|\eta_V| \ll 1$, with η_V defined in (3.27). This implies the condition:

$$\frac{\partial^2 V}{\partial \phi^2} \lesssim \frac{V}{M_{pl}^2}, \tag{3.34}$$

therefore, if we express the Quintessence mass squared as $m_\phi^2 = \frac{\partial^2 V}{\partial \phi^2}$, we obtain the following constrain today:

$$m_\phi^2 \lesssim \frac{V_0}{M_{pl}^2} \simeq H_0^2, \tag{3.35}$$

as it is required by observations of the accelerated expansion today. This means that:

$$m_\phi \lesssim 10^{-33} eV, \tag{3.36}$$

thus, to be compatible with observations the Quintessence scalar field needs to have an extremely small mass. This leads to some problems: a nearly massless field should give rise to long-range forces with ordinary matter, which should be observable; furthermore, it might be unstable against radiative corrections [10]. Within particle physics, some solutions are present, for example a possibility is constituted by the class of models where the Quintessence field is a Pseudo-Nambu-Goldstone Boson (PNGB) of a spontaneously broken shift symmetry. More details can be found in [41].

3.4.2 Phantom models

Energy Conditions

In General Relativity, it is sometimes useful to be able to understand the properties of Einstein's equations without the need of specifying the theory of matter from which $T_{\mu\nu}$ is derived. The properties that are studied in this context will then hold for different sources. In this frame, it is usual to impose some energy conditions on the stress-energy tensor $T_{\mu\nu}$.
To impose energy conditions, we need to build scalars from $T_{\mu\nu}$, having therefore coordinate-invariant bounds. To translate the energy conditions in physical terms, it is useful to consider the stress-energy tensor of the perfect fluid (1.2).
The most common energy conditions are [13]:

- Weak Energy Condition (WEC):
  $T_{\mu\nu} t^\mu t^\nu \geq 0$ with t^μ time-like vector.
  For a perfect fluid, it translates: $\rho \geq 0$ and $\rho + P \geq 0$.

- Null Energy Condition (NEC):
  $T_{\mu\nu}l^\mu l^\nu \geq 0$ with l^μ null vector.
  For a perfect fluid, it translates: $\rho + P \geq 0$. The energy density might now be negative, as long as the pressure compensates.

- Dominant Energy Condition (DEC):
  $T_{\mu\nu}t^\mu t^\nu \geq 0$ with t^μ time-like vector and $T_{\mu\nu}t^\mu$ is a non space-like vector, that means $T_{\mu\nu}T^\nu_\lambda t^\lambda t^\mu \leq 0$.
  For a perfect fluid, it translates: $\rho \geq |P|$.

- Null Dominant Energy Condition (NDEC):
  $T_{\mu\nu}l^\mu l^\nu \geq 0$ with l^μ null vector and $T_{\mu\nu}l^\mu$ is a non space-like vector, that means $T_{\mu\nu}T^\nu_\lambda l^\lambda l^\mu \leq 0$. It is the DEC conditions specialised for null vectors.
  For a perfect fluid, we have the same condition of the DEC and, in addition, the condition: $\rho = -P$, under which also negative energy densities are allowed.

- Strong Energy Condition (SEC):
  $T_{\mu\nu}t^\mu t^\nu \geq \frac{1}{2}T^\lambda_\lambda t^\sigma_\sigma$ with t^μ time-like vector.
  For a perfect fluid, it translates: $\rho + P \geq 0$ and $\rho + 3P \geq 0$.

Clearly, the energy conditions are helpful to identify non physical properties of a fluid; for example, considering a perfect fluid with $\rho \geq 0$, then all the energy conditions imply that the equation of state parameter is $w \geq -1$.

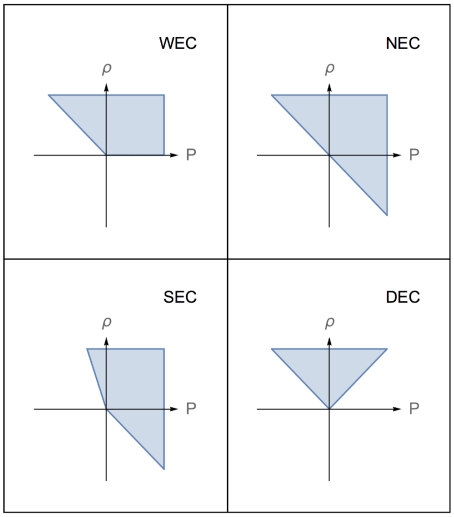

Figure 3.3: Energy conditions for the perfect fluid. Taken from [23].

On the other hand, the dark energy equation of state parameter is not constrained by observation to be grater than -1; therefore, from an observational point of view, the regime with $w_{DE} < -1$ is not excluded. Nevertheless, as we said before, for example the WMAP 5-years release gives $-1.097 < w_{DE} < -0.858$ at 95% confidence level, so the value is constrained to stay near the bound -1.
From a theoretical point of view, it was therefore necessary to explore the so called phantom regime. To do so, the phantom theories need to break the Null Dominant Energy Condition. The simplest phantom model can be realized exploiting a scalar field χ with negative kinetic energy (using the signature $(-+++)$ for the metric tensor) [24]:

$$\mathcal{L}_\chi = \frac{1}{2}\partial_\mu\chi\partial^\mu\chi - V(\chi). \tag{3.37}$$

Similarly to the Quintessence case, we can obtain the stress energy tensor:

$$T^{\chi}_{\mu\nu} = -\partial_\mu\chi\partial_\nu\chi + g_{\mu\nu}\left[\frac{1}{2}g^{\alpha\beta}\partial_\alpha\chi\partial_\beta\chi - V(\chi)\right] \tag{3.38}$$

and then the associated pressure and energy density:

$$\begin{aligned} T^0_0 &= \frac{\dot{\chi}^2}{2} - V(\chi) = -\rho_\chi, \\ T^i_j &= -\left[\frac{\dot{\chi}^2}{2} + V(\chi)\right]\delta^i_j = P_\chi\delta^i_j, \end{aligned} \tag{3.39}$$

where we have assumed again a spatially constant field. Finally the equation of state parameter:

$$w_\chi = \frac{P_\chi}{\rho_\chi} = -\frac{\frac{\dot{\chi}^2}{2} + V(\chi)}{-\frac{\dot{\chi}^2}{2} + V(\chi)}, \tag{3.40}$$

which is clearly smaller than -1 for $\frac{\dot{\chi}^2}{2} < V(\chi)$.
Varying the action with respect to the field, now we obtain the following equation of motion:

$$\Box\chi = -\frac{\partial V(\chi)}{\partial\chi}, \tag{3.41}$$

which is the usual Klein-Gordon equation for the scalar field, with a opposite sign in the right hand side. In a FLRW metric:

$$\ddot{\chi} + 3H\dot{\chi} = V_{,\chi}\,, \tag{3.42}$$

where $V_{,\chi} = \frac{\partial V(\chi)}{\partial\chi}$. The equation of motion describes a field that tends to run up, not down, the potential.
Finally, it is possible to study the perturbations of the phantom field, considering the following perturbed FLRW metric in the synchronous gauge :

$$ds^2 = -dt^2 + a(t)^2(\delta_{ij} + h_{ij})d\vec{x}^2, \tag{3.43}$$

where h_{ij} is the trace part of the metric perturbation that can be rewritten in terms of its trace h as $h_{ij} = \frac{h}{3}\delta_{ij}$. It is then possible to re-derive the equation of motion in the perturbed metric, admitting a space dependence for the field χ:

$$\ddot{\chi} + 3H\dot{\chi} + \frac{1}{2}\dot{h}\dot{\chi} - \frac{\nabla^2\chi}{a^2}\left(1 - \frac{h}{3}\right) = V_{,\chi}\,, \tag{3.44}$$

for a perturbation $\chi(t,\vec{x}) = \chi(t) + \delta\chi(t,\vec{x})$, the first-order perturbed equation in Fourier space is:

$$\ddot{\delta\chi} + 3H\dot{\delta\chi} + \left(\frac{k^2}{a^2} - V_{,\chi\chi}\right)\delta\chi = -\frac{\dot{h}\dot{\chi}}{2}. \tag{3.45}$$

In this equation the sign of the $V_{,\chi\chi}$ is opposite with respect to the standard case, as a consequence of the negative kinetic term in the field Lagrangian. It is possible to show that small scales perturbations are suppressed, while, on larger scale and in the case $\left(\frac{k^2}{a^2} - V_{,\chi\chi}\right) < 0$, the field perturbation $\delta\chi$ develops a growing instability [24]. If the instability manifests on a timescale shorter than the age of the Universe, then the phantom model is not a viable candidate for dark energy.
It is worth to notice that a good option to recover an effective equation of state parameter less than -1 might be realized with a non-minimally coupled dark energy model or with an alternative theory of gravity [5].

3.4.3 Brans-Dicke theories

Brans-Dicke (BD) theories are among the simplest examples of modified gravity theories with an additional scalar degree of freedom. Being φ the BD scalar field, the general action is [40]:

$$S = \int d^4x\sqrt{-g}\left(\frac{1}{2}\varphi R - \frac{\omega_{BD}}{2\varphi}(\partial_\mu\varphi\partial^\mu\varphi) - U(\varphi)\right) + \int d^4x\sqrt{-g}\mathcal{L}_M(g_{\mu\nu},\psi_M). \tag{3.46}$$

It contains a non-minimal coupling between gravity and the scalar field, a non-canonical kinetic term and the field potential. ω_{BD} is called Brans-Dicke parameter. In the original formulation of the theory in 1961 [41], the self interaction potential was not present, thus this case is known as massless BD theory.
In BD theories the scalar field can take the role of a point-dependent gravitational coupling:

$$\varphi = M_{pl}^2(x) = \frac{1}{8\pi G(x)}, \tag{3.47}$$

therefore the BD scalar field sets the strength of the gravitational interaction at each point of the space-time [40].
An extension of Brans-Dicke theories is called Generalized Brans-Dicke whose action is [67]:

$$S = \int d^4x\sqrt{-g}\left(\frac{M_{pl}^2}{2}F(\varphi)R - \frac{1}{2}K(\varphi)(\partial_\mu\varphi\partial^\mu\varphi) - U(\varphi)\right) + \int d^4x\sqrt{-g}\mathcal{L}_M(g_{\mu\nu},\psi_M), \tag{3.48}$$

where now the first two terms in the action are multiplied for generic functions of the scalar field. The freedom in choosing the $F(\varphi)$ and $K(\varphi)$ functions provides the possibility of choosing the desired expansion history. In these theories the equation of state of the scalar field, that takes the role of an effective dark energy fluid, depends on the function $F(\varphi)$ and it can indeed change sign going in the phantom regime.
A further generalization of (3.48) can be realize making the first term a free function of both the scalar field and the Ricci scalar, these theories are also known as extended Quintessence, as they propose a non-minimally coupled scalar field with a generalized kinetic term and the scalar potential [68]-[69].
A particular kind of Brans-Dicke theories are $f(R)$ theories, as we will see in more details in the next paragraph.

3.4.4 $f(R)$ theories

$f(R)$ theories modify the Einstein-Hilbert action by adding to it a generic function of the Ricci scalar R [35]:

$$S = \int d^4x\sqrt{-g}\frac{M_{pl}^2}{2}(R + f(R)) + \int d^4x\sqrt{-g}\mathcal{L}_M(g_{\mu\nu},\psi_M). \tag{3.49}$$

Some examples of this kind were already presented in the context of inflation in 1979 by Starobinsky. Indeed, adding in the Lagrangian terms like $\sqrt{-g}R^n$ with $n > 1$, brings modifications of cosmology at early times and in particular it leads to a deSitter phase. Subsequently, it was shown that, for $n < 0$, these modifications become relevant in the late Universe [33]. Thus, they might be an appropriate choice of the $f(R)$ term in (3.49) to explain late time cosmic acceleration.
The modified field equation can be found varying the action with respect to the metric, similarly to Einstein's one, apart for the additional term:

$$\begin{aligned}\frac{\delta\sqrt{-g}f(R)}{\delta g^{\mu\nu}} &= \frac{\delta\sqrt{-g}}{\delta g^{\mu\nu}}f(R) + \sqrt{-g}\frac{\delta f(R)}{\delta g^{\mu\nu}} \\ &= -\frac{1}{2}\sqrt{-g}g_{\mu\nu}f(R) + f_R\left(\frac{\delta R_{\alpha\beta}}{\delta g^{\mu\nu}}g^{\alpha\beta} + R_{\mu\nu}\right),\end{aligned} \tag{3.50}$$

where $f_R = \frac{\partial f(R)}{\partial R}$. In General Relativity the second term of (3.50) vanishes since it can be rewritten as a total derivative. Having a function of the Ricci scalar, in $f(R)$ gravity, it is not

possible to do the same, therefore it needs to be computed. To do so, we can exploit the following relation [34]:

$$\delta R_{\alpha\beta} g^{\alpha\beta} = D_\lambda((g^{\lambda\alpha} g^{\nu\beta} - g^{\lambda\nu} g^{\alpha\beta}) D_\nu \delta g_{\alpha\beta}), \tag{3.51}$$

that applied to the second term of (3.50) gives:

$$\begin{aligned}(\delta R_{\alpha\beta} g^{\alpha\beta}) f_R &= f_R D_\lambda((g^{\lambda\alpha} g^{\nu\beta} - g^{\lambda\nu} g^{\alpha\beta}) D_\nu \delta g_{\alpha\beta}) \\ &= (D^\beta D^\alpha f_R - g^{\alpha\beta} D_\nu D^\nu f_R) \delta g_{\alpha\beta},\end{aligned} \tag{3.52}$$

where in the second line we have integrated per parts twice to free the metric variation. Then, using:

$$\delta(g_{\alpha\nu} g^{\nu\mu}) = 0 \longrightarrow \delta g_{\alpha\beta} = -g_{\mu\beta} g_{\alpha\nu} \delta g^{\mu\nu}, \tag{3.53}$$

we obtain:

$$(\delta R_{\alpha\beta} g^{\alpha\beta}) f_R = (g_{\mu\nu} \Box f_R - D_\mu D_\nu f_R) \delta g^{\mu\nu}. \tag{3.54}$$

Therefore, the resulting $f(R)$ field equation is:

$$(1 + f_R) R_{\mu\nu} - \frac{1}{2} g_{\mu\nu}(R + f(R)) + (g_{\mu\nu} \Box - D_\mu D_\nu) f_R = 8\pi G T_{\mu\nu}, \tag{3.55}$$

that can be rewritten absorbing the non-GR terms in an effective stress energy tensor:

$$8\pi G T^{eff}_{\mu\nu} = f_R R_{\mu\nu} - \frac{1}{2} g_{\mu\nu} f(R) + (g_{\mu\nu} \Box - D_\mu D_\nu) f_R. \tag{3.56}$$

Assuming as always the stress energy tensor of a perfect fluid and specifying (3.55) for a flat FLRW background, it is possible to obtain the modified Friedman equations [5]:

$$\begin{aligned} &H^2 + \frac{f(R)}{6} - \frac{\ddot{a}}{a} f_R + H \dot{f_R} = \frac{8\pi G}{3} \rho, \\ &\frac{\ddot{a}}{a} - f_R H^2 + \frac{f(R)}{6} + \frac{\ddot{f_R}}{2} = -\frac{4\pi G}{3}(\rho + 3P). \end{aligned} \tag{3.57}$$

It is interesting to take the trace of equation (3.55):

$$R f_R - R - 2f(R) + 3\Box f_R = 8\pi G T. \tag{3.58}$$

Ror a perfect fluid the trace of the stress energy tensor is $T = g_{\mu\nu} T^{\mu\nu} = -\rho + 3P$, therefore, we can rewrite (3.58) as:

$$\Box f_R = \frac{1}{3}(R + 2f(R) - R f_R) - \frac{8\pi G}{3}(\rho + 3P) \equiv \frac{\partial V_{eff}}{\partial f_R}, \tag{3.59}$$

which is clearly a dynamical equation for f_R, making it a propagating scalar degree of freedom of the theory. This scalar degree of freedom, called scalaron, obeys an equation of motion with a standard kinetic term and an effective potential V_{eff}. The mass of the scalar is:

$$m^2_{f_R} = \frac{\partial^2 V_{eff}}{\partial f_R^2} = \frac{\partial R}{\partial f_R} \frac{\partial}{\partial R} \frac{\partial V_{eff}}{\partial f_R} = \frac{1}{3}\left(\frac{1 + f_R}{f_{RR}} - R\right). \tag{3.60}$$

To be consistent at high curvature, $f(R)$ theories need to have $f_R \to 0$ and $|R f_{RR}| \ll 1$ [5], therefore:

$$m^2_{f_R} \sim \frac{1}{3 f_{RR}}, \tag{3.61}$$

which then means that we also need to impose $f_{RR} > 0$ to have a positive mass squared. These are only some of the viability conditions for $f(R)$ theories, indeed more bounds need to be impose in order to avoid instabilities and to guarantee agreement with local tests of gravity [35], as we will see better in the next chapter.
Finally, it can be shown that $f(R)$ theories are a particular sub-class of the Brans-Dicke theories. More on this topic and on f(R) theories in Jordan and Einstein frames can be found in the Appendix C.

3.4.5 Scalar-tensor theories

From a more general point of view, scalar-tensor theories are some of the most studied modified gravity theories. Indeed, essentially all MG theories result in theories with additional degrees of freedom; for example both Brans-Dicke and $f(R)$ theories are sub-classes of scalar-tensor theories. Moreover, thanks to the relatively simple structure of their field equations, analytic solutions can be found.
The most general action for a four dimensional scalar-tensor theory with second-order field equations is [27]:

$$S = \int d^4x\sqrt{-g}\Big[\sum_{i=2}^{5}\mathcal{L}_i + \mathcal{L}_M(g_{\mu\nu},\psi)\Big], \tag{3.62}$$

with:

$$\begin{aligned}
\mathcal{L}_2 =& K(\phi,X),\\
\mathcal{L}_3 =& -G_3(\phi,X)\Box\phi,\\
\mathcal{L}_4 =& G_4(\phi,X)R + G_{4,X}[(\Box\phi)^2 - (D_\mu D_\nu\phi)(D^\mu D^\nu\phi)],\\
\mathcal{L}_5 =& G_5(\phi,X)G_{\mu\nu}(D^\mu D^\nu\phi) - \frac{1}{6}G_{5,X}[(\Box\phi)^3 - 3(\Box\phi)(D_\mu D_\nu\phi)(D^\mu D^\nu\phi)\\
&+ 2(D^\mu D_\alpha\phi)(D^\alpha D_\beta\phi)(D^\beta D_\mu\phi)],
\end{aligned} \tag{3.63}$$

where K and G_i $(i = 3, 4, 5)$ are function of the scalar field ϕ and its kinetic term $X = -\frac{1}{2}g_{\mu\nu}\partial^\mu\phi\partial^\nu\phi$, R is the Ricci scalar, $G_{\mu\nu}$ the Einstein tensor and $G_{i,X}$, $G_{i,\phi}$ the derivative of the function with respect to X and ϕ.
It is worth to notice that, even if the action contains higher order terms, the equations of motion are second order.
The above action is the so called Generalized Galileons action, that historically comes from the Covariant Galileons theory [28]. Indeed, Galileons theories were first written as the the most general action having second-order equations of motion and satisfying the so called Galilean symmetry in Minkowski spacetime. The Galileon in fact is a scalar field with a symmetry under the transformation:

$$\phi \to \phi + b_\mu x^\mu + c, \tag{3.64}$$

that is called Galilean shift symmetry, from an analogy to the Galilei transformation in classical mechanics. Introducing gravity, the Galilean shift symmetry is broken, due to the necessity of introducing non-minimal couplings of the scalar field to the curvature, and, in the Covariant Galieons theories, only the requirement of second-order equations of motion survives. The Covariant Galileons action is still a sub-class of the Generalized Galileons theories; it corresponds to the following choice of the Generalized Galileons functions [27]:

$$K = c_2X, \qquad G_3 = -\frac{c_3}{M^3}X, \qquad G_4 = \frac{M_{pl}^2}{2} - \frac{c_4}{M^6}X^2, \qquad G_5 = \frac{c_5}{M^9}X^2, \tag{3.65}$$

where c_2, c_3, c_4 and c_5 are dimensionless constants while M is a constant with dimension of a mass. Between the Covariant Galileon models, it is usual to distinguish the models with $c_2, c_3 \neq 0$ and $c_4 = c_5 = 0$ referred to as Cubic Galileons, while the cases with $c_4 \neq 0$ and $c_5 \neq 0$ are respectively Quartic and Quintic Galileons.

Similarly, the Generalized Galileons Lagrangian is found starting from the most general action in Minkowski spacetime with second-order field equations, requiring to have at most second derivatives of ϕ and to be polynomial in $\partial_\mu\partial_\nu\phi$.
The Generalized Galileons are also known as Hordenski theories, that, as already said, are the most general scalar-tensor theories with second-order field equations in four dimension. Indeed, the first at writing the action was Hordeski in 1974; in the context of Lovelock gravity, he worked under different assumptions from that used to find the Generalized Galileons. As a consequence,

the Hordenski Lagrangian presents in a very different, but equivalent, form [28]:

$$\begin{aligned}\mathscr{L} = \delta^{\alpha\beta\gamma}_{\mu\nu\sigma}\left[\kappa_1\phi^{,\mu}_{,\alpha}R_{\beta\gamma}{}^{\nu\sigma} + \frac{2}{3}\kappa_{1X}\phi^{,\mu}_{,\alpha}\phi^{,\nu}_{,\beta}\phi^{,\sigma}_{,\gamma} + \kappa_3\phi_{,\alpha}\phi^{,\mu}R_{\beta\gamma}{}^{\nu\sigma} + 2\kappa_{3X}\phi_{,\alpha}\phi^{,\mu}\phi^{,\nu}_{,\beta}\phi^{,\sigma}_{,\gamma}\right] \\ +\delta^{\alpha\beta}_{\mu\nu}[(F+2W)R_{\alpha\beta}{}^{\mu\nu} + 2F_X\phi^{,\mu}_{,\alpha}\phi^{,\nu}_{,\beta} + 2\kappa_8\phi_{,\alpha}\phi^{,\mu}\phi^{,\nu}_{,\beta}] \\ -6(F_\phi + 2W_\phi - X_{\kappa_8})\Box\phi + \kappa_9,\end{aligned} \tag{3.66}$$

where $\delta^{\alpha\alpha_1\alpha_2\cdots}_{\mu\mu_1\mu_2\cdots} = n!\delta^{[\alpha}_{\mu}\ldots\delta^{\alpha_n]}_{\mu_n}$ is the generalized Kronecker delta, κ_1, κ_3, κ_8 and κ_9 are functions of ϕ and its kinetic term X, F is a κ_i-dependent function of ϕ and X, and W is another ϕ function that can be reabsorbed in F. Thus, like for the Generalized Galileons, the free functions are only ϕ and X. It was indeed shown that the two theories can be mapped one in the other through [29]:

$$\begin{aligned}K &= \kappa_9 + 4X\int^X dX'(\kappa_{8\phi} - 2\kappa_{3\phi\phi}), \\ G_3 &= 6F_\phi - 2X\kappa_8 - 8X\kappa_{3\phi} + 2\int^X dX'(\kappa_8 - 2\kappa_{3\phi}), \\ G_4 &= 2F - 4X\kappa_3, \\ G_5 &= -4\kappa_1.\end{aligned} \tag{3.67}$$

Beyond Hordenski

As we saw, Hordenski and Galileons theories were built with the indispensable request of describing systems with second-order field equations. Thanks to it, the theories are clearly free of Ostrogradsky instabilities, which are due to higher order time derivatives.
Nevertheless, it is possible to show that healthy theories beyond Horndeski gravity can be constructed free from Ostrogradsky instabilities. To achieve it, we need to drop the crucial postulate of Ostrogradsky theorem that asks for a non-degenerate Lagrangian of the system.
It is interesting to see this, in a simple toy model Lagrangian [30]:

$$\mathscr{L} = \frac{a}{2}\ddot{\phi}^2 + b\ddot{\phi}\ddot{q} + \frac{c}{2}\ddot{q}^2 + \frac{1}{2}\dot{\phi}^2 - \frac{1}{2}\phi^2 - \frac{1}{2}q^2. \tag{3.68}$$

It is then easy to compute the Euler-Lagrange equations for the two fields, applying (3.12):

$$a\dddot{\phi} + b\dddot{q} - \ddot{\phi} - \phi = 0, \tag{3.69}$$

$$b\dddot{\phi} + c\ddot{q} + q = 0, \tag{3.70}$$

thus, clearly the system presents higher order time derivatives in both the fields. Therefore, as Ostrogradsky predicts the system should be unstable and not viable for physical purposes. To avoid this, we can choose a degenerate system. To clarify it, we can introduce the kinetic matrix, which contains the coefficients of the highest order derivatives terms:

$$M = \begin{pmatrix} a & b \\ b & c \end{pmatrix}, \tag{3.71}$$

if it is degenerate $det(M) = ac - b^2 = 0$, then the system contains only two healthy degrees of freedom. Indeed, we can consider the combination of the field equations $(c \cdot (3.69)) - (b \cdot \frac{d(3.70)}{dt})$, that, for a degenerate system leads to:

$$\ddot{\phi} + \frac{b}{c}\dot{q} + \phi = 0, \tag{3.72}$$

then multiplying (3.72) by b and subtracting it to (3.70), we can obtain:

$$\ddot{q}\left(\frac{b^2}{c^2} - 1\right) + \frac{b}{c}\dot{\phi} - \frac{q}{c} = 0. \tag{3.73}$$

Therefore, thanks to the degeneracy of the system, we have obtained two second-order equations for ϕ and q, showing that the system is free from Ostrogradsky instabilities despite the higher order Euler-Lagrange equations.

The Beyond Hordenski class of theories that exploits this mechanism are called Degenerate Higher-Order Scalar-Tensor (DHOST) theories.
Examples are the Gleyzes-Langlois-Piazza-Vernizzi (GLPV) theories, where the covariant version of the original Galileons Lagrangian is exploited [31]-[32].

Chapter 4

Viability conditions

4.1 Screening mechanism

As already anticipated, General Relativity is really well tested within the solar system and astrophysical scale [47], therefore it is necessary for new physics to provide a mechanism to hide itself from local observation. This mechanisms are known as screening mechanism.
To better understand how these mechanisms can work, it is useful to study the connection between fields in the Lagrangian and the potential that introduce new long range forces.

Following [20], we can consider a general scalar field theory coupled to non-relativistic matter through a coupling $g(\phi)$, which depends on the scalar field itself. We suppose to have a point-like matter source, with a stress-energy tensor with trace $T^{\mu}_{\mu} = -\rho = -M\delta^3(x)$, M is the mass of the matter source. Being $Z^{\mu\nu}$ a generic tensor built by derivatives of the field and expanding the field ϕ around a background value $\bar{\phi}$ as $\phi = \bar{\phi} + \varphi$, it is possible to find the generic equation of motion for the perturbation:

$$Z^{\mu\nu}(\ddot{\varphi} - c_s^2(\bar{\phi})\nabla^2\varphi) + m^2(\bar{\phi})\varphi = g(\bar{\phi})M\delta^3(x), \tag{4.1}$$

where c_s is an effective sound speed. It is possible to show that the resulting static potential around the point-like source is:

$$V(r) = -\frac{g^2(\bar{\phi})}{Z(\bar{\phi})c_s^2(\bar{\phi})}\frac{e^{-\frac{m(\bar{\phi})r}{\sqrt{Z(\bar{\phi})}c_s(\bar{\phi})}}}{4\pi r}M, \tag{4.2}$$

thus, a light scalar fields mediates an attractive long-range force that goes as $F \propto 1/r^2$. This is clearly forbidden by local tests of gravity, therefore we need a mechanism to suppress it on small scales. From (4.2), it is straightforward to see how it can work:

- *Weak coupling*:
  It consists in letting the coupling to matter $g(\bar{\phi})$ to depend on the background. This allows to have a small coupling in high density regions and suppress the fifth force.

- *Large mass*:
  Similarly, another possibility is to let the mass of the fluctuations $m(\bar{\phi})$ to depend on the environment. For a large mass indeed the potential is exponentially suppressed; thus the mass should be able to vary from large value in high density regions to small one on cosmological scales. For example, the so called chameleon screening mechanisms exploits this idea, as we will see.

- *Large inertia*:
  Finally, another possibility is offered by the kinetic function $Z(\bar{\phi})$. Similarly to the mass, we need the kinetic function to be large on solar system scales. The kind of mechanism that relies on second-order derivatives is known as Vainshtein screening mechanism.

Clearly, also $c_s(\bar{\phi})$ might be a candidate parameter to provide a screening mechanism. However, screening mechanisms due to the effective sound speed are not really efficient so they are usually excluded.

4.1.1 Chameleon mechanism

Chameleon mechanism realizes the screening of many scalar-tensor theories such as Brans-Dicke and $f(R)$ theories. It describes a fifth force mediated by the additional scalar degree of freedom, with the peculiarity of being so called environmental dependent. In particular, as we are going to see, the range of the force decreases with increasing ambient matter density, thus providing a mechanism to hide the new degree of freedom from local tests of gravity.
To explain the chameleon mechanism, we start from the following action:

$$S = \int d^4x\sqrt{-g}\left[\frac{M_{pl}^2}{2}R - \frac{1}{2}(\partial\phi)^2 - V(\phi)\right] + \int d^4x\mathcal{L}_M(\tilde{g}^{(i)}_{\mu\nu}, \psi_M^{(i)}), \tag{4.3}$$

with:

$$\tilde{g}^{(i)}_{\mu\nu} = e^{\frac{2\beta_i\phi}{M_{pl}}} g_{\mu\nu}, \tag{4.4}$$

where β_i are dimensionless constants. This is nothing else than the action of a modified gravity theory with an additional scalar field in the Einstein frame, i.e. in the frame where the gravity sector of the action remains unchanged, while a non-minimal coupling between gravity and the matter field is induced. Indeed (4.4) is a conformal transformation between the metric $g_{\mu\nu}$ in the Einstein frame and its conformally related $\tilde{g}^{(i)}_{\mu\nu}$ (for more details about conformal transformations and the procedure to go from Jordan to Einstein frame, see Appendix B and C).
Taking the variation of (4.3) with respect to the scalar field ϕ, it is easy to find:

$$\frac{\delta S}{\delta\phi} = \sqrt{-g}(\Box\phi - V_{,\phi}) + \sqrt{-\tilde{g}}\sum_i e^{-\frac{2\beta_i\phi}{M_{pl}}}\frac{\beta_i}{M_{pl}}T^{(i)}_{\mu\nu}g^{\mu\nu} = 0, \tag{4.5}$$

where the last term is due to the variation of the matter action and it is found using the definition for the conformal stress energy tensor $\frac{\delta\mathcal{L}_M}{\delta g^{\mu\nu(i)}} = -\frac{\sqrt{-\tilde{g}}}{2}T^{(i)}_{\mu\nu}$. Then exploiting (B.2) and (B.3), we find the field equation:

$$\Box\phi = V_{,\phi} - \sum_i \frac{\beta_i}{M_{pl}} e^{\frac{4\beta_i\phi}{M_{pl}}} T^{(i)}_{\mu\nu}\tilde{g}^{\mu\nu}_{(i)}. \tag{4.6}$$

Choosing, for simplicity, to have only one single component of non relativistic matter:

$$T_{\mu\nu}\tilde{g}^{\mu\nu} = -\tilde{\rho} = -e^{\frac{-3\beta\phi}{M_{pl}}}\rho, \tag{4.7}$$

where ρ is the matter energy density in the Einstein frame and hence ϕ independent. Thus we obtain the final expression, for a single matter component:

$$\Box\phi = V_{,\phi} + \frac{\beta}{M_{pl}} e^{\frac{\beta\phi}{M_{pl}}}\rho \equiv \frac{\partial V_{eff}}{\partial\phi}, \tag{4.8}$$

so the dynamics of the chameleon scalar field is not affected by the potential $V(\phi)$ but rather by the effective potential:

$$V_{eff}(\phi) = V(\phi) + \rho e^{\frac{\beta\phi}{M_{pl}}}. \tag{4.9}$$

In order to have a minimum of the effective potential, the scalar potential $V(\phi)$ is usually assumed to have a runaway form, i.e. to be monotonically decreasing in ϕ. Then, to have a minimum of the effective potential, we just need $\beta > 0$.

Indeed the minimum should satisfy the condition:

$$\left.\frac{\partial V_{eff}}{\partial\phi}\right|_{\phi_{min}} = V_{,\phi}|_{\phi_{min}} + \frac{\beta}{M_{pl}} e^{\frac{\beta\phi_{min}}{M_{pl}}}\rho = 0, \tag{4.10}$$

while for the mass of the fluctuations around the minimum:

$$m^2|_{\phi_{min}} = \left.\frac{\partial^2 V_{eff}}{\partial\phi^2}\right|_{\phi_{min}} = \left.\frac{\partial^2 V}{\partial\phi^2}\right|_{\phi_{min}} + \rho\frac{\beta^2}{M_{pl}^2} e^{\frac{\beta\phi_{min}}{M_{pl}}}. \tag{4.11}$$

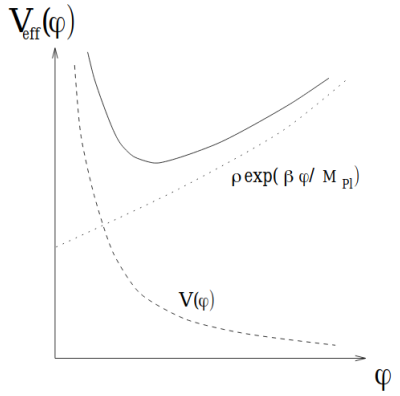

Figure 4.1: The chameleon effective potential (solid curve) found as the sum of a scalar potential (dashed curve) and the density-dependent term (dotted curve). Taken from [45].

A typical choice of the potential is the inverse power law potential, already considered for the Quintessence field, that has the following analytic form:

$$V(\phi) = \frac{M^{4+n}}{\phi^n}. \tag{4.12}$$

Thus for the inverse power law potential, (4.10) and (4.11) give:

$$\phi_{min} = \left(\frac{nM^{4+n}}{\rho\beta}M_{pl}\right)^{\frac{1}{n+1}} \tag{4.13}$$

and the effective mass:

$$m^2|_{\phi_{min}} = n(n+1)M^{4+n}\left(\frac{\rho\beta}{nM^{4+n}M_{pl}}\right)^{\frac{n+2}{n+1}} + \rho\frac{\beta^2}{M_{pl}^2}, \tag{4.14}$$

where we have exploited the fact that $\phi \ll M_{pl}$ for the relevant field range [44]. We have found the so called environmental dependence: both ϕ_{min} and the mass around this value depend on the background matter energy density. In particular the mass is an increasing function of it, while the minimum of the field shifts to smaller values for higher ρ .

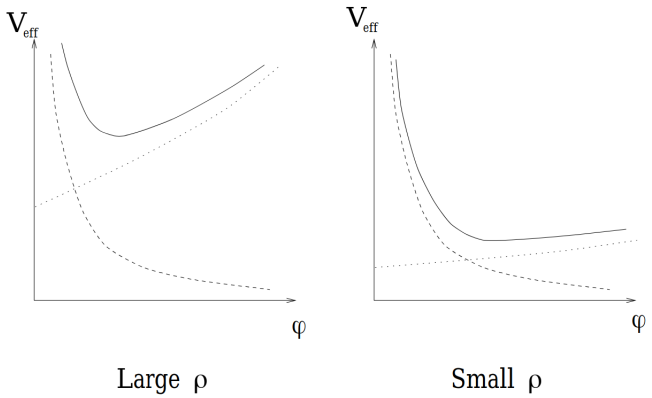

Figure 4.2: Chameleon effective potential for large and small ρ. As ρ decreases, the minimum shifts to larger values of φ (in our notation ϕ) and the mass of small fluctuations decreases. Taken from [46].

Chameleon fifth force

As we see from action (4.3), there is a coupling between the matter and the chameleon field due to the conformal metric $\tilde{g}^{(i)}_{\mu\nu}$. Indeed, free particles follow geodesic of the metric $\tilde{g}^{(i)}_{\mu\nu}$ rather than the standard $g_{\mu\nu}$ [48]. Thus, a free test particle of mass M of the species i, has the following equation of motion:

$$\ddot{x}^\rho + \tilde{\Gamma}^\rho_{\mu\nu}\dot{x}^\mu\dot{x}^\nu = 0, \tag{4.15}$$

where $\tilde{\Gamma}^\rho_{\mu\nu}$ are the Christoffel symbols in the $\tilde{g}_{\mu\nu}$ metric. Then applying (B.4) for the conformal transformation (4.4):

$$\begin{aligned}\tilde{\Gamma}^\rho_{\mu\nu} &= \frac{1}{2}\tilde{g}^{\sigma\rho}(\tilde{g}_{\mu\sigma,\nu} + \tilde{g}_{\nu\sigma,\mu} - \tilde{g}_{\mu\nu,\sigma}) \\ &= \Gamma^\rho_{\mu\nu} + \frac{\beta_i}{M_{pl}}(g^\rho_\mu\phi_{,\nu} + g^\rho_\nu\phi_{,\mu} - g_{\mu\nu}g^{\sigma\rho}\phi_{,\sigma}),\end{aligned} \tag{4.16}$$

that, substituted in (4.15), gives:

$$\ddot{x}^\rho + \Gamma^\rho_{\mu\nu}\dot{x}^\mu\dot{x}^\nu + \frac{\beta_i}{M_{pl}}(2\phi_{,\mu}\dot{x}^\mu\dot{x}^\rho + g^{\sigma\rho}\phi_{,\sigma}) = 0, \tag{4.17}$$

which is the standard geodesic equation plus an additional term $\propto \beta_i/M_{pl}$ which is the Chameleon force. Indeed, in the non relativistic limit and in presence of a static Chameleon field, the test particle considered experiences the force:

$$\vec{F}_\phi = -M\frac{\beta_i}{M_{pl}}\vec{\nabla}\phi, \tag{4.18}$$

thus ϕ can be identify as the potential of this "fifth" force [48].
As we describe in Appendix D, it is possible to show that under the condition of a "thin shell" object, the Chameleon force will be successfully suppressed, thanks to the environmental dependence of both the field and the mass of the fluctuations.

4.2 Instabilities

As we saw, the Ostrogradsky theorem is a powerful tool to predicts instabilities of some DE/MG theories. These theories indeed, introduce new degrees of freedom to source cosmic acceleration in a dynamical way. However, it might happen that the extra degrees of freedom lead to an unstable system and thus not viable to describe our Universe.
It is then possible to study the dynamics of the perturbations of a specific action and perform a diagnostic of it; this allows to identify conditions, for example on the viable values of the model parameters, to avoid these instabilities.
These kinds of instabilities are typical of the Effective Field Theory (EFT) approach, which is a framework often used to investigate new physics beyond ΛCDM, as we will see better in Chapter 5. EFTs are indeed an effective description of low-energy physics, thus they are valid up to an energy scale Λ, called cutoff of the theory. Beyond the cutoff, the theory is not trustable, and some more fundamental theory is needed. This high energy wider theory is called UV completion [20].
It is worth to notice that instabilities in EFTs can be ignored as long as their energy scales lie above the cutoff of the theory. In this case indeed, we can interpret the unstable behaviour as due to the truncation of the EFT expansion at finite order and appeal to the UV completion to cure the instability.

4.2.1 Ghost instabilities

A possible pathology of MG/DE theories is called ghost; they are fields whose particles have negative energy indicating an instability of the theory. They manifest mainly as fields with the wrong kinetic sign. Indeed, an example is the phantom theory (3.37), where we saw that a possible instability is present if, considering (3.37) as an Effective Field Theory, the instability timescale is

smaller than the age of the Universe [49].
The Lagrangian of a ghost field is (always considering the signature $(-+++)$):

$$\mathscr{L}_{ghost} = \frac{1}{2}(\partial\chi)^2 - \frac{1}{2}m^2\chi^2, \tag{4.19}$$

where $(\partial\chi)^2 = g_{\mu\nu}\partial^\mu\chi\partial^\nu\chi$. The pathology of this theory might arise when the field couples to another field with canonical kinetic term, for example [20]:

$$\mathscr{L} = \frac{1}{2}(\partial\chi)^2 - \frac{1}{2}m_\chi^2\chi^2 - \frac{1}{2}(\partial\phi)^2 - \frac{1}{2}m_\phi^2\phi^2 + \lambda\phi^2\chi^2. \tag{4.20}$$

The vacuum of this theory is then unstable under the process $0 \to \phi\phi + \chi\chi$, indeed the two particles have opposite sign energy thus the process might cost zero energy. The rate of the process will be infinite and the theory will be not viable.

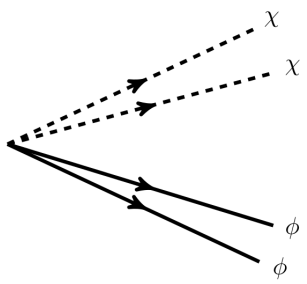

Figure 4.3: The vacuum of theory plagued by ghost is unstable to rapid pair production of ghost particles and healthy particles. Taken from [20].

The divergence can be avoided if we consider our theory not as fundamental, i.e. valid up to arbitrary high momenta, but rather as an effective theory valid below a cutoff scale Λ. For example, [49] demonstrated that, under specific assumptions, a phantom theory is valid only for energies below the cutoff of 100 MeV, which is uncomfortably low but still within the observed energy range of late time cosmic acceleration that is $\sim 10^{-3}eV$ for the vacuum energy today.

Furthermore, ghost instabilities might also arise in theories with higher order equations of motion, in this case ghost instabilities correspond to the Ostrograndsky instabilities that we have already encountered in Chapter 3. Following [20], we can proof this considering the following theory:

$$\mathscr{L} = -\frac{1}{2}(\partial\psi)^2 + \frac{1}{2\Lambda^2}(\Box\psi)^2 - V(\psi), \tag{4.21}$$

where Λ is the cutoff of the effective theory, meaning that this theory is well defined as long as we work with energies far below Λ.
By varying the Lagrangian with respect to the field ψ, we obtain the following equation of motion:

$$\Box\psi + \frac{1}{\Lambda^2}\Box(\Box\psi) = V(\psi)_{,\psi}, \tag{4.22}$$

therefore (4.21) has fourth order equation of motion. Therefore, Ostrogradsky theorem predicts instability of the system. In particular, we can see that the instability is ghost-like. To do so, we can introduce an auxiliary field χ and rewrite (4.21) as:

$$\mathscr{L} = -\frac{1}{2}(\partial\psi)^2 + \chi\Box\psi - \frac{\Lambda^2}{2}\chi^2 - V(\psi). \tag{4.23}$$

The equivalence between (4.21) and (4.23) can be easily checked computing the field equation for χ:

$$\chi = \frac{1}{\Lambda^2}\Box\psi, \tag{4.24}$$

that substituted back in (4.23), return the Lagrangian (4.21). Finally, we can remove the kinetic mixing in (4.23), through the field redefinition $\psi = \phi - \chi$, that applied to (4.23) gives:

$$\begin{aligned}\mathscr{L} &= -\frac{1}{2}(\partial\phi)^2 - \frac{1}{2}(\partial\chi)^2 + \partial_\mu\phi\partial^\mu\chi + \chi\Box\phi - \chi\Box\chi - \frac{\Lambda^2}{2}\chi^2 - V(\chi,\phi) \\ &= -\frac{1}{2}(\partial\phi)^2 + \frac{1}{2}(\partial\chi)^2 - \frac{\Lambda^2}{2}\chi^2 - V(\chi,\phi),\end{aligned} \tag{4.25}$$

where in the second line we have integrated by parts the third and fifth terms of the first line. Thus, we have found that (4.21) is equivalent to a theory with two scalar degrees of freedom, one healthy and one ghost.

4.2.2 Gradient instabilities

Another possible pathology, that makes a theory non-predictive, is the gradient instability which manifests in a wrong sign for the spatial gradient term. For example, a free scalar field theory plagued by gradient instability can be written with the following Lagrangian [20]:

$$\mathscr{L}_{gradient} = \frac{1}{2}\dot{\chi}^2 + \frac{1}{2}(\vec{\nabla}\chi)^2, \tag{4.26}$$

which is clearly non-Lorentz invariant. By varying the action with respect to the scalar field, it is possible to find its equation of motion, that in Fourier space assumes the form:

$$\ddot{\chi} - k^2\chi = 0. \tag{4.27}$$

Differently from the standard case, (4.27) does not have the plane-waves solution but instead it has solutions of the form:

$$\chi \sim e^{\pm kt}, \tag{4.28}$$

where in particular the growing mode increases exponentially without any bounds, making the theory unstable on a timescale:

$$t_{inst} \sim k^{-1}, \tag{4.29}$$

thus, the higher the energy modes, the sooner their instability will manifest, so the major contribution to the instability comes from high k.
It is also possible to show that considering such a Lagrangian, an EFT approach is not feasible: introducing a cut off is not sufficient to circumvent the gradient instability [20].

4.2.3 Tachyonic instabilities

Another possible instability, that can plague a certain theory, is the so called tachyonic instability. In an Effective Field Theory, a tachyonic instability is due to the fact that we are not perturbing around the true vacuum of the theory, and indeed, it manifests as a field with negative mass squared. Therefore, this kind of instability is not due to an intrinsic pathology of the theory but instead, it is a signal that the system is unstable because the considered value of the field is a local maximum of its potential energy, i.e. the false vacuum.
Following [20], it is possible to learn about the tachyonic instability from a toy example, considering the Lagrangian:

$$\mathscr{L}_{tachyon} = -\frac{1}{2}(\partial\chi)^2 + \frac{m^2}{2}\chi^2. \tag{4.30}$$

As before, by varying the action with respect to the field, it is easy to find the equation of motion in Fourier space:

$$\ddot{\chi} + (k^2 - m^2)\chi = 0, \tag{4.31}$$

that admits solutions of the form:

$$\chi \sim e^{\pm\sqrt{m^2-k^2}t}, \tag{4.32}$$

which in the limit $k \to 0$, becomes:

$$\chi \sim e^{\pm mt}, \tag{4.33}$$

thus, we have found again the unstable growing mode solution. Unlike for the gradient instability, the timescale of the instability is now dependent on the mass of the field:

$$\tau_{inst} \sim m^{-1}. \tag{4.34}$$

It is clear that, to avoid the instability, we can consider modes with $k \gg m$, where indeed everything remains well defined. In particular, for an EFT with a cut off Λ, we can require that $m \ll k \ll \Lambda$.

4.3 Gravitational waves aftermath

A turning point for multi-messenger astrophysics is the famous, first measurement of gravitational waves and electromagnetic radiation from the same astrophysical source, dated on August 17, 2017. The gravitational signal was detected by the Laser Interferometer Gravitational-Wave Observatory (LIGO) [70]; approximately 1.7 s after the Fermi Gamma-ray Burst Monitor (GBM) triggered a short Gamma-Ray Burst, GRB 170817A. In addition, the GRB signal was independently confirmed by the INTernational Gamma-ray Astrophysics Laboratory (INTEGRAL) [71].
This measurement has had also a crucial impact on DE/MG models since it greatly improved our understanding of gravity at a fundamental level. Indeed, the joint observations allowed to put stringent bounds on the speed of propagation of the gravitational waves c_T [71]:

$$-3 \cdot 10^{-5} < \frac{c_T}{c} - 1 < 7 \cdot 10^{-16}. \tag{4.35}$$

Such a constraint has brought very important consequences for the late time cosmic acceleration theoretical landscape: additional degrees of freedom coupled to gravity, such that the ones introduced in many DE/MG models, can effect the speed of propagation of standard gravitational waves. As a consequence, models that predict an anomalous c_T were immediately ruled out by GW170817 [72]-[73]-[74].
Within General Relativity, the equation of motion of transerve-traceless tensor perturbations of the metric, i.e. gravitational waves, can be obtained by perturbing the Einstein equations; at linear order and in absence of sources, it is possible to find in Fourier space:

$$\ddot{h}^T_{ij} + 3H\dot{h}^T_{ij} + c_T^2 k^2 h^T_{ij} = 0. \tag{4.36}$$

In the frame of a general scalar-tensor theory, the equation of motion assumes a slightly different form [73]:

$$\ddot{h}^T_{ij} + (3 + \alpha_M)H\dot{h}^T_{ij} + (1 + \alpha_T)k^2 h^T_{ij} = 0, \tag{4.37}$$

which depends on two functions of time: the tensor speed excess α_T, that accounts for modifications of the speed of gravitational waves (clearly in GR, $\alpha_T = 0$ thus $c_T = 1$) and the running of the effective Planck mass α_M, that possibly modifies the friction term due to the expansion of the Universe. These functions, whose explicit expressions are given by the specific Lagrangian, depend on the dynamics of the additional scalar field and on the parameters of the theory, thus allowing to establish constraints on the viable parameters space of a theory.
Indeed it was found that, excluding the possibility to accept a fine-tuning of the parameters space, several interesting models are effectively ruled out as viable late time cosmic acceleration theories. This class includes quartic and quintic Hordenski, as well as quartic and quintic GLPV and many other beyond Hordenski theories [73].

Chapter 5

EFT approach

The Effective Field Theory (EFT) approach for dark energy is the framework in which we will work in the next Chapter. The advantage of this approach is the possibility of working in a model independent framework using a parametrized action. Indeed, thanks to this unified approach, it is possible to study not only specific viable models but also perform agnostic tests of gravity.
The EFT approach, firstly introduced in Cosmology to study inflation with a single inflaton field [75], was later extended as a framework for the late time cosmic acceleration [77], where it allows to have a model independent language testable by observations and that unifies single field models of DE and MG.

5.1 Unified action in Unitary Gauge

The EFT Lagrangian is written in the Jordan frame and unitary gauge and it is expanded around a Friedmann-Lemaitre-Robertson-Walker Universe. In this gauge, the spacetime is foliated by constant time hypersurfaces that correspond to the constant scalar field ones: this makes the scalar field not to appear explicitly in the EFT action but to be hidden inside the metric degrees of freedom. Indeed, the spacetime slicing is realized by the time evolving scalar field $\phi_0(t)$, meaning that we are choosing the scalar field itself as the time coordinate, and its perturbations as vanishing, i.e. $\delta\phi(\vec{x},t)=0$. More in details, in the frame of Cosmological Perturbation Theory, applying (2.8), the scalar field perturbations transform under a gauge transformation as:

$$\delta\tilde{\phi}=\delta\phi+\dot{\phi}_0\alpha, \tag{5.1}$$

where α is the time component of the field along which we are computing the Lie derivative. With a proper choice of α, it is therefore possible to work in the gauge where there are not perturbations of the scalar field but only metric fluctuations. Thus, it is usually said that the scalar field perturbation has been eaten by the metric.
In particular, we can define the unit vector perpendicular to the constant scalar field hypersurfaces as:

$$n_\mu=\frac{\partial_\mu\phi}{\sqrt{-(\partial\phi)^2}}\rightarrow\frac{\delta^0_\mu}{\sqrt{-g_{00}}}, \tag{5.2}$$

where the last expression is valid in unitary gauge.
It is now possible to write down the most general Lagrangian in this gauge [76], the requirement will be to use operators that are function of the metric $g_{\mu\nu}$ and that are invariant under time-dependent spatial diffeomorphisms. It follows that, beside 4-dimensional covariant terms, such as the Ricci scalar, in the dark energy action many other terms are allowed, due to the fact that time diffeomorphisms have been fixed and therefore they are not a symmetry of the system anymore. As a consequence, the action will contain terms proportional to tensors with free 0 upper indices, such as g^{00} and R^{00}, which are scalar under spatial diffeomorphisms. Furthermore, tensors built from the contraction of the orthonormal vector n_μ or its covariant derivative are also allowed and they indeed described the preferred foliation of the spacetime. Finally, any term in the action can be multiplied by a generic function of time.

Under this assumptions, it is possible to show that the most generic Lagrangian can be written up to quadratic order in perturbations as [78]:

$$\begin{aligned} S_{EFT} = \int d^4x\sqrt{-g}\Big(&\frac{M_{pl}^2}{2}(1+\Omega(t))R + \Lambda(t) - c(t)\delta g^{00} + \\ &+ \frac{M_2^4(t)}{2}(\delta g^{00})^2 - \frac{\bar{M}_1^3(t)}{2}\delta g^{00}\delta K - \frac{\bar{M}_2^2(t)}{2}(\delta K)^2 - \frac{\bar{M}_3^2(t)}{2}\delta K^\mu_\nu \delta K^\nu_\mu \\ &+ \frac{\hat{M}^2(t)}{2}\delta g^{00}\delta\mathcal{R} + m_2^2(t)h^{\mu\nu}\partial_\mu g^{00}\partial_\nu g^{00} + ...\Big) + S_M(g_{\mu\nu},\psi_M), \end{aligned} \tag{5.3}$$

where the dots are for terms of higher order in the perturbations. $h^{\mu\nu} = g^{\mu\nu} + n^\mu n^\nu$ is the spatial metric on constant-time hypersurfaces, $\mathcal{R}_{\mu\nu}$ is the three dimensional Ricci tensor and $\mathcal{R}$ its trace, $K_{\mu\nu} = h^\lambda_\mu D_\lambda n_\nu$ is the extrinsic curvature, K its trace. Then, δg^{00}, $\delta\mathcal{R}$, $\delta K_{\mu\nu}$ and δK are respectively the perturbations of the zero-zero upper component of the metric, of the trace of the three dimensional Ricci tensor, of the extrinsic curvature and of its trace.
Moreover, the functions $\{\Omega, \Lambda, c, M_2^4, \bar{M}_1^3, \bar{M}_2^2, \bar{M}_3^2, \hat{M}^2 m_2^2\}$ are free functions of time, usually called EFT functions and they are used to map any specif model into the EFT language. In particular, as we will see, only the first three of them $\{\Omega, \Lambda, c\}$ enter in the equations for the background and indeed they are usually called background EFT functions.
This EFT action, describing the most general single-scalar field model of dark energy, accounts for most of the theories of cosmological interest; the four major subclasses of theories covered by the EFT action are [80]:

- Scalar-tensor theories such as Brans-Dicke and f(R) theories which are described only by the background EFT functions.
- Hordenski theories, for which the relation $\bar{M}_2^2 = -\bar{M}_3^2 = 2\hat{M}^2$ must be satisfied.
- GLPV theories which require $\bar{M}_2^2 = -\bar{M}_3^2$.
- Lorentz violating theories, like Horava gravity [79].

5.1.1 Background evolution equations

As we said, the background evolution is completely determined by the first line of (5.3), that corresponds to the action:

$$S_{EFT}^{(0)} = \int d^4x\sqrt{-g}\left(\frac{M_{pl}^2}{2}(1+\Omega(t))R + \Lambda(t) - c(t)\delta g^{00}\right) + S_M(g_{\mu\nu},\psi_M), \tag{5.4}$$

from which it is possible to obtain the evolution equations for the background quantities. By varying (5.4) with respect to the metric in a spatially flat FLRW metric, it is possible to obtain [80]:

$$\begin{aligned} &3M_{pl}^2(\Omega+1)H^2 + 3M_{pl}^2 H\dot{\Omega} = \sum_i \rho_i - \Lambda + 2c, \\ &3M_{pl}^2 H^2(\Omega+1) + 2M_{pl}^2\dot{H}(\Omega+1) + M_{pl}^2\ddot{\Omega} + 2M_{pl}^2 H\dot{\Omega} = -\sum_i p_i - \Lambda, \end{aligned} \tag{5.5}$$

where ρ_i and p_i are respectively the background energy density and pressure of the i^{th} matter component, that are usually assumed to be pressureless matter and radiation. They can be easily rewritten as:

$$\begin{aligned} \Lambda &= -\sum_i p_i - M_{pl}^2[(3H^2 + 2\dot{H})(\Omega+1) + \ddot{\Omega} + 2H\dot{\Omega}], \\ c &= -\frac{\sum_i(\rho_i + p_i)}{2} - \frac{M_{pl}^2}{2}[2\dot{H}(\Omega+1) + \ddot{\Omega} - H\dot{\Omega}]. \end{aligned} \tag{5.6}$$

It is worth to notice that, fixing the expansion history with H and assuming a form for one of the three EFT background functions, usually Ω, the background evolution is fully determined from (5.6) and solving the continuity equations for the matter components.
It is interesting to rewrite (5.5) in a more familiar form:

$$\begin{aligned} H^2 &= \frac{1}{3M_{pl}^2(\Omega+1)}\left(\sum_i \rho_i + \rho_{DE}\right), \\ \dot{H} &= -\frac{1}{2M_{pl}^2(\Omega+1)}\left(\sum_i \rho_i + p_i + \rho_{DE} + p_{DE}\right), \end{aligned} \tag{5.7}$$

where:

$$\begin{aligned} \rho_{DE} &= -\Lambda + 2c - 3M_{pl}^2 H\dot{\Omega}, \\ p_{DE} &= \Lambda + M_{pl}^2\ddot{\Omega} + 2M_{pl}^2 H\dot{\Omega}. \end{aligned} \tag{5.8}$$

These equations preserve the structure of the Friedmann equations with the explicit dependence on the function Ω linked to the non-minimal coupling between the scalar field and the metric.
Deriving with respect to the time the first equation of (5.7) and exploiting the second one, it is possible to obtain a sort of continuity equation for the dark energy fluid:

$$\dot{\rho}_{DE} = -3H(\rho_{DE} + p_{DE}) + 3M_{pl}^2\dot{\Omega}H^2, \tag{5.9}$$

where the last term expresses a non-conservation of the dark energy fluid, regulated by the time derivative of the EFT function Ω.

5.1.2 Stückelberg trick

As we have seen, in unitary gauge the scalar field does not appear explicitly in the action (5.3). This is useful in order to identify the operators that enter in the action and to select and map many DE/MG theories in the EFT language. On the other hand, the unitary gauge results unsuitable for the study of the evolution of linear cosmological perturbations. Indeed, in order to obtain the evolution equation for the scalar field, it is better to make it manifest through the so called Stückelberg trick, which allows to restore non linearly the time diffeomorphism invariance [81]. The procedure consists in performing the following infinitesimal time coordinate transformation [80]:

$$t \to \tilde{t} = t + \pi(x^\mu), \qquad x^i \to \tilde{x}^i = x^i, \tag{5.10}$$

where $\pi(x)$ represents the additional scalar degree of freedom that will appear explicitly in the action. Indeed, under this procedure, time-dependent functions in (5.3) will transform as:

$$f(t) \to f(t+\pi(x)) = f(t) + \dot{f}(t)\pi + \frac{\ddot{f}(t)}{2}\pi^2 + ... \tag{5.11}$$

since they are typically Taylor expanded in π. Furthermore, operators that are not 4-dimensional covariant, transform under (5.10) with the tensor transformation law, providing terms with derivatives of π. For example, the zero-zero component of the metric tensor:

$$g^{00} \to \tilde{g}^{00} = g^{00} + 2\partial_\mu\pi g^{0\mu} + \partial_\mu\pi\partial_\nu\pi g^{\mu\nu}, \tag{5.12}$$

that can be used to find the transformation for the perturbation δg^{00}. This brings the EFT action in the following form:

$$\begin{aligned} S = \int d^4x\sqrt{-g}\Big(&\frac{M_{pl}^2}{2}(1+\Omega(t+\pi))R + \Lambda(t+\pi) - c(t+\pi)[\delta g^{00} \\ &- 2\dot{\pi} + 2\dot{\pi}\delta g^{00} + 2\partial_i\pi\delta g^{0i} - \dot{\pi}^2 + \dot{\pi}^2\delta g^{00} + 2\dot{\pi}\partial_i\pi\delta g^{0i} + g^{ij}\partial_i\pi\partial_j\pi] + ...\Big) + S_M(g_{\mu\nu}, \psi_M), \end{aligned} \tag{5.13}$$

where we have considered only the background EFT functions to show the mechanism. By varying the action with respect to π, it is then possible to obtain the dynamical equation for the extra scalar degree of freedom. Given that, the Stückelberg trick has taken us out from the unitary gauge, it becomes then convenient to choose a gauge associated with the metric perturbations. The typical choice that is adopted by the cosmological code CAMB [82] and its modified version which we will use in following, is to work in the synchronous gauge, whose line element is defined in (2.20). Considering only scalar metric perturbations, the spatial perturbation of the metric h_{ij} contains two scalar degrees of freedom which are usually written in Fourier space as [83]:

$$h_{ij}(x,\tau) = \int d^3k e^{i\vec{k}\cdot\vec{x}}[k_i k_j h(k,\tau) + (k_i k_j - \frac{1}{3}\delta_{ij})6\eta(k,\tau)], \tag{5.14}$$

with h the trace of h_{ij}. Then, starting from the action in terms of the Stückelberg field it is possible to derive the equations for the perturbations at linear order. It is worth to notice that, while in the background equations only the Ω, Λ, c functions appear, in the perturbed equations all the remaining functions in action (5.3) will also affect the dynamics at linear order.
In particular, by varying the action with respect to the π field it is possible to find the dynamical equation for the additional scalar degree of freedom, which has the following form:

$$A\ddot{\pi} + B\dot{\pi} + C\dot{\pi} + k^2 D\pi + E = 0, \tag{5.15}$$

where A, B, C, D, E contains the contribution of the metric and matter perturbations and they are functions of time and scale. Their explicit expressions can be found in [83].

5.2 Mapping in the EFT language

As previously said, the advantage of the EFT formalism is the possibility of employing it for two different purposes. The first possible approach is to work in a model-independent framework where we can perform agnostic test of gravity by studying the effect of the different operators in the EFT action on the dynamics of linear perturbations. This use is usually called pure EFT approach.
On the other hand, the second possibility of applying the formalism is with the mapping EFT approach. Indeed, an advantage of the EFT language is in its capability of encompassing dark energy and modified gravity models with a single additional scalar field. This means that all these models can be found as particular cases of the EFT action. In this framework, the EFT functions of (5.3) can be expressed in terms of the functions appearing in the specific scalar-tensor theory and, as a consequence, they can reproduce the phenomenology of the specific theory. An application of this procedure will be shown in Chapter 6.
In order to map a specific theory in the EFT language, it is possible to start from the covariant action and impose the unitary gauge. Then, the two actions can be compared to identify the terms corresponding to the EFT ones. To exemplify, we can consider the simple case of the Quintessence Lagrangian (3.23) and rewrite it in unitary gauge:

$$-\frac{1}{2}\partial_\mu\phi\partial_\nu\phi g^{\mu\nu} - V(\phi) \longrightarrow -\frac{1}{2}\dot{\phi}_0^2(t)g^{00} - V(\phi_0(t)). \tag{5.16}$$

Writing the zero-zero component of the metric as $g^{00} = -1 + \delta g^{00}$ and comparing the Quintessence action with (5.3), it is straightforward to see that the mapping can be written as:

$$\Omega(t) = 0, \qquad \Lambda(t) = \frac{1}{2}\dot{\phi}_0^2 - V(\phi_0), \qquad c(t) = \frac{1}{2}\dot{\phi}_0^2, \tag{5.17}$$

while all the other EFT functions are zero.
Despite the fact that the procedure appears easy here, for some more complicated theories finding the mapping can be more cumbersome. It is then possible to work in a more general framework, exploiting the ADM decomposition of spacetime. Thanks to it, a general mapping can be derived and used to translate any model in the EFT language.

5.2.1 ADM decomposition

A natural formalism that is usually employed when dealing with the EFT approach to dark energy is the so called Arnowitt-Deser-Misner (ADM) decomposition of spacetime. The ADM formalism indeed is often used as a convenient platform for finding mapping relations between specific dark energy and modified gravity models into the EFT language. It offers a general procedure to map specific scalar-tensor theories in the EFT formalism by providing a mapping between a general Lagrangian in ADM formalism and unitary gauge and the EFT Lagrangian.
The line element in ADM coordinates is:

$$ds^2 = -N^2 dt^2 + h_{ij}(dx^i + N^i dt)(dx^j + N^j dt), \tag{5.18}$$

where N^i is the shift function, N the lapse function and h_{ij} the three-dimensional spatial metric. In this coordinate, the most general Lagrangian can be written as [87]:

$$L = L(N, \mathcal{R}, \mathcal{S}, K, \mathcal{Z}, \mathcal{U}, \mathcal{Z}_1, \mathcal{Z}_2, \alpha_1, \alpha_2, \alpha_3, \alpha_4, \alpha_5, t), \tag{5.19}$$

where in details we have:

$$\begin{aligned} &\mathcal{S} = K_{\mu\nu}K^{\mu\nu}, \;\; \mathcal{Z} = \mathcal{R}_{\mu\nu}\mathcal{R}^{\mu\nu}, \;\; \mathcal{U} = \mathcal{R}_{\mu\nu}K^{\mu\nu}, \\ &\mathcal{Z}_1 = D_i\mathcal{R}D^i\mathcal{R}, \;\; \mathcal{Z}_2 = D_i\mathcal{R}_{jk}D^i\mathcal{R}^{jk}, \;\; \alpha_1 = a^i a_i, \\ &\alpha_2 = a^i D_k D^k a_i, \;\; \alpha_3 = \mathcal{R}D_i a^i, \;\; \alpha_4 = a_i(D_k D^k)^2 a^i, \;\; \alpha_5 = D_k D^k \mathcal{R} D_i a^i, \end{aligned} \tag{5.20}$$

where $a = n^\mu D_\mu n_\nu$ and $n_\mu = N\delta_{\mu 0}$ is the normal vector to the hypersurfaces of constant time. This general action needs then be expanded up to quadratic order in perturbations while, on the other side, the EFT action needs to be rewritten in ADM form. At this point a complete mapping is naturally found comparing the two results. For more details [78].

5.3 Code implementation of the EFT formalism

A very useful application of the EFT approach to dark energy is its implementation in the Code for Anisotropies in the Microwave Background (CAMB) [82], which is a publicly available cosmological code that allows to study observables of interest in Cosmology such as the Cosmic Microwave Background, growth of structure or gravitational lensing. The implementation of the EFT approach in the Einstein-Bolzmann solver CAMB is called EFTCAMB and it is a powerful tool to study the evolution of scalar linear perturbations in the frame of dark energy and modified gravity models [83]. Indeed, thanks to the fact that it is based on the EFT formalism, it can be used both as a model-independent framework to test gravity by looking at possible modifications of linear perturbations linked to the EFT operators, but also it allows to study specific dark energy and modified gravity models that can be mapped in the EFT language.
A positive feature of the EFTCAMB code is the fact that it works without relying on any Quasi-Static approximation, that means without neglecting the time variation of the gravitational potentials and scalar field with respect to their spatial gradients. Therefore EFTCAMB is able to evolve the full set of perturbed equations, inclusive of the Klein-Gordon equation for the Stückelberg field, on all linear scales. Moreover it also checks if the considered theory is acceptable in view of viability conditions such as the ones presented in Chapter 4.
It is worth to notice that some other Einstein-Boltzmann codes, that can treat scalar-tensor theories, are available today, such as hi-class [84] and COOP [85]. Thanks to them, it was possible to check the compatibility of the their results with the ones of EFTCAMB for the overlapping regions of working of the codes [86].

EFTCAMB is structured by an hierarchy of flags that control the behaviour of the code, allowing to choose its preferred application. The main code flags called EFTflags are the starting point of the computational process and they are [18]:

- *Standard CAMB*: the code evolves the standard set of Boltzmann-Einstein equations, as predicted by General Relativity and excluding every EFT modification.

- *Pure EFT*: it is necessary to specify the background expansion history by selecting a parametrization for the equation of state of the dark energy and to choose the functional forms of the EFT functions.
- *Alternative parametrizations*: it allows to choose model-independent parametrizations present in the literature written in terms of the EFT functions.
- *Designer mapping EFT*: the expansion history needs to be chosen by selecting a parametrization for the equation of state of the dark energy. Then, using the mapping for the model of interest, the code computes the EFT functions evolution.
- *Full EFT mapping*: the model needs to be fully specified, in particular the background expansion history is found solving the specific equations of the model.

It is worth to notice that the code works with the following second-order EFT functions, redefined in order to be dimensionless:

$$\begin{aligned} &\gamma_1 = \frac{M_2^4}{M_{pl}^2 H_0^2}, \quad \gamma_2 = \frac{\bar{M}_1^3}{M_{pl}^2 H_0}, \quad \gamma_3 = \frac{\bar{M}_2^2}{M_{pl}^2}, \\ &\gamma_4 = \frac{\bar{M}_3^2}{M_{pl}^2}, \quad \gamma_5 = \frac{\hat{M}^2}{M_{pl}^2}, \quad \gamma_6 = \frac{m_2^2}{M_{pl}^2}. \end{aligned} \tag{5.21}$$

5.3.1 Full-mapping approach

In view of the following Chapter, it is interesting to explore in more details how to implement in EFTCAMB a new model with the full-mapping approach.
In this framework, a fully specified model needs to be chosen and the background expansion history is found solving the equations of the model. For the implementation in EFTCAMB, this translates to some steps that provide to the code the right information.
Firstly, a complete mapping between the covariant action of the chosen model and the EFT action needs to be derived, as explained in the previous paragraph. Then, one has to create a new module of the code by means of which the cosmological and model parameters are fed to EFTCAMB, which uses them to solve the specific background equations of the theory. Under these conditions, the time evolution of the EFT functions can be derived and they can be used to evolve the full set of perturbed Einstein-Boltzmann equations.
In the next Chapter, we will apply this procedure to study a specific MG model, called Generalized Brans-Dicke theory.

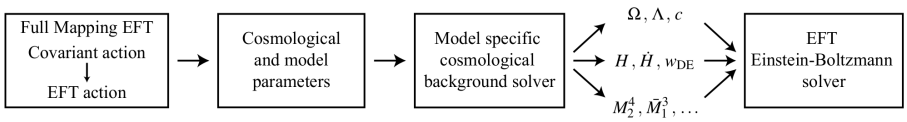

Figure 5.1: Logical steps of the full-mapping implementation in EFTCAMB. Taken from [88].

Chapter 6

Generalized Brans-Dicke model

This last Chapter consists in the analysis of a specific modified gravity model, called Generalized Brans-Dicke theory. This theory was firstly proposed and studied in the original paper [89]. In the following, applying all the notions exposed in the previous part of this Thesis, I will outline my work of studying the Generalized Brans-Dicke theory via the Effective Field Theory approach to dark energy and the cosmological code EFTCAMB using a Full-Mapping procedure.

6.1 Generalized Brans-Dicke model

The action of the considered Generelized Brans-Dicke theory is [89]:

$$S = \int d^4x\sqrt{-g}\left(\frac{1}{2}F(\phi)R - \frac{1}{2}B(\phi)\partial_\mu\phi\partial^\mu\phi + \xi(\phi)\Box\phi\partial_\mu\phi\partial^\mu\phi\right) + S_M(g_{\mu\nu},\psi_M), \tag{6.1}$$

in which we have an additional scalar degree of freedom ϕ, that is non-minimally coupled to the metric via the term $F(\phi)R$ in the action and with the term $\xi(\phi)\Box\phi\partial_\mu\phi\partial^\mu\phi$ which describes a non-linear self-interaction of the scalar field. $F(\phi)$, $B(\phi)$ and $\xi(\phi)$ are functions of the scalar field. Clearly, this theory is a further extension of the canonical Generalized Brans-Dicke theories present in the literature with action (3.48). Indeed, (6.1) describes a theory without the field potential and with the characterising term $\xi(\phi)\Box\phi\partial_\mu\phi\partial^\mu\phi$, which can be found in the Cubic Galileons action, in (3.62).
It is known that this class of theories have screening mechanisms that allow to recover General Relativity in high density regimes constrained by local tests of gravity in the solar system, as explained in Chapter 4. Indeed, the mechanisms at work when considering the broad class of Brans-Dicke theories are essentially two. The Chameleon mechanism usually provides the screening for Brans-Dicke theories with the field potential, where it is possible to find the environmental dependence for the effective mass of the field. Furthermore, in the presence of terms of non-linear self-interaction of the scalar field, as $\xi(\phi)\Box\phi\partial_\mu\phi\partial^\mu\phi$, the Vainshtein mechanism can also come into play allowing to recover General Relativity for scales smaller than the so called Vainshtein radius [20].
By varying the action with respect to the metric and using (1.4) it is possible to find the covariant equation:

$$\begin{aligned}&-\frac{1}{2}g_{\mu\nu}\left(\frac{1}{2}F(\phi)R - \frac{1}{2}B(\phi)(g^{\alpha\beta}\partial_\alpha\phi\partial_\beta\phi) - \xi(\phi)\Box\phi(\partial_\sigma\phi\partial^\sigma\phi)\right) + \frac{1}{2}F(\phi)R_{\mu\nu} - \frac{1}{2}(D_\nu D_\mu F(\phi) - F(\phi)g_{\mu\nu})\\ &-\frac{1}{2}B(\phi)\partial_\mu\phi\partial_\nu\phi - D_\mu(\xi(\phi)\partial_\nu\phi(\partial_\sigma\phi\partial^\sigma\phi)) + \frac{1}{2}g_{\mu\nu}D_\rho(\xi(\phi)\partial^\rho\phi(\partial_\sigma\phi\partial^\sigma\phi)) + \xi(\phi)\partial_\mu\phi\partial_\nu\phi = \frac{T_{\mu\nu}}{2},\end{aligned} \tag{6.2}$$

then, assuming a flat FLRW spacetime and perfect fluids of pressureless matter and radiation as the matter components, it is possible to find the following equations:

$$\begin{aligned} 3FH^2 &= \frac{B\dot{\phi}^2}{2} - 3HF_{,\phi}\dot{\phi} + (6H\xi - \xi_{,\phi}\dot{\phi})\phi^3 + \rho_m + \rho_r, \\ -2F\dot{H} &= (F_{,\phi} - 2\xi\dot{\phi}^2)\ddot{\phi} + [B\dot{\phi} + F_{,\phi\phi}\dot{\phi} - HF_{,\phi} + \dot{\phi}^2(6H\xi - 2\xi_{,\phi})]\dot{\phi} + \rho_m + \frac{4\rho_r}{3}, \end{aligned} \tag{6.3}$$

were we consider the background value of the scalar field, therefore we have $\phi = \phi(t)$. They are respectively the (00) and the (ij) components of (6.2). Under the same assumptions, varying the action with respect to the scalar field, it is possible to find:

$$(B - 4\dot{\phi}^2\xi_{,\phi} + 12H\xi\dot{\phi})\ddot{\phi} + [3HB + \frac{B_{,\phi}\dot{\phi}}{2} - \xi_{,\phi\phi}\dot{\phi}^3 + 6\xi(3H^2 + \dot{H}\dot{\phi})]\dot{\phi} - 3F_{,\phi}(2H^2 + \dot{H}) = 0, \tag{6.4}$$

where we have adopted the notation $_{,\phi} = \frac{\partial}{\partial\phi}$.
Following [89], we then restrict the three functions $F(\phi)$, $B(\phi)$ and $\xi(\phi)$ in action (6.1) to a power-law form:

$$F(\phi) = M_{pl}^2\left(\frac{\phi}{M_{pl}}\right)^{3-n}, \quad B(\phi) = \omega\left(\frac{\phi}{M_{pl}}\right)^{1-n}, \quad \xi(\phi) = (\lambda/\mu^3)\left(\frac{\phi}{M_{pl}}\right)^{-n}, \tag{6.5}$$

where n, ω and λ are dimensionless constants while μ is a constant with dimension of a mass. It is possible to see that, for the theory to be viable, we need to have $\lambda > 0$ [89]. The choice (6.5) is due to the requirement of obtaining deSitter attractor solutions at late time, which is essential in order to have an alternative theory that can explain the late time accelerated expansion of our Universe discussed in Chapter 1.
Indeed, defining the dimensionless variable:

$$x = \frac{\dot{\phi}}{H\phi}, \tag{6.6}$$

it is possible to solve (6.3) and (6.4) looking for deSitter solutions in which x and H are constant, respectively with the value x_{ds} and H_{ds}. Studying the algebraic equations at the deSitter fixed point it is then possible to fix some of the constants of the model: the values of λ and of the mass scale μ can be found as a function of x_{ds} and H_{ds}, thus they can be fixed from the request of having late time cosmic acceleration. In particular the mass scale μ can be fixed as:

$$\mu = (M_{pl}H_{ds}^2)^{1/3}. \tag{6.7}$$

Moreover it is worth to notice that, under the assumption (6.5), the choice $n = 2$ allows to recover the original Brans-Dicke action [41] with $\omega = \omega_{BD}$. Similarly for $n = 3$ the $F(\phi)$ function is constant and (6.1) corresponds to a k-essence theory. Clearly, in both cases we have the additional term $\propto \xi(\phi)$.
In order to find a more familiar form for the constraint equation of (6.3), we can rewrite it in term of the x variable defined in (6.6):

$$1 = \frac{B\phi^2}{6F}x^2 - \frac{\phi F_{,\phi}}{F}x + \frac{2\xi\phi^3}{F}H^2x^3\left(1 - \frac{\phi\xi_{,\phi}}{6\xi}x\right) + \frac{\rho_m}{3FH^2} + \frac{\rho_r}{3FH^2}. \tag{6.8}$$

It is now convenient to redefine the density parameters in the following way:

$$\Omega_r := \frac{\rho_r}{3FH^2}, \qquad \Omega_m := \frac{\rho_m}{3FH^2} \tag{6.9}$$

and introducing another dimensionless variable:

$$y = \lambda x^2\frac{H^2}{H_{ds}^2}, \tag{6.10}$$

it is now possible to rewrite the constraint equation (6.8) as:

$$1 = \Omega_{DE} + \Omega_r + \Omega_m, \tag{6.11}$$

with:

$$\Omega_{DE} = \frac{\omega x^2}{6} - (3 - n)x + 2xy\left(1 + \frac{nx}{6}\right). \tag{6.12}$$

6.2 Mapping into EFT language

As anticipated, our purpose is to study the cosmology of the Generalized Brans-Dicke model, in particular cosmological perturbations, and we have decided to do so implementing the Generalized Brans-Dicke theory in the cosmological code EFTCAMB, via the Full-Mapping approach. This requires to find a mapping between the considered action and the EFT action (5.3).
To do so, we will need to rewrite (6.1) in unitary gauge and expand it up to second order in perturbations. Having done this, finding the mapping between the two actions will simply consist in the identification of functional form of the EFT functions in the Generalized Brans-Dicke action by comparing the two Lagrangians.
Looking at (6.1), it is clear that for the first two terms the computations are straightforward. On the other hand, the term $\xi(\phi)\Box\phi\partial_\mu\phi\partial^\mu\phi$ will require some more calculations. In order to find a more convenient form for this last term we have to consider some of the basic quantities in EFT formalism. In particular, it is useful to compute the trace of the extrinsic curvature $K_{\mu\nu}$:

$$K = g^{\mu\nu}K_{\mu\nu} = h^{\mu\nu}K_{\mu\nu} = D_\mu n^\mu, \tag{6.13}$$

where we have exploited the definition of the spatial metric on constant-time hypersurfaces $h^{\mu\nu} = g^{\mu\nu} + n^\mu n^\nu$ and of the extrinsic curvature $K_{\mu\nu} = h^\lambda_\mu D_\lambda n_\nu$, with n^μ the unit vector defined in (5.2) and we have used the property $n^\mu K_{\mu\nu} = 0$ [87].
According to the EFT approach, we want to expand our quantities around a flat FLRW background. It is then easy to check that:

$$K = -3H + \delta K. \tag{6.14}$$

We can now rewrite the last term in the action in a more convenient form:

$$\begin{aligned}
\xi(\phi)\Box\phi(\partial\phi)^2 =& -\partial_\mu(\xi(\phi)(\partial\phi)^2)\partial^\mu\phi \\
=&(-(\partial\phi)^2)^{3/2}\xi_{,\phi}(\phi)\partial_\mu\phi\frac{\partial^\mu\phi}{\sqrt{-(\partial\phi)^2}} + \frac{2}{3}\xi(\phi)\partial_\mu(-(\partial\phi)^2)^{3/2}\frac{\partial^\mu\phi}{\sqrt{-(\partial\phi)^2}} \\
=& -\xi_{,\phi}(\phi)(-(\partial\phi)^2)^2 - \frac{2}{3}(-(\partial\phi)^2)^{3/2}D_\mu\left(\xi(\phi)\frac{\partial^\mu\phi}{\sqrt{-(\partial\phi)^2}}\right) \\
=& -\xi_{,\phi}(\phi)(-(\partial\phi)^2)^2 - \frac{2}{3}(-(\partial\phi)^2)^{3/2}\xi_{,\phi}(\phi)\partial_\mu\phi\frac{\partial^\mu\phi}{\sqrt{-(\partial\phi)^2}} - \frac{2}{3}(-(\partial\phi)^2)^{3/2}\xi(\phi)K \\
=& -\frac{\xi_{,\phi}(\phi)}{3}(-(\partial\phi)^2)^2 - \frac{2}{3}\xi(\phi)(-(\partial\phi)^2)^{3/2}K,
\end{aligned} \tag{6.15}$$

where we have integrated by parts twice and we have rearranged the term in order to obtain the expression (6.13) for the trace of the extrinsic curvature.
Exploiting the last expression of (6.15), we can go in unitary gauge:

$$\begin{aligned}
\xi\Box\phi(\partial\phi)^2 \to& -\frac{\xi_{,\phi}}{3}(-g^{00})^2\dot\phi^4 - \frac{2}{3}[(-g^{00})^{3/2}-1]\dot\phi^3\xi K - \frac{2}{3}\dot\phi^3\xi K \\
=& -\frac{\xi_{,\phi}}{3}(-g^{00})^2\dot\phi^4 - \frac{2}{3}[(-g^{00}))^{3/2}-1]\dot\phi^3\xi K - \frac{2}{3}\xi_{,\phi}\dot\phi^4\sqrt{-g^{00}} - 2\xi\dot\phi^2\ddot\phi\sqrt{-g^{00}} \\
=& -\frac{\xi_{,\phi}}{3}(-g^{00})^2\dot\phi^4 + 2H\xi\dot\phi^3[(-g^{00})^{3/2}-1] - \frac{2}{3}\xi\dot\phi^3[(-g^{00})^{3/2}-1]\delta K \\
&-\frac{2}{3}\xi_{,\phi}\dot\phi^4\sqrt{-g^{00}} - 2\xi\dot\phi^2\ddot\phi\sqrt{-g^{00}},
\end{aligned} \tag{6.16}$$

where in the second line we have integrated by parts the last term and in the third line we have exploited (6.14).
Thus, writing the full action (6.1) in unitary gauge we get:

$$\begin{aligned}
S = \int d^4x\sqrt{-g}\Big(&\frac{1}{2}FR - \frac{B}{2}g^{00}\dot\phi^2 - \frac{\xi_{,\phi}}{3}(-g^{00})^2\dot\phi^4 + 2H\xi\dot\phi^3[(-g^{00})^{3/2}-1] \\
&-\frac{2}{3}\xi\dot\phi^3[(-g^{00})^{3/2}-1]\delta K - \frac{2}{3}\xi_{,\phi}\dot\phi^4\sqrt{-g^{00}} - 2\xi\dot\phi^2\ddot\phi\sqrt{-g^{00}}\Big).
\end{aligned} \tag{6.17}$$

Considering the metric perturbation $\delta g^{00} = 1 + g^{00}$ and expanding up to second order, we can find the final form:

$$S = \int d^4x\sqrt{-g}\Big[\frac{1}{2}FR + \frac{B}{2}\dot{\phi}^2 - \xi_{,\phi}\dot{\phi}^4 - 2\xi\dot{\phi}^2\ddot{\phi} - \Big(\frac{B}{2}\dot{\phi}^2 - \xi_{,\phi}\dot{\phi}^4 + 3H\xi\dot{\phi}^3 - \xi(t)\dot{\phi}^2\ddot{\phi}\Big)\delta g^{00} + \frac{1}{2}\Big(-\frac{1}{2}\xi_{,\phi}\dot{\phi}^4 + \frac{3}{2}H\xi\dot{\phi}^3 + \frac{1}{2}\xi\dot{\phi}^2\ddot{\phi}\Big)(\delta g^{00})^2 - \frac{1}{2}(-2\xi\dot{\phi}^3)\delta g^{00}\delta K + ...\Big]. \tag{6.18}$$

Comparing (6.18) and (5.3), it is now trivial to find the following mapping for the Generalized Brans-Dicke theory:

$$\begin{aligned}
\Omega(\phi) &= \frac{F(\phi)}{M_{pl}^2} - 1,\\
\Lambda(\phi) &= \frac{1}{2}B(\phi)\dot{\phi}^2 - \xi_\phi\dot{\phi}^4 - 2\ddot{\phi}\dot{\phi}^2\xi(\phi),\\
c(\phi) &= \frac{1}{2}B(\phi)\dot{\phi}^2 + \dot{\phi}^2\xi(\phi)(3H\dot{\phi} - \ddot{\phi}) - \xi_\phi\dot{\phi}^4,\\
\bar{M}_1^3(\phi) &= -2\xi(\phi)\dot{\phi}^3,\\
M_2^4(\phi) &= \frac{1}{2}\xi(\phi)\dot{\phi}^2(3H\dot{\phi} + \ddot{\phi}) - \frac{1}{2}\xi_\phi\dot{\phi}^4,
\end{aligned} \tag{6.19}$$

and all the other EFT functions are zero.
For a reason that will become clear in the next paragraph, it is useful to rewrite the mapping relations (6.19) in terms of the dimensionless variable x and y defined in (6.6) and (6.10) and of the function F:

$$\begin{aligned}
\Omega(t) &= \frac{F}{M_{pl}^2} - 1,\\
\Lambda(t) &= \Big(\frac{\omega x^2}{2} - \frac{2\dot{x}y}{H} - \frac{2\dot{H}xy}{H^2} - 2x^2y + nx^2y\Big)FH^2,\\
c(t) &= \Big(\frac{\omega x^2}{2} + 3xy - \frac{\dot{x}y}{H} - \frac{\dot{H}xy}{H^2} - x^2y + nx^2y\Big)FH^2,\\
\bar{M}_1^3(t) &= -2xyFH,\\
M_2^4(t) &= \Big(\frac{3xy}{2} + \frac{\dot{x}y}{2H} + \frac{\dot{H}xy}{2H^2} + \frac{x^2y}{2} + \frac{nx^2y}{2}\Big)FH^2.
\end{aligned} \tag{6.20}$$

It is then clear that we can recover the time evolution of the EFT functions solving the background equations of the theory for the x, y, F and H variables.

6.3 Background solution

As anticipated, the next step in our work is to find the time evolution of the x, y, F and H variables. To do so we will have to solve three dynamical equations while the dynamics of the fourth variable can be found thanks to the constraint equation (6.8).
Considering the assumption (6.5) for the F function and deriving it with respect to $N = ln(a)$, it is possible to find the following first-order differential equation for F:

$$F' = (3 - n)Fx, \tag{6.21}$$

where $' = \frac{d}{dN}$ and we used that fact that $\frac{d}{dN} = \frac{1}{H}\frac{d}{dt}$.
Similarly, from (6.3) and (6.4) it is possible to find the following first-order differential equations for x and y [89]:

$$x' = -\frac{d_2}{d_1}x - \frac{9x}{2\omega d_1}(3 - n - 2y)\Big(\Omega_m + \frac{4}{3}\Omega_r\Big) + \frac{6(3-n)x}{\omega d_1} - x^2 - x\frac{H'}{H}, \tag{6.22}$$

$$y' = -2y\left[\frac{d_2}{d_1} + \frac{9}{2\omega d_1}(3-n-2y)\left(\Omega_m + \frac{4}{3}\Omega_r\right) - \frac{6(3-n)}{\omega d_1} + x\right], \tag{6.23}$$

with:

$$d_1 = \frac{12}{\omega}y + x\left[1 + \frac{4n}{\omega}y + \frac{3}{2\omega}(3-n-2y)^2\right], \tag{6.24}$$

$$\begin{aligned} d_2 =& \frac{18}{\omega}y + x\left[3 + \frac{1-n}{2}x - \frac{n(n+1)}{\omega}xy + 3(3-n-2y)\left(\frac{x}{2}\right.\right. \\ &\left.\left. + \frac{(3-n)(2-n)}{2\omega}x - \frac{3-n}{2\omega} + \frac{3}{\omega}y\left(1 + \frac{n}{3}x\right)\right)\right] \end{aligned} \tag{6.25}$$

and

$$\begin{aligned} \frac{H'}{H} =& \frac{1}{2}(3-n-2y)\left[\frac{d_2}{d_1}x + \frac{9x}{2\omega d_1}(3-n-2y)\left(\Omega_m + \frac{4}{3}\Omega_r\right) - \frac{6(3-n)}{\omega d_1}x\right] \\ &- \frac{1}{2}x[\omega x + (3-n)(2-n)x - (3-n) + y(6+2nx)] - \frac{3}{2}\Omega_m - 2\Omega_r. \end{aligned} \tag{6.26}$$

where (6.26) can be substituted in (6.22) and (6.23) to find the evolution of x and y. It is worth to underline that Ω_r and Ω_m are the variables defined in (6.9).
Therefore, considering equations (6.21), (6.22) and (6.23), we have a dynamical system of first-order coupled differential equations that can be solved numerically. Once the solution of the dynamical system is obtained, it is possible to recover the evolution of the Hubble parameter exploiting the constraint equation (6.11). Indeed, rearranging the equation and substituting (6.9), we get:

$$H = \sqrt{\frac{\rho_m + \rho_r}{3F(1-\Omega_{DE})}}, \tag{6.27}$$

that can be easily solved knowing the evolution of x, y and F and using (6.12). Furthermore for the matter and radiation fluids, we assume the standard continuity equations.
It is worth to notice that, in order to recover General Relativity in the early Universe, we have to require that the initial value of the field ϕ_i is close to M_{pl} [89]. This constrains the initial value of F to be $F_i \simeq M_{pl}^2$, as we can see from (6.5).
In order to solve numerically the dynamical system of differential equations, we can now write a Python script with the differential equations, in particular we have decided to use a fourth order Runge-Kutta method [90].
As we can see from Figure 6.1, the x variable is very small during the radiation and matter epoch meaning that the initial value of the field remains almost frozen. Only at recent times x grows to the order of unity and the scalar field starts to evolve allowing the Universe to enter a period of accelerated expansion.

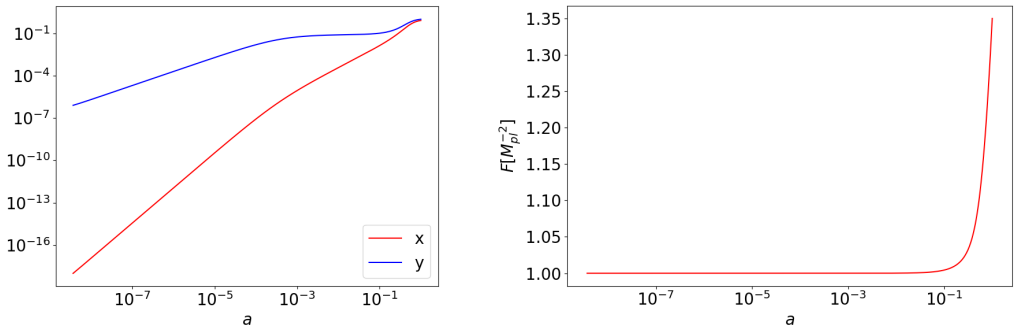

Figure 6.1: Evolution of the x, y (left panel) and F (right panel) variables as a function of the scale factor a for $n = 2.5$ and $\omega = -10$. These solutions are obtained integrating (6.21), (6.22) and (6.23) from $a_i = 3.7 \cdot 10^{-9}$ to $a_0 = 1$ and assuming $x_i \sim 10^{-18}$ and $y_i \sim 8 \cdot 10^{-7}$.

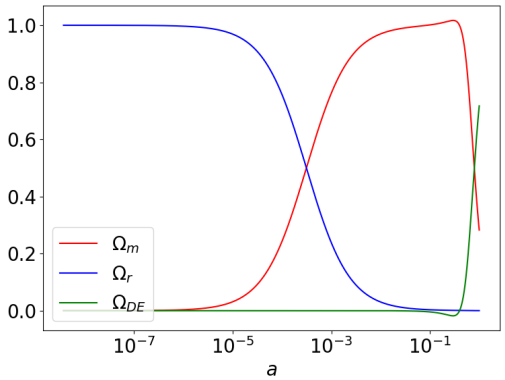

Figure 6.2: Time evolution of the densities parameters as defined in (6.9) and (6.12) obtained solving the background equations with $n = 2.5$ and $\omega = -10$. As before, we have integrated from $a_i = 3.7 \cdot 10^{-9}$ to $a_0 = 1$ and assumed $x_i \sim 10^{-18}$ and $y_i \sim 8 \cdot 10^{-7}$.

6.4 Generalized Brans-Dicke in EFTCAMB

To implement the Generalized Brans-Dicke theory (6.1) in EFTCAMB via the Full-Mapping approach, we have to write a new module of EFTCAMB that provides to the code all the information needed to compute the time evolution of the EFT functions.
As before, the module has to solve the background equations of the specific model but, unlike the python script, it has to be written in the proper way in order to interface with the whole EFTCAMB code. Indeed, we have to use the Fortran programming language, and to specify some subroutines that initialise and solve the background of the model by integrating the dynamical system of differential equations. Moreover, the mapping relations (6.20) are also implemented in the code to recover the time evolution of the EFT functions.
More in details, in the code we require the system of first-order differential equations to satisfy the following boundary condition today:

$$\Omega^0_{DE} = \frac{\omega x_0^2}{6} - (3-n)x_0 + 2x_0 y_0 \left(1 + \frac{n x_0}{6}\right), \tag{6.28}$$

that imposes to recover the observed dark energy parameter density today. This can be realized tuning one of the two initial condition of the x or y variable with a bisection algorithm [90]. This method consists in iteratively solving the background equation starting from different initial conditions, for example for the x variable. At the end of each iteration the code will then compute the tolerance between the expected and obtained dark energy density parameter. When the required tolerance is met, the iterations stop and the code computes the time evolution of the EFT functions. In this way, the code can reproduce the today values of the cosmological density parameters exactly.
As a consequence, the free parameters of the theory reduce to be only two: the n parameter which is linked to the exponent of the power-law shape assumed for the free-functions in action (6.1) and the ω parameter that multiplies the kinetic term, as we can see from (6.5). The two model parameters together with all the cosmological parameters can be set with a parameter file. Changing the values of the parameters in this file allows to use the code without having to touch its root modules.
We validated the results using the Python script that solves the same set of equations and computing quantities of interest with and without employing the mapping relations. Finding good agreement for all the different checks of both the mapping and the background solver, we were able to establish that our new module is properly working in EFTCAMB. Consequently, the computational power of the code can now be exploited to study the Generalized Brans-Dicke model and its phenomenological peculiarities. For example, as we can see in Figure 6.3, a useful quantity that we can plot using EFTCAMB is the ratio of the Hubble parameter of the Generalized Brans-Dicke

theory and the ΛCDM theory.

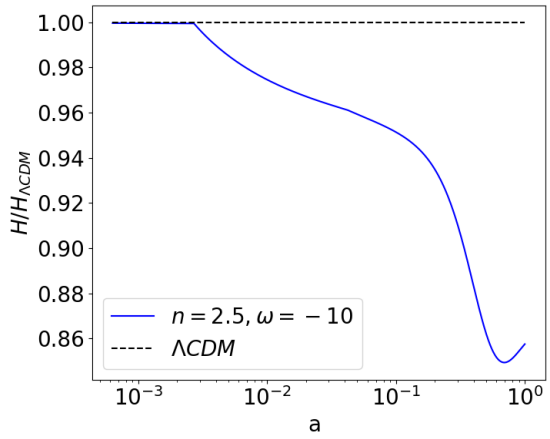

Figure 6.3: Ratio of Hubble parameter of the Generalized Brans-Dicke model, with $n = 2.5$ and $\omega = -10$, and the ΛCDM model computed via EFTCAMB.

6.5 Viable parameter space

The first part in our analysis of the Generalized Brans-Dicke model consists in restricting the viable region of the model parameter space with the requirement of avoiding unstable behaviour of the theory.
To do so, we can exploit the viability priors, already implemented in EFTCAMB, which apply to the EFT functions in order to ensure the stability of the considered theory. In particular, we can use EFTCAMB to check for both mathematical and physical conditions. In the full set of physical priors, ghost and gradient instabilities are considered for the full class of Horndeski models, which includes also the Generalized Brans-Dicke theory. In addition, the code is also provided with a set of mathematical, or classical, stability conditions that check the stability of the perturbations in the dark sector. They can be recovered studying the equation (5.15) for the π Stückelberg field . In particular, they require the π equation to be well-defined and to avoid exponential growth of π perturbations.

For the Generalized Brans-Dicke model, we checked the stability at recent times between $a_i = 0.1$ and a_0, sampling the parameter space for different combinations of the two model parameters. Indeed, as we saw in the previous section, the effect of the additional scalar field becomes relevant only recently in the Universe expansion history.
We obtain that we have to restrict the viable parameter space to negative values of the ω parameter and to $n \lesssim 3$. Then, we can notice that the lower bound on n decreases with the value of ω which does not have a lower bound. In particular, as we can see from Figure 6.4, for $\omega > -3$, the n parameter is restricted in the interval $2 \lesssim n \lesssim 3$. This interval quickly shrinks towards $n \sim 3$ as ω goes to zero. Our result is consistent with the conditions obtained via the dynamical analysis in [89], that studies the viability conditions for the system of dynamical equations at the fixed points correspondent to the matter and deSitter cosmological epochs.
Finally, we can find a second region where $n \lesssim 2$ and the background equations fail in reproducing a viable expansion history. For example, we observe that for combinations of parameters in this area, the dark energy density parameter always tends to negative values making the background solutions unphysical.
The results obtained in this section will be used to set theoretical priors for the MCMC likelihood analysis of the next section.

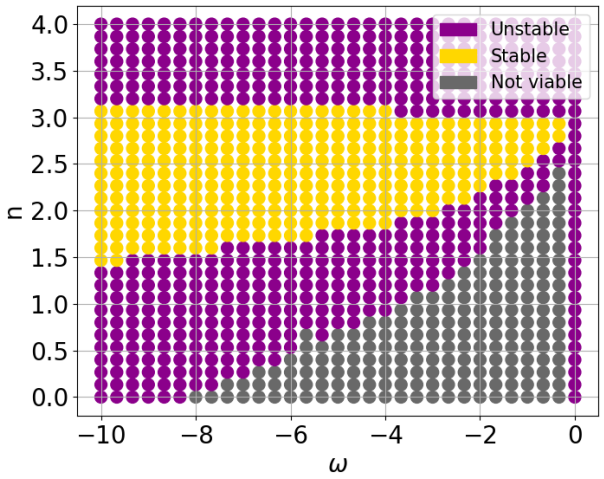

Figure 6.4: Viable parameter space for the ω and n parameters of the Generalized Brans-Dicke action, obtained imposing physical and mathematical theoretical priors.

6.6 Cosmological features

Once we have studied the effects of the theoretical priors on the parameter space, we can start investigating the phenomenology of cosmological perturbations assuming the Generalized Brans-Dicke model, looking at power spectra of interest that can be easily computed with EFTCAMB. For example, in Figure 6.5 and in Figure 6.6 we plot the temperature anisotropies power spectrum, the matter power spectrum and the CMB lensing power spectrum for the same choice of parameters.

It is possible to notice that the Generalized Brans-Dicke model entails two kind of modifications to the CMB temperature anisotropies power spectrum: the shift in positions of the acoustic peaks and a modification of the Integrated Sachs-Wolfe (ISW) effect on large scales.

In particular, for lower values of n, the shape at low multipoles is substantially different from that predicted by the ΛCDM model. Indeed, taking $n = 2$, which is close to the lower bound of the viable range for the n parameter, the spectrum displays a bump on large scales, that increases for bigger values of ω. On the contrary, considering values of n close to the upper bound of the viable range, the anomaly is cured and the shape of ISW plateau tracks better the trend of the ΛCDM model. This effect can be linked to a modification in the late time evolution of the gravitational potentials, whose time derivatives directly impact the ISW tail. Moreover, we already know that the internal consistency of the ΛCDM model shows a mild tension between Planck CMB temperature anisotropies data and the ΛCDM fit at low multipoles, as noticed in [3]. In particular, a conspicuous dip, not easily explainable in terms of instrumental systematic or foreground, is observed for $20 \lesssim l \lesssim 30$. Noticing that the Generalized Brans-Dicke model can introduce modifications at large scale, we expect the data to prefer values of the model parameters that produce a decrease in the amplitude at low multipoles. This is possible for values of n close to 3.

On the other hand, the shift in the positions of the acoustic peaks might be understood in terms of the modifications of the background expansion history, which can affect the distance to the surface of last scattering. As we can see in Figure 6.3, while at early times the Hubble parameter of the Generalized Brans-Dicke theory mimics the time evolution of the ΛCDM, at late time this is no more true and H is smaller than $H_{\Lambda CDM}$ featuring the late time dips in the ratio $H/H_{\Lambda CDM}$. A smaller Hubble parameter can indeed affect, in particular increase, the angular diameter distance to the surface of last scattering, producing the observed shift in the peaks positions.

Furthermore, considering the matter and the CMB lensing power spectra we can see that the Generalized Brans-Dicke theory predicts an enhancement in both spectra with respect to ΛCDM. Therefore, the result for the matter power spectrum indicates that the modification of gravity

introduced by the Generalized Brans-Dicke model increases the formation of linear structures, conclusion in agreement with other results in the literature regarding cubic Galileon theories [91]-[92]. Moreover, especially for the lensing power spectrum we clearly observe that the enhancement increases for smaller value of n. This, together with the feature already observed on the ISW effect, are first hints that stringent constraints on the parameter space will come from the analysis with cosmological data.

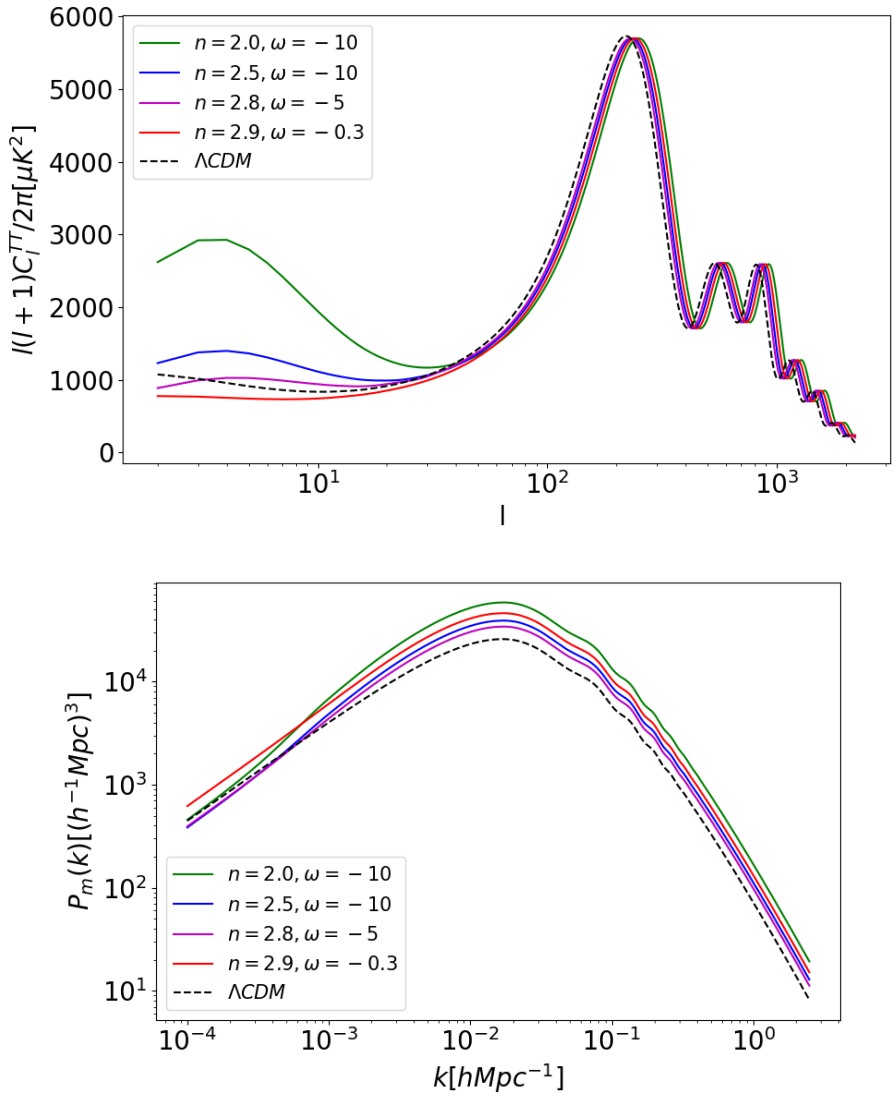

Figure 6.5: From top to bottom: temperature anisotropies and matter power spectra for different choices of the model parameters within the viable parameter space, obtained from the theoretical priors. The coloured lines are the Generalized Brans-Dicke theoretical predictions, the black dotted line is the ΛCDM expectation.

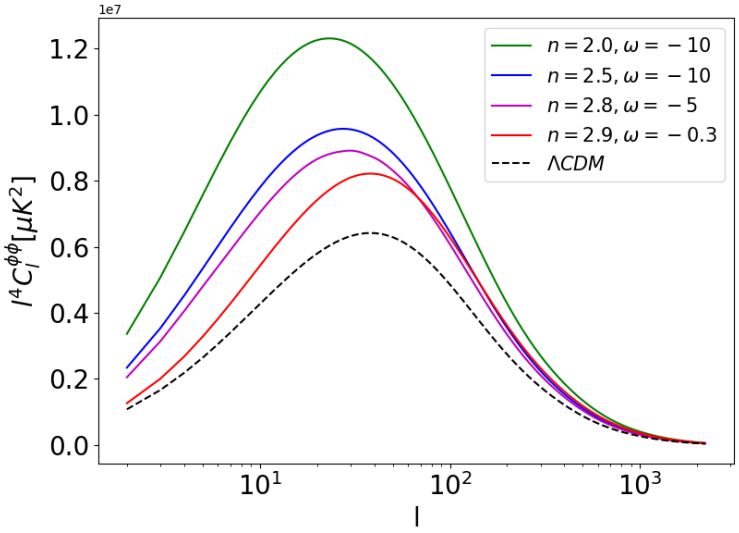

Figure 6.6: CMB lensing (right) power spectrum for different choices of the model parameters within the viable parameter space, obtained from the theoretical priors. The coloured lines are the Generalized Brans-Dicke theoretical predictions, the black dotted line is the ΛCDM expectation.

6.7 MCMC likelihood analysis

We now want to constraint the model parameters using recent cosmological dataset. Indeed, until now our approach consisted in computing the expected distribution of data, assuming the parameters as known. Oppositely, we can change approach and use the data for parameter estimations, that means to find the posterior probability distribution of the parameters given the data.
To do so, we can employ the Monte Carlo Markov Chain (MCMC) technique based on a Bayesian analysis. Identifying with θ the set of parameters that we want to estimate and x the cosmological data, the Bayes's theorem states [93]:

$$p(\theta|x) = \frac{p(x|\theta)p(\theta)}{p(x)}, \tag{6.29}$$

where $p(\theta|x)$ is the posterior probability distribution of the set of parameters, $p(x|\theta)$ is the likelihood, that is the probability distribution of data given the parameters, and $p(\theta)$ is the parameters prior, that can be known from the theory or from previous experiment, in our case we have already seen some theoretical priors that constrain the model parameters. Finally, $p(x)$ is called the evidence and, for our purposes, it is just a normalisation factor.
Clearly, computing these quantities is a complicated task since we have to take into account a multi-dimensional parameter space. To make this feasible, a useful approach is to sample the parameter space with MCMC approach. With MCMC we can generate a set of points in the parameter space whose distribution function allows to recover the posterior probability. The MCMC moves in the parameter space following a Markov process, this means that each step depends only on the previous one, every new point is accepted or rejected in the chain with a probability that depends on the ratio between the likelihood at the previous and at new point. One of the most popular algorithm is the Metropolis-Hastings, which calculates the probability of transition from an old to a new point randomly generated from a proposal distribution of steps.
Given that the Markov Chain starts from a random point, there will be an early part of the chain in which a dependence on the starting point is still preserved, this is called burn-in phase and it has to be ignored in the analysis.
Finally, in order to check the convergence of the theory it is crucial to use a proper convergence test; in the CosmoMC software, on which the following work is based on, the Gelman-Rubin convergence criterion is implemented. The basic idea under this criterion is the fact that, running

different chains based on the same data, we expect that the mean of each chain should agree within some tolerance with the mean of the combined chains as a single dataset.
A useful quantity that can be extrapolated is the marginal distribution of a single parameter and it is obtained by integrating over all the other parameters with a process called marginalisation. A result often used is the marginalisation of the parameters in pairs since it allows to explore more complex results.
As anticipated, the MCMC technique is implemented in the CosmoMC software [94]-[95]. In particular, a modified version of the CosmoMC software has been created and it can interface with the EFTCAMB code. This allows to explore and further constrain the parameter space of DE/MG models implemented in EFTCAMB, performing a fit to cosmological data.

6.7.1 MCMC analysis of Generalized Brans-Dicke model

Datasets

For the likelihood analysis we considered mainly two datasetes: the JLA ('Joint Light-curve Analysis') dataset [96], which allows to probe the background, and Planck 2018 data for CMB, as the perturbations observable.
The JLA contains data of Type Ia SNe from SDSS-II (Sloan Digital Sky Suervey) and SNLS (Supernova Legacy Survey) collaborations, gathering a total of 740 Type Ia SNe from low redshift ($z < 1$) to high redshift ($z \sim 1$). For the Planck data instead, we used the TEB Plik likelihood which contains the temperature and polarization data at all multipoles [3].
For both the datasets we run simultaneously a total of 8 chains and we constrain the ω and n parameter with the theoretical priors discussed in the previous paragraph.

Results

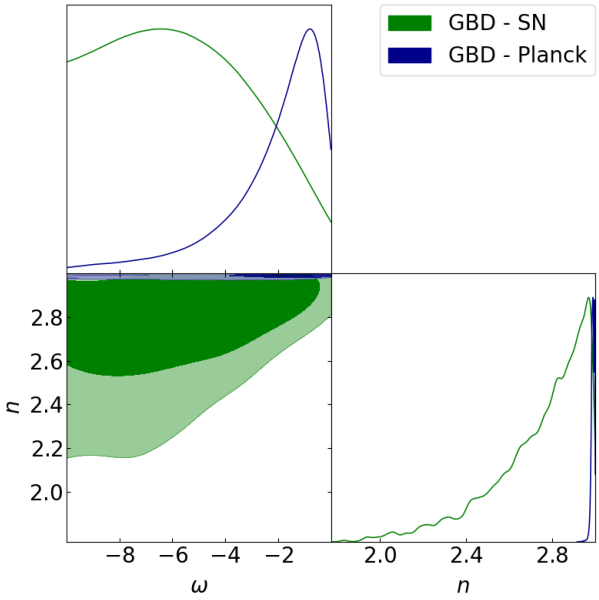

Figure 6.7: Two-dimensional observational bounds on the combinations of (ω, n) model parameters. The colored regions correspond to the parameter space constrained by the Planck (blue) and Supernovae (SN) (green) datasets at 68% (inside) and 95% (outside) CL limits. The one-dimensional plots show the marginalized parameter constraints.

As we can see in Figure 6.7, the (ω, n) parameter space is strongly constrained by the data. In particular, both the Planck and SNe data find as best fit for the n parameter values very close to 3, which represents the upper bound of the allowed region for this parameter. As already mentioned, thanks to the stability analysis, we know that theories with values of n greater than this upper

	SN best fit	SN	Planck best fit	Planck
ω	-0.3	-5.7 ± 2.6	-0.45	-3.02 ± 4.54
n	3.0	2.7 ± 0.2	2.995	2.989 ± 0.008

Table 6.1: Best fit values and marginalized means with standard deviation for the model parameters ω and n from Supernovae (SN) dataset and Planck dataset.

bound are considered not viable because they are plagued by some instabilities. This result is clearly consistent with what we have observed from the analysis of the power spectra. In fact, for smaller values of n the deviations at low multipoles in the CMB temperature anisotropies power spectrum increase, making these theories excluded by the data.
In Figure 6.8 we also plot the posterior distribution of the base ΛCDM parameters as found fitting the Planck data with the Generalized Brans-Dicke theory and ΛCDM model. We have $h = H_0/(100\ km/s/Mpc)$, θ_{MC} is an approximation of the acoustic scale angle θ_s, τ is the optical depth at reionization, A_S is the initial super-horizon amplitude of curvature perturbations (at the pivot scale $k_0 = 0.05 Mpc^{-1}$) and n_s the scalar spectral index.
It is worth to notice that the Generalized Brans-Dicke theory has (ω, n) as two more model parameters compared to ΛCDM; this allows to have more freedom to fit the data.
We can notice that fitting the Planck temperature and polarization data with the Generalized Brans-Dicke model we obtain slightly different, but still compatible, estimations for the base cosmological parameters with respect to the ΛCDM case, as we can see in Table 6.2, where all parameters appear to be shifted between the two models. In particular, we can observe that the Generalized Brans-Dicke model prefers smaller values for $\Omega_c h^2$ parameter which accounts for most of the matter in the Universe, thus leading to a decrease in the $\Omega_m h^2$ derived parameter. Furthermore, we can also observe some degeneracies between pairs of parameters in Figure 6.8 both for the Generalized Brans-Dicke model and the ΛCDM case. In particular, the overall nature of the correlations seems to be similar between the two models. For example, a large degeneracy between the τ and A_S parameters is present in both models, due to the fact that the observed amplitude of the acoustic peaks, measured with high precision by Planck, is sensitive to a combination of the two parameters. The degeneracy is expected to be significantly broken by CMB lensing data. Moreover, mild degeneracies between the baryon and cold dark matter density parameters and the scalar spectral index as well as between the scalar spectral index and the optical depth can also be observed. This is due to the fact that these parameters affect the scale-dependence of the CMB spectra in different ways.

	GBD - Planck	ΛCDM - Planck
$\Omega_b h^2$	0.02264 ± 0.00025 (0.02238)	0.02226 ± 0.00023 (0.02225)
$\Omega_c h^2$	0.1163 ± 0.0023 (0.1180)	0.1195 ± 0.0022 (0.1203)
$100\theta_{MC}$	1.04144 ± 0.00059 (1.04082)	1.04094 ± 0.00049 (1.04077)
τ	0.063 ± 0.020 (0.049)	0.077 ± 0.019 (0.069)
$ln(10^{10} A_S)$	3.053 ± 0.039 (3.026)	3.087 ± 0.038 (3.071)
n_s	0.975 ± 0.007 (0.970)	0.9663 ± 0.0064 (0.9630)

Table 6.2: Marginalized mean and standard deviation for Generalized Brans-Dicke and ΛCDM model with Planck dataset. In parenthesis, the maximum likelihood values for these parameters are also displayed.

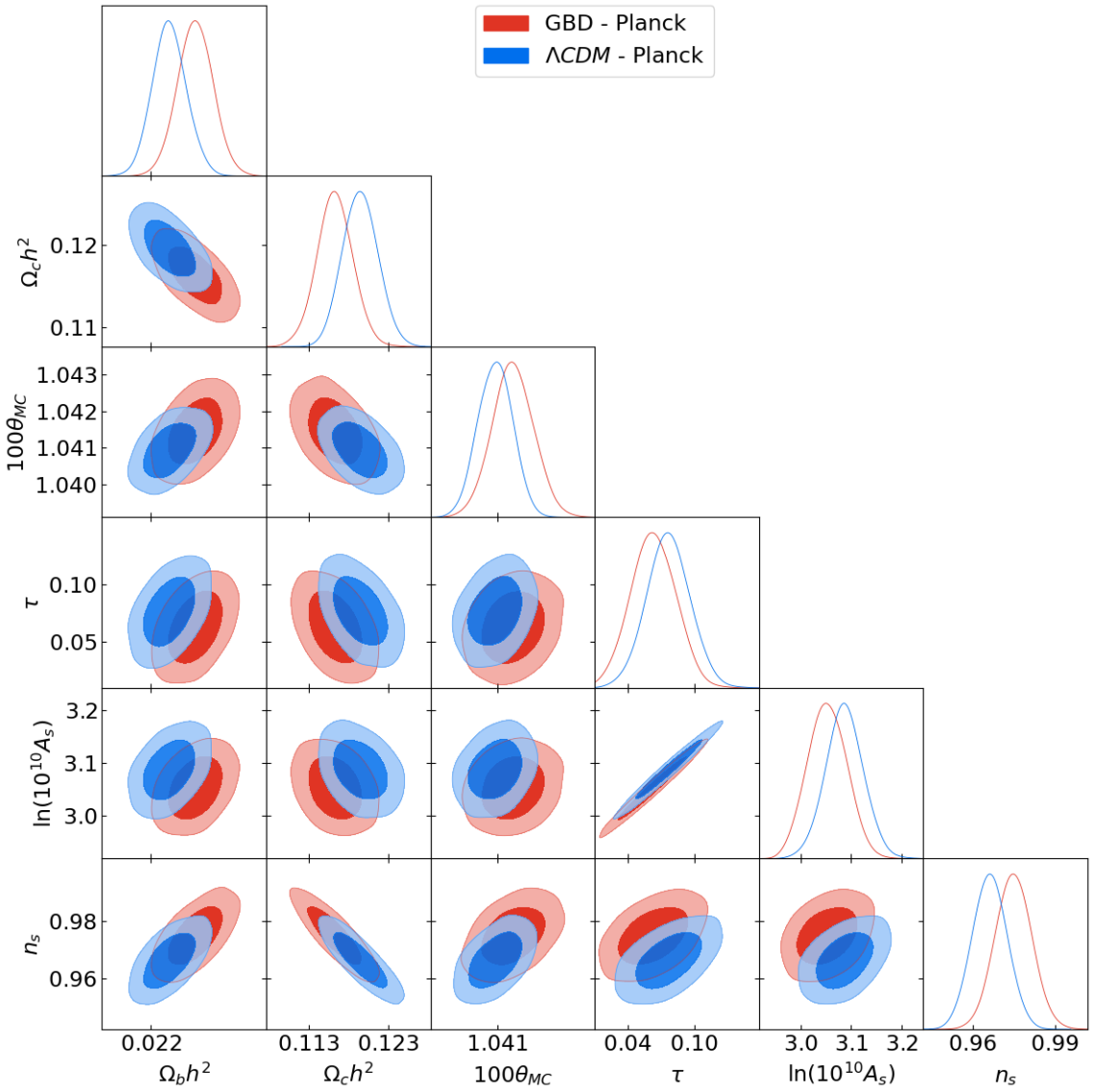

Figure 6.8: Two-dimensional observational bounds of cosmological parameters. The Planck dataset is used and the colored regions correspond to the parameter space constrained for the Generalized Brans-Dicke model (red) and ΛCDM model (blue) with 68% (inside) and 95% (outside) CL limits. The upper plots show the marginalized parameter constraints.

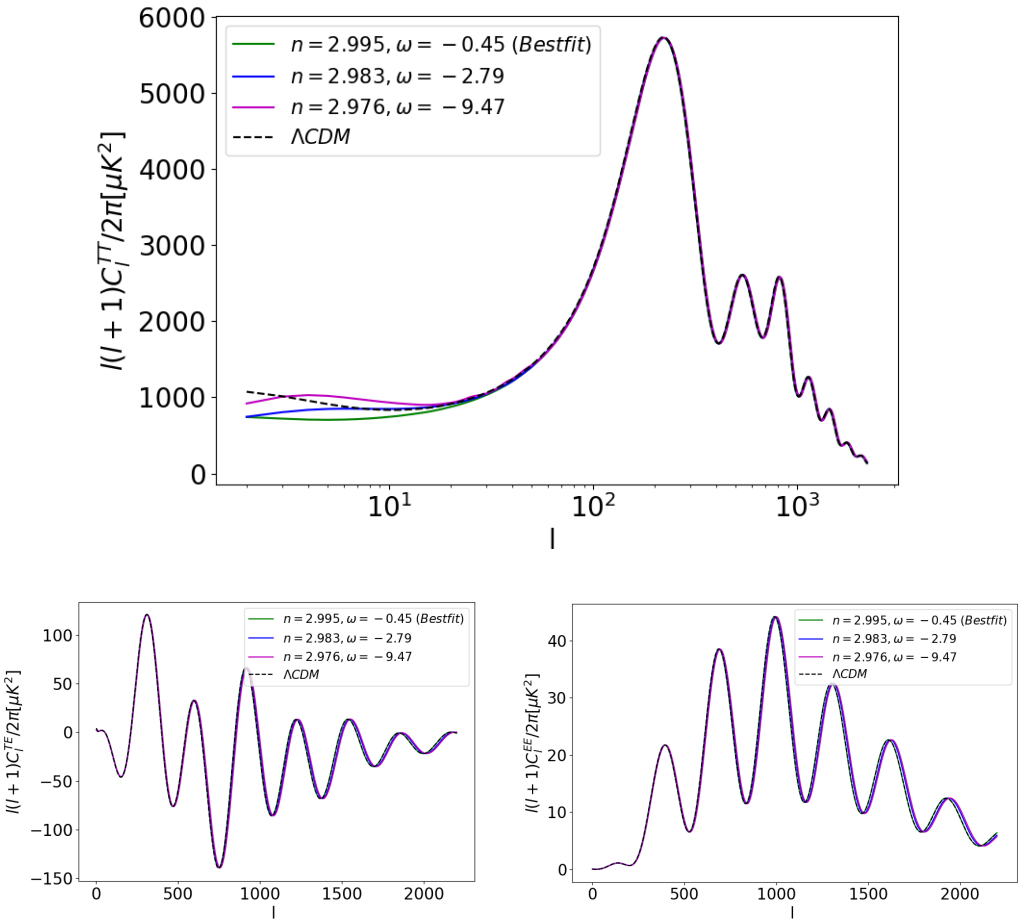

Figure 6.9: Top pannel: temperature anisotropies power spectrum for the Generalized Brans-Dicke best fit to Planck TEB dataset (green) and values of the ω and n parameters at 1σ (blue) and 2σ (purple). Bottom panels: the temperature-polarization (TE) cross-spectrum (on the left), the E mode of polarization (EE) power spectrum (on the right).

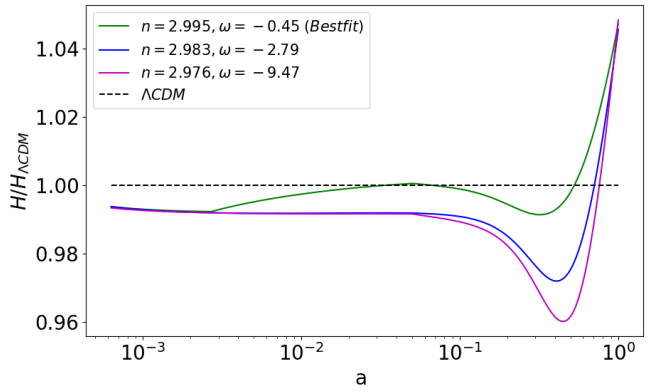

Figure 6.10: Ratio of the Hubble parameter for the Generalized Brans-Dicke best fit (green) and the ΛCDM. The other curves correspond to values of the ω and n parameters at 1σ (blue) and 2σ (purple).

In Figure 6.9, we plot the CMB temperature anisotropies power spectrum for the Generalized Brans-Dicke best fit. We notice that for the best fit values of the cosmological and model parameters, the shift in the position of the peaks is not present anymore and we produce a decrease in the amplitude at low multipoles which is preferred by the data; indeed, at these scales the ΛCDM model displays some differences from the data and the error bars are larger due to cosmic variance. For completeness, we report also the temperature-polarization and the E mode polarization CMB power spectra.
Moreover, in Figure 6.10, we plot the ratio of the Hubble parameter for the Generalized Brans-Dicke best fit and ΛCDM; as we can observe, choosing the best fit cosmological parameters for the Generalized Brans-Dicke theory, we obtain a larger expansion rate today. This can be explained by the fit of the CMB peak positions: larger values of the Hubble parameter today can compensate the intrinsically smaller values at late time in order to preserve the angular diameter distance to the surface of last scattering and in turns the positions of the peaks.

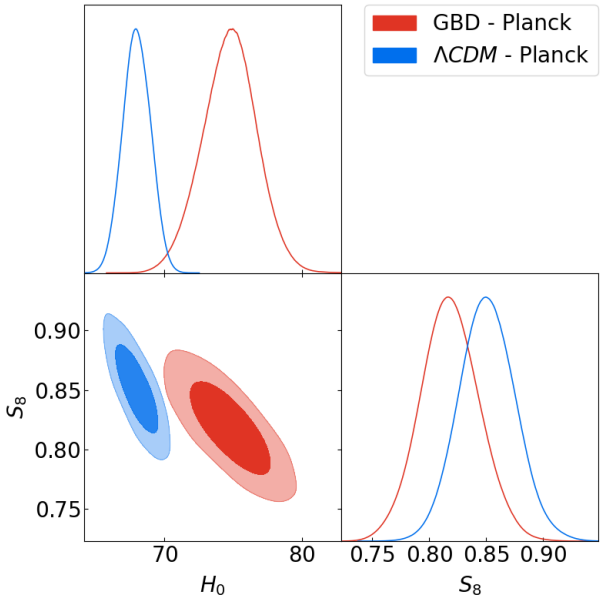

Figure 6.11: Two-dimensional observational bounds on the combinations of H_0 and S_8 derived parameters. The Planck dataset is used and the colored regions correspond to the parameter space constrained for the Generalized Brans-Dicke model (red) and ΛCDM model (blue) with 68% (inside) and 95% (outside) CL limits. The upper plots show the marginalized parameter constraints.

As a final part of this work, we check the effect of the Generalized Brans-Dicke theory (6.1) on the cosmological tensions. Indeed, as we have mentioned in Chapter 3, these internal inconsistencies of the ΛCDM model are often used to motivate the quest of DE/MG models.

It is therefore natural to verify the effect of the Generalized Brans-Dicke model in the estimation of the H_0 and S_8 derived parameters. As we can see from Figure 6.11, the observational bounds obtained from the Planck TEB dataset for the H_0 and S_8 parameters show interesting results. The data constraint H_0 to higher values and simultaneously S_8 to smaller values with respect to the ΛCDM case. This means that the values of these derived parameters move in the right direction in order to alleviate both tensions. In particular, assuming the Generalized Brans-Dicke model, from the Planck dataset we obtain the following marginalized mean values:

$$\begin{cases} H_0 = (74.75 \pm 1.98)\ km/s/Mpc \\ S_8 = 0.818 \pm 0.026 \end{cases} \tag{6.30}$$

and the matter density parameter $\Omega_m = 0.249 \pm 0.016$ which is a smaller value with respect to the

ΛCDM case.
This result makes the Generalized Brans-Dicke model very interesting in view of understanding the cosmological tensions. At this point, it will be crucial to understand which is the physics of this model that produces these values for the H_0 and S_8 parameters: a better understanding of the effect might shed light on possible new physics hidden behind these cosmological tensions.
Moreover, better constraints on these two parameters, as well as on all the other cosmological and model parameters, can come from fitting different dataset with the Generalized Brans-Dicke theory, such as data from BAO or CMB lensing. In particular, given the effect of the model on lensing observable, we expect interesting results from the CMB lensing dataset. We might also expect that other datasets help in breaking degeneracies between pairs of parameters.
This second and deeper part of the analisys of the model goes beyond the scope of this Thesis and it is left for future work.

Conclusions

In this Thesis, we have studied one of the most remarkable unresolved puzzle in modern Cosmology, that is the late time accelerated expansion of our Universe, due to a still unknown form of dark energy. In particular, adopting a phenomenological point of view, we have learned about how to create a bridge between theoretical models and cosmological data in order to shed light on possible intriguing scenarios that go beyond ΛCDM, the standard model of Cosmology.

We have started from a general introduction about the ΛCDM model, which nowadays successfully provides an accurate fit to the most recent cosmological data, such as the latest Planck 2018 release [3]. Surprisingly, the spectacular agreement is obtained fixing only six cosmological parameters. Within the ΛCDM model the source of the expansion resides in a cosmological constant which is usually interpreted by modern field theory as the vacuum energy density.
Moreover, we have seen some observational evidences which reveal the fact that our Universe is mostly filled with dark energy. Along the way, we have explored the characteristics of the cosmological probes which allow to open an observational window on our Universe. Looking at the Universe with different probes we can test our understanding of both the background expansion history and the evolution of cosmological perturbations. This is crucial in order to check the cosmic concordance of observables of interest and identify internal inconsistencies of the theoretical model, such as the cosmological tensions. These unresolved issues, together with the "Cosmological constant problem" and the "Coincidence problem" motivate the quest for cosmological models that go beyond the ΛCDM model. The theoretical landscape that explores alternatives to the ΛCDM model is extremely rich and the already available cosmological data have the key role to survey and verify all dark energy and modified gravity models. Furthermore, the upcoming generation of cosmological missions, such as the EUCLID [99] and DESI [100] experiments, will allow us to test gravity on cosmological scales with unprecedented precision.

On the other hand, when exploring the field of dark energy and modified gravity, some essential guidance have to be taken into account. For example, Lovelock's theorem assures the robustness of General Relativity and puts stringent bounds on the way in which we can try to modify it on cosmological scales. Solar system and astrophysical experiments of General Relativity require to provide modified gravity theories with screening mechanisms that hide possible new physics from local observations and allow to manifest it only on cosmic regimes. As an example to understand better this matter, we have focused on the Chameleon mechanism which usually applies to standard Brans-Dicke theories and we have seen how it is able to provide a method to hide the effects of an additional scalar field introduced to modify the usual General Relativity action.
Furthermore, important theoretical priors on alternative cosmological theories are set by the requirement of satisfying stability criteria. We have indeed presented the Ostrogradsky theorem as well as described some of the most relevant instabilities that can plague a theory, such as ghost, gradient and tachyonic instabilities.
Finally, we have briefly outlined the aftermath of the recent gravitational waves observations on dark energy and modified gravity models. The measurement of the speed of propagation of tensor perturbations reveals itself as a crucial constraint that a viable cosmological model needs to satisfy.

In the second part of this Thesis, we have presented the Effective Field Theory (EFT) approach to dark energy as a suitable formalism to compare theory and observations, keeping in mind the needed theoretical priors. Its unified language is an excellent tool to prepare the basis for a

confrontation of scalar-tensor theories with data. We have also seen its implementation in the cosmological code EFTCAMB [83].
The application of the EFT formalism and of the EFTCAMB code has allowed to realize the original part of this Thesis, which is about the study of a specific Generalized Brans-Dicke theory. We have implemented the Generalized Brans-Dicke theory in EFTCAMB and we have checked the effect of this cosmological model on the background quantities and on the evolution of cosmological perturbations. This has implied the necessity of mapping the Generalized Brans-Dicke theory in the EFT language and of computing the background solution solving the equations of motion of the theory. Furthermore, a deeper knowledge of computational methods in Cosmology and of Fortran and Python programming languages have been necessary to successfully implement the Generalized Brans-Dicke theory in the EFTCAMB code. The stability criteria have been also applied to constrain the viable parameter space of the Generalized Brans-Dicke theory.

As a result of this work, we have presented power spectra of interest such as the CMB temperature anisotropies, the matter and the CMB lensing power spectra and we have studied them as functions of the two free parameters of the model. We have clearly noticed that the effect of the additional scalar degree of freedom introduced by the Generalized Brans-Dicke theory on the CMB temperature anisotropies power spectrum is mainly two-fold. Firstly, it introduces modifications at low multipoles, linked to the Integrated Sachs-Wolfe effect which are due to a different evolution of the gravitational potentials with respect to the ΛCDM case. As we have seen, looking at these modifications at low multipoles we were able to forecast stringent constraints on the model parameter space from data that probe the cosmological perturbations. Secondly, we have noticed a shift in the position of the acoustic peaks which we have linked to the different background expansion history with respect to the ΛCDM one. Moreover, we have observed an enhancement in both the matter and CMB lensing power spectra. This results are consistent with the ones present in the literature for Cubic Galileons theory, of which the Generalized Brans-Dicke theory can be seen as a subcase.
Finally, we have concluded with a parameter estimation analysis, carried with a Monte Carlo Markov Chain approach and employing the CosmoMC software. Considering Supernovae and CMB TEB Planck dataset, we have been able to further constrain the parameter space and to check the conclusions obtained studying the power spectra. Indeed, we have seen that both the dataset constrain the n model parameter to be very close to the value of 3, which corresponds to the upper bound established by theoretical priors. It is worth to notice that in this limit the Generalized Brans-Dicke theory loses the non-minimal coupling between the additional scalar field and the metric and it becomes a k-essence theory with a higher derivative term for the scalar field. Then, exploiting the Planck dataset best fit, we have plotted again the power spectra with the best fit cosmological parameters. As a result, we have found that the modifications of the CMB temperature power spectrum reduce mainly to the ones at low multipoles where differences between the ΛCDM best fit and the data are also known. We have also checked that the background expansion history changes consistently.
We have reported the final and unexpected result of the MCMC likelihood analysis with the Planck TEB dataset, which constrains the H_0 and S_8 parameters respectively to higher and smaller values with respect to the ΛCDM case. As we have mentioned, this makes the Generalized Brans-Dicke theory interesting in view of the cosmological tensions since both parameters move in the right direction to alleviate them.
A better understanding of the physics of the Generalized Brans-Dicke model that produces this result, as well as a complementary analysis with other cosmological probes, such as BAO and CMB lensing data, is expected to render very interesting results and it is left for future work.

Acknowledgements

I really would like to thank Prof. Alessandra Silvestri for offering me the opportunity of being part of the Cosmology group in Leiden and for her guidance during all the duration of the work; Prof. Sabino Matarrese for having led me in the choice of the project and having always supervised during it; Dr. Simone Peirone for the useful knowledge he transmitted to me and the time dedicated helping with my work.

Appendix A

First-order gravitational perturbations

For completeness, we report here the covariant expressions of the scalar perturbed quantities of the left hand side of Einstein equation.
Starting from the Christoffel symbols:

$$\Gamma^{\alpha}_{\mu\nu} = \frac{1}{2} g^{\alpha\rho}(\partial_\mu g_{\rho\nu} + \partial_\nu g_{\rho\mu} - \partial_\rho g_{\mu\nu}). \tag{A.1}$$

Computing them in a FLRW background metric in conformal time, we find the following non null unperturbed components:

$$\Gamma^0_{00} = \frac{a'}{a}, \qquad \Gamma^i_{0j} = \frac{a'}{a}\delta^i_j, \qquad \Gamma^0_{ij} = \frac{a'}{a}\delta_{ij}. \tag{A.2}$$

Then the first-order scalar perturbations of the Christoffel symbols are:

$$\begin{aligned}
\delta\Gamma^0_{00} &= \Psi', \\
\delta\Gamma^0_{0i} &= \partial_i\Psi + \frac{a'}{a}\partial_i\omega^{\parallel}, \\
\delta\Gamma^i_{00} &= \frac{a'}{a}\partial^i\omega^{\parallel} + \partial^i(\omega^{\parallel})' + \partial^i\Psi, \\
\delta\Gamma^0_{ij} &= -2\frac{a'}{a}\Psi\delta_{ij} - \partial_i\partial_j\omega^{\parallel} - 2\frac{a'}{a}\Phi\delta_{ij} - \Phi'\delta_{ij} - \frac{a'}{a}D_{ij}\chi^{\parallel} + \frac{1}{2}D_{ij}(\chi^{\parallel})', \\
\delta\Gamma^i_{0j} &= -\Phi\delta^i_j + \frac{1}{2}D^i_j(\chi^{\parallel})', \\
\delta\Gamma^i_{jk} &= -\partial_j\Phi\delta^i_k - \partial_k\Phi\delta^i_j + \partial^i\Phi\delta_{jk} - \frac{a'}{a}\partial^i\omega^{\parallel}\delta_{jk} + \frac{1}{2}\partial_j D^i_k\chi^{\parallel} + \frac{1}{2}\partial_k D^i_j\chi^{\parallel} - \frac{1}{2}\partial^i D_{jk}\chi^{\parallel}.
\end{aligned} \tag{A.3}$$

The Ricci tensor is defined as:

$$R_{\mu\nu} = \partial_\alpha\Gamma^\alpha_{\mu\nu} - \partial_\mu\Gamma^\alpha_{\nu\alpha} + \Gamma^\alpha_{\sigma\alpha}\Gamma^\sigma_{\mu\nu} - \Gamma^\alpha_{\sigma\nu}\Gamma^\sigma_{\mu\alpha} \tag{A.4}$$

and in the FLRW background it has the following non null components:

$$R_{00} = -3\frac{a''}{a} + 3\left(\frac{a'}{a}\right)^2, \qquad R_{ij} = \left[\frac{a''}{a} + \left(\frac{a'}{a}\right)^2\right]\delta_{ij} \tag{A.5}$$

and the first-order perturbed components of the Ricci tensor are:

$$\begin{aligned}
\delta R_{00} =& \frac{a'}{a}\partial_i\partial^i\omega^{\parallel} + \partial_i\partial^i(\omega^{\parallel})' + \partial_i\partial^i\Psi + 3\Phi'' + 3\frac{a'}{a}\Phi' + 3\frac{a'}{a}\Psi', \\
\delta R_{0i} =& \frac{a''}{a}\partial_i\omega^{\parallel} + \left(\frac{a'}{a}\right)^2\partial_i\omega^{\parallel} + 2\partial_i\Phi' + 2\frac{a'}{a}\partial_i\Psi + \frac{1}{2}\partial_k D_i^k(\chi^{\parallel})', \\
\delta R_{ij} =& \Big[- \frac{a'}{a}\Psi' - 5\frac{a'}{a}\Phi' - 2\frac{a''}{a}\Psi - 2\left(\frac{a'}{a}\right)^2\Psi - 2\frac{a''}{a}\Phi - 2\left(\frac{a'}{a}\right)^2\Phi - \Phi'' + \partial_k\partial^k\Phi \\
& - \frac{a'}{a}\partial_k\partial^k\omega^{\parallel}\Big]\delta_{ij} - \partial_i\partial_j(\omega^{\parallel})' + \frac{a'}{a}D_{ij}(\chi^{\parallel})' + \frac{a''}{a}D_{ij}\chi^{\parallel} + \left(\frac{a'}{a}\right)^2 D_{ij}\chi^{\parallel} + \frac{1}{2}D_{ij}(\chi^{\parallel})'' \\
& + \partial_i\partial_j\Phi - \partial_i\partial_j\Psi - 2\frac{a'}{a}\partial_i\partial_j\omega^{\parallel} + \frac{1}{2}\partial_k\partial_i D_j^k\chi^{\parallel} + \frac{1}{2}\partial_k\partial_j D_i^k\chi^{\parallel} - \frac{1}{2}\partial_k\partial^k D_{ij}\chi^{\parallel}.
\end{aligned} \tag{A.6}$$

Then, the Ricci scalar which is defined as:

$$R = R_{\mu\nu}g^{\mu\nu}. \tag{A.7}$$

In a FLRW background:

$$R = \frac{6}{a^2}\frac{a''}{a} \tag{A.8}$$

and its first-order perturbation:

$$\delta R = \frac{1}{a^2}\Big(- 6\frac{a'}{a}\partial_i\partial^i\omega^{\parallel} - 2\partial_i\partial^i(\omega^{\parallel})' - 2\partial_i\partial^i\Psi - 6\Phi'' - 6\frac{a'}{a}\Psi' - 18\frac{a'}{a}\Big). \tag{A.9}$$

Finally, putting all together we can find the Einstein tensor:

$$G_{\mu\nu} = R_{\mu\nu} - \frac{1}{2}g_{\mu\nu}R, \tag{A.10}$$

that in FLRW has the following components:

$$G_0^0 = -\frac{3}{a^2}\left(\frac{a'}{a}\right)^2, \qquad G_j^i = -\frac{1}{a^2}\left[2\frac{a''}{a} - \left(\frac{a'}{a}\right)^2\right]\delta_j^i \tag{A.11}$$

and the first-order perturbations:

$$\begin{aligned}
\delta G_0^0 =& \frac{1}{a^2}\left[6\left(\frac{a'}{a}\right)^2\Psi + 6\frac{a'}{a}\Phi' + 2\frac{a'}{a}\nabla^2\omega^{\parallel} - 2\nabla^2\Phi - \frac{1}{2}\partial_k\partial^i D_i^k\chi^{\parallel}\right], \\
\delta G_i^0 =& \frac{1}{a^2}\Big(- 2\frac{a'}{a}\partial_i\Psi - 2\partial_i\Phi' - \frac{1}{2}\partial_k D_i^k(\chi^{\parallel})'\Big), \\
\delta G_j^i =& \frac{1}{a^2}\Big[\Big(2\frac{a'}{a}\Psi' + 4\frac{a''}{a}\Psi - 2\left(\frac{a'}{a}\right)^2\Psi + \nabla^2\Psi + 4\frac{a'}{a}\Phi' + 2\Phi'' - \nabla^2\Phi + 2\frac{a'}{a}\nabla^2\omega^{\parallel} \\
& + \nabla^2(\omega^{\parallel})' + \frac{1}{2}\partial_k\partial^m D_m^k\chi^{\parallel}\Big)\delta_j^i - \partial^i\partial_j\Psi + \partial^i\partial_j\Phi - 2\frac{a'}{a}\partial^i\partial_j\omega^{\parallel} - \partial^i\partial_j(\omega^{\parallel})' \\
& + \frac{a'}{a}D_j^i(\chi^{\parallel})' + \frac{1}{2}D_j^i(\chi^{\parallel})'' + \frac{1}{2}\partial_k\partial^i D_j^k\chi^{\parallel} + \frac{1}{2}\partial_k\partial_j D^{ik}\chi^{\parallel} - \frac{1}{2}\partial_k\partial^k D_j^i\chi^{\parallel}\Big].
\end{aligned} \tag{A.12}$$

Appendix B

Conformal transformation

Considering two manifolds $\mathscr{M}$ and $\tilde{\mathscr{M}}$, respectively with metrics $g_{\mu\nu}$ and $\tilde{g}_{\mu\nu}$ and covered by the same coordinate system x_μ, they are said to be conformal to each other if they are related by the following transformation [36]:

$$\tilde{g}_{\mu\nu}(x) = \Omega^2(x) g_{\mu\nu}(x) \tag{B.1}$$

i.e. if they are related by a conformal transformation. Ω is called conformal function and it needs to be a twice-differentiable function of the coordinates x_μ and to assume values in the range $0 < \Omega < \infty$.
Unlike a change of coordinates, which relabels the name of the points, a conformal transformation changes the physics of the conformally related manifolds $\mathscr{M}$ and $\tilde{\mathscr{M}}$. Indeed, it consists in the shrink or stretch of the distance between two points described by the same coordinates system on the two manifolds, while the angles between vectors are preserved. This means that, the casual structure of the two manifolds is equivalent, since the angles between null vectors, which defines light cones, remain unchanged. Indeed, conformal transformations are localized transformations that, in the case $\Omega = const$, become the so called scale transformations.
It is then possible to see that the following relations hold:

$$\tilde{g}^{\mu\nu}(x) = \Omega^{-2}(x) g^{\mu\nu}(x), \tag{B.2}$$

$$\sqrt{-\tilde{g}} = \Omega^4 \sqrt{-g}, \tag{B.3}$$

where $g = det(g_{\mu\nu})$.
Then, applying the transformation to the Christoffel symbols, it is possible to find [37]:

$$\begin{aligned} \tilde{\Gamma}^\lambda_{\mu\nu} &= \Gamma^\lambda_{\mu\nu} + \frac{1}{\Omega}(g^\lambda_\mu \Omega_{,\nu} + g^\lambda_\nu \Omega_{,\mu} - g_{\mu\nu} g^{\lambda\kappa} \Omega_{,\kappa}), \\ \Gamma^\lambda_{\mu\nu} &= \tilde{\Gamma}^\lambda_{\mu\nu} - \frac{1}{\Omega}(\tilde{g}^\lambda_\mu \Omega_{,\nu} + \tilde{g}^\lambda_\nu \Omega_{,\mu} - \tilde{g}_{\mu\nu} \tilde{g}^{\lambda\kappa} \Omega_{,\kappa}). \end{aligned} \tag{B.4}$$

Similarly, the Ricci tensors in the two conformal metrics are:

$$\begin{aligned} \tilde{R}_{\mu\nu} &= R_{\mu\nu} + \Omega^{-2}[4\Omega_{,\mu}\Omega_{,\nu} - \Omega_{,\sigma}\Omega^{,\sigma} g_{\mu\nu}] - \Omega^{-1}[2\Omega_{;\mu\nu} + \Box\Omega g_{\mu\nu}], \\ R_{\mu\nu} &= \tilde{R}_{\mu\nu} - 3\Omega^{-2}\Omega_{,\rho}\Omega^{,\rho}\tilde{g}_{\mu\nu} + \Omega^{-1}[2\Omega_{;\mu\nu} + \tilde{g}_{\mu\nu}\tilde{\Box}\Omega] \end{aligned} \tag{B.5}$$

and the Ricci scalars:

$$\begin{aligned} \tilde{R} &= \Omega^{-2}\left[R - 6\frac{\Box\Omega}{\Omega}\right], \\ R &= \Omega^2\left[\tilde{R} + 6\frac{\tilde{\Box}\Omega}{\Omega} - 12\tilde{g}^{\mu\nu}\frac{\Omega_{,\mu}\Omega_{,\nu}}{\Omega}\right], \end{aligned} \tag{B.6}$$

where $\tilde{\Box}$ is the d'Alembertian operator taken with respect to the metric $\tilde{g}_{\mu\nu}$, differently from $\Box$ of the conformally rescaled metric $g_{\mu\nu}$.
The conformal transfomation preserves the Weyl curvature tensor, which in D dimensions is :

$$C_{\mu\nu\rho\sigma} = R_{\mu\nu\rho\sigma} + \frac{2}{D-2}(g_{\mu[\sigma}R_{\rho]\nu} + g_{\nu[\rho}R_{\sigma]\mu}) + \frac{2}{(D-1)(D-2)} R g_{\mu[\rho}g_{\sigma]\nu}, \tag{B.7}$$

indeed, under a conformal transformation (B.1):

$$\tilde{C}_{\mu\nu\rho\sigma} = C_{\mu\nu\rho\sigma}. \tag{B.8}$$

Appendix C

More on f(R). Jordan and Einstein frame

$f(R)$ theories are also a sub-class of Brans-Dicke theories; to see this, we start from the action (3.49) and we reabsorb the Ricci scalar inside the definition of $f(R)$:

$$S = \int d^4x\sqrt{-g}\frac{M_{pl}^2}{2}f(R) + \int d^4x\sqrt{-g}\mathcal{L}_M(g_{\mu\nu},\psi_M), \tag{C.1}$$

introducing an auxiliary field χ [38], we can rewrite this action in a dynamically equivalent form [39]:

$$S = \int d^4x\sqrt{-g}\frac{M_{pl}^2}{2}[f(\chi) + f_\chi(\chi)(R-\chi)] + S_M(g_{\mu\nu},\psi_M), \tag{C.2}$$

where $f_\chi(\chi) = \frac{\partial f}{\partial \chi}$. The equivalence between the two actions (C.1) and (C.2) is easy to see: varying (C.2) with respect to the auxiliary field, we obtain the equation of motion of the field:

$$f_{\chi\chi}(\chi - R) = 0, \tag{C.3}$$

if $f_{\chi\chi} \neq 0$, the field equation gives $\chi = R$, that recasts the original action. Then, following [38], we can define another intermediate field as:

$$\varphi = f_\chi(\chi) \tag{C.4}$$

and rewriting (C.2), in terms of the new field φ:

$$\begin{aligned} S &= \int d^4x\sqrt{-g}\frac{M_{pl}^2}{2}[\varphi R - \varphi\chi(\varphi) + f(\chi(\varphi))] + S_M(g_{\mu\nu},\psi_M) \\ &= \int d^4x\sqrt{-g}\left[\frac{M_{pl}^2}{2}\varphi R - U(\varphi)\right] + S_M(g_{\mu\nu},\psi_M), \end{aligned} \tag{C.5}$$

with:

$$U(\varphi) = \frac{\varphi\chi(\varphi) - f(\chi(\varphi))}{2M_{pl}^{-2}}. \tag{C.6}$$

Thus, confronting (C.5) with the Brans-Dicke action (3.46) (and setting $M_{pl}^2 = 1$), it is clear that $f(R)$ theories are a sub-class of Brans-Dicke with $\omega_{BD} = 0$, that is without the kinetic term.

From Jordan to Einstein frame

Finally, it is worth to see that there is an equivalent frame in which $f(R)$ theories and other MG theories can be described, in this context, the additional scalar degree of freedom manifests even more explicitly. Indeed, the action (3.49) is written in the so called Jordan frame, where the

gravitational part of the action is modified. As we will see, there exists another possibility, called Einstein frame, in which the gravitational part of the action remains the standard Einstein-Hilbert action while a non-minimal coupling between the matter fields and gravity is introduced in the matter action.
To go from Jordan to Einstein frame and viceversa, a conformal transformation of the metric is needed. A conformal transformation consists in a local re-scale of units that leaves the angles unchanged (see Appendix B). In particular, here we choose the following transformation [38]:

$$\tilde{g}_{\mu\nu} = \Omega^2(x) g_{\mu\nu} = e^{2\omega(x)} g_{\mu\nu}, \tag{C.7}$$

from (B.5), we find for the Ricci tensor:

$$R = \Omega^2(\tilde{R} + 6\tilde{\Box}\omega - 6\tilde{g}^{\mu\nu}\partial_\mu\omega\partial_\nu\omega). \tag{C.8}$$

Starting again from (C.5), we apply the conformal transformation (C.7). Exploiting (B.3), the result is:

$$S = \int d^4x\sqrt{-\tilde{g}}\left[\frac{M_{pl}^2}{2}\varphi\Omega^{-2}(\tilde{R} + 6\tilde{\Box}\omega - 6\tilde{g}^{\mu\nu}\partial_\mu\omega\partial_\nu\omega) - \Omega^{-4}U(\varphi)\right] + S_M(\Omega^{-2}\tilde{g}_{\mu\nu}, \psi_M). \tag{C.9}$$

This is the result of a general conformal transformation. To go to the Einstein frame, we want to recover the Einstein-Hilbert part of the action. As a consequence, a suitable choice is to consider:

$$\Omega^2 = \varphi, \tag{C.10}$$

that allows to recover a linear term in $\tilde{R}$. Furthermore, we introduce a new field ϕ [38]:

$$\frac{\phi}{M_{pl}} = \sqrt{\frac{3}{2}} ln(\varphi). \tag{C.11}$$

Putting together (C.10) and (C.11), we can find:

$$\omega = \frac{1}{\sqrt{6}}\frac{\phi}{M_{pl}}. \tag{C.12}$$

Plugging all these choices in (C.9), we finally find the $f(R)$ action in the Einstein frame:

$$S = \int d^4x\sqrt{-\tilde{g}}\frac{M_{pl}^2}{2}\tilde{R} + \int d^4x\sqrt{-\tilde{g}}\left[-\frac{1}{2}\tilde{g}^{\mu\nu}\partial_\mu\phi\partial_\nu\phi - V(\phi)\right] + S_M\left(e^{-\sqrt{\frac{2}{3}}\frac{\phi}{M_{pl}}}\tilde{g}_{\mu\nu}, \psi_M\right), \tag{C.13}$$

with:

$$V(\phi) = e^{-\sqrt{\frac{8}{3}}\frac{\phi}{M_{pl}}}U(\phi), \tag{C.14}$$

where the term $\propto \tilde{\Box}\omega$ does not contribute since it can easily rewritten as a four-divergence term, exploiting the relation $\Box\omega = \frac{1}{\sqrt{-g}}(\sqrt{-g}g^{\mu\nu}\omega_{,\nu})_{,\mu}$.
Thus, in the Einstein frame, the additional degree of freedom manifests explicitly as a canonical scalar field with the density Lagrangian:

$$\mathscr{L}_\phi = -\frac{1}{2}\tilde{g}^{\mu\nu}\partial_\mu\phi\partial_\nu\phi - V(\phi), \tag{C.15}$$

where the potential under which ϕ evolves is determined by the original form of $f(R)$. Clearly, this additional degree of freedom can play the role of dynamical dark energy, and so it exemplifies the equivalence between DE/MG models.
It is also important to underline that, through the matter action, the scalar field is coupled with matter and the particles fall along geodesics of the conformally related metric $g_{\mu\nu}$.

Appendix D

Chameleon mechanism: solution for a compact object

To better understand the chameleon screening mechanism, it is useful to derive an approximate solution for ϕ for a compact object. In particular, for simplicity, we will assume to have a spherically symmetric body of radius R_C and to be in the static case. Then the mass of the object is $M_C = \frac{4\pi}{3}\rho_C R_C^3$. Following [46], we approximate the geometry to Minkowsky space-time $g_{\mu\nu} \simeq \eta_{\mu\nu}$, thus ignoring the back-reaction of the metric. Under this assumption, we can rewrite (4.8) as:

$$\frac{d^2\phi}{dr^2} + \frac{2}{r}\frac{d\phi}{dr} = V_{,\phi} + \rho(r)\frac{\beta}{M_{pl}}e^{\frac{\beta\phi}{M_{pl}}}, \tag{D.1}$$

that can be found computing the Christoffel symbols for Minkowsky space-time in spherical coordinates: $ds^2 = -dt^2 + dr^2 + r^2 d\Omega^2$. In particular, $\Gamma^{\theta}_{\theta r} = \Gamma^{\varphi}_{\varphi r} = \frac{1}{r}$. The energy density $\rho(r)$ is assumed to have the following profile:

$$\rho = \begin{cases} \rho_C & \text{for } r < R_C \\ \rho_\infty & \text{for } r > R_C \end{cases} \tag{D.2}$$

where ρ_∞ is the homogeneous energy density of the background that surrounds the spherical body. Indeed, considering for example solar system bodies, the surrounding background is not not empty but rather filled by baryonic gas and dark matter with an approximately homogeneous energy density of $\rho_\infty \sim 10^{-24} g/cm^3$.
Then, we denote with ϕ_C the value of the field that minimizes the effective potential for $r < R_C$ and with m_C the mass of the fluctuations associated with this minimum. Similarly, for $r > R_C$ the minimum is for ϕ_∞ with mass m_∞.
Equation (D.1) is a second-order differential equation, thus to solve we need two boundary conditions:

$$\begin{aligned} &\frac{d\phi}{dr} = 0 \quad \text{at} \quad r = 0, \\ &\phi \to \phi_\infty \quad \text{at} \quad r \to \infty. \end{aligned} \tag{D.3}$$

It is now possible to find the solution for (D.1). For sufficiently large objects, for $r < R_C$, the field should be indeed equal to ϕ_C; this is true everywhere inside the object except for a shell ΔR_C below the surface. In particular, it is necessary that the shell is thin with respect to the radius of the object.

Thus, considering to have a thin-shell, that is $\frac{\Delta R_C}{R_C} \ll 1$, we have that the field is nearly frozen inside the object, till a critical radius R_{roll} when the field starts to roll. Indeed the friction term $\propto 1/r$ dominates for small radius, and the field starts to roll only when the friction becomes small enough. Thus we have:

$$\phi \simeq \phi_C \quad \text{for} \quad 0 < r < R_{roll}. \tag{D.4}$$

As soon as the value of the field displaces from the minimum ϕ_C, then we have that $|V_{,\phi}| \ll \rho(r)\frac{\beta}{M_{pl}}e^{\frac{\beta\phi}{M_{pl}}}$. Furthermore, as we have already said, $\phi \ll M_{pl}$ in the range that we are considering;

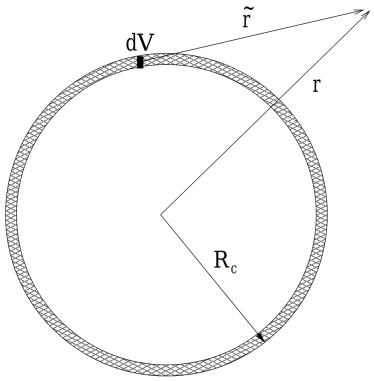

Figure D.1: Schematic representation of the spherical object of radius R_C and of the thin shell ΔR_C (shaded region). Taken from [46].

thus (D.1) becomes:

$$\frac{d^2\phi}{dr^2} + \frac{2}{r}\frac{d\phi}{dr} \simeq \rho_C \frac{\beta}{M_{pl}}, \tag{D.5}$$

that has the following solution [46]:

$$\phi(r) = \frac{\beta\rho_C}{3M_{pl}}\left(\frac{r^2}{2} + \frac{R_{roll}^2}{r}\right) - \frac{\beta\rho_C R_{roll}^2}{2M_{pl}} + \phi_C \quad \text{for} \quad R_{roll} < r < R_C. \tag{D.6}$$

The separation of the solutions for the two regimes inside the object is valid thanks to the thin-shell assumption.
At $r = R_C$ then ρ goes discontinuously from ρ_C to ρ_∞. Therefore, the speed of the field is initially large with respect to the curvature of the potential and (D.1) becomes:

$$\frac{d^2\phi}{dr^2} + \frac{2}{r}\frac{d\phi}{dr} \simeq 0. \tag{D.7}$$

By matching the solution at $r = R_C$, we have [46]:

$$\phi(r) = -\left(\frac{\beta}{4\pi M_{pl}}\right)\left(\frac{3\Delta R_C}{R_C}\right)\frac{M_C e^{-m_\infty(r-R_C)}}{r} + \phi_\infty \quad \text{for} \quad r > R_C, \tag{D.8}$$

with:

$$\frac{\Delta R_C}{R_C} = \frac{\phi_\infty - \phi_C}{6\beta M_{pl}\Phi_C} \ll 1, \tag{D.9}$$

with $\Phi_C = M_C/8\pi M_{pl}^2 R_C$ is the Newtonian potential at the surface of the object. Thus in the thin shell case, the difference between the value of minimum of the field inside and outside the source is much smaller than the Newtonian potential of the source. Clearly, the thin shell assumption is satisfied better by massive objects. In this farme, the chameleon mechanism predicts a successful screening of the "fifth" force from local tests of gravity.

On the other hand, the thick shell case is realized when $\frac{\Delta R_C}{R_C} > 1$. In this case, it is not possible to separate two different regimes of solution inside the object because there is no clear separation between regions for $r < R_C$. Thus a solution valid for the entire range $0 < r < R_C$ is needed. In such solution there is no friction dominated regime and the field starts to roll as soon as it is released from $r = 0$; in this case the screening mechanism is not successful and the source remains unscreened.

Thus summarizing, if the source body has a thin shell, then the Chameleon field will settle to

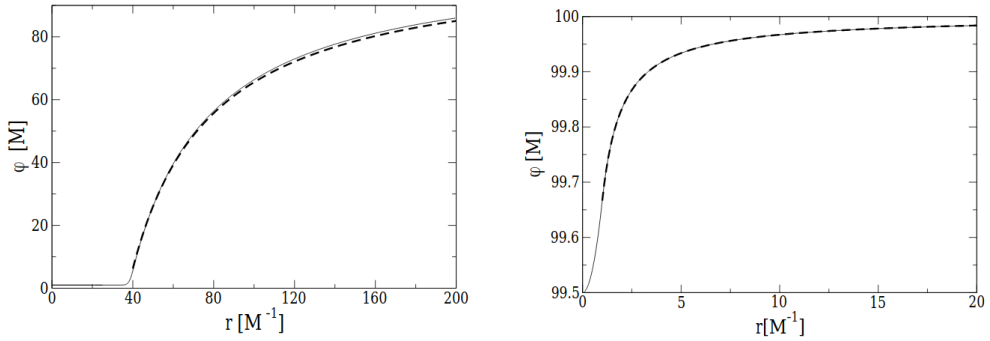

Figure D.2: On the left: Chameleon field solution with thin shell. On the right: Chameleon field with thick shell. Taken from [45].

a minimum over most of the source. The Chameleon force, which is $\propto \vec{\nabla}\phi$, will then be suppressed, thanks to the fact that the field is almost constant inside the body. The environmental dependence of the mass of the fluctuations makes the field massive and therefore, assuming that the fifth force interaction is parametrized by a Yukawa potential $V(r) \propto e^{-m_\phi r}/r$, the interaction will be exponentially suppressed. The interpolation between outer and inner values of the field will take place in the thin shell, further suppressing the intensity of the field also outside the source. Indeed, in this scenario, the source will be successfully screened.
On the other hand, for a thick shell body the chameleon field will change throughout all the source. This means that the Chameleon force will not be null inside the body and the field will not be massive enough to suppress interactions inside the source. Thus the source will be unscreened and the field will not be hidden from local tests of gravity.

The requirement of having a successful screening puts stringent bounds on the viable parameters of a theory. For example, the request for the Earth to have a thin shell allows to put constraints on the parameters of the inverse power law potential (4.12). Indeed, assuming to have β and n of the order of unity, we need for the mass scale M to satisfy [45]:

$$M \lesssim 10^{-3} eV, \tag{D.10}$$

that, as we saw at the beginning of Chapter 3, coincides with the observed energy scale of dark energy.

Bibliography

[1] S.Perlmutter et al., *Measurements of Omega and Lambda from 42 High-Redshift Supernovae*, Astrophys.J.517:565-586, (1999).

[2] A. Riess et al., *Observational Evidence from Supernovae for an Accelerating Universe and a Cosmological Constant*, Astron.J.116:1009-1038, (1998).

[3] Planck Collaboration, *Planck 2018 results. VI. Cosmological parameters*, arXiv:1807.06209 [astro-ph.CO], (2018).

[4] W. Hu, *CMB Temperature and Polarization Anisotropy Fundamentals*, Ann.Phys.303:203-225, (2003).

[5] A. Silvestri, M. Trodden, *Approaches to Understanding Cosmic Acceleration*, Rept.Prog.Phys.72:096901, (2009).

[6] D. H. Weinberg et al. *Observational Probes of Cosmic Acceleration*, arXiv:1201.2434 [astro-ph.CO], (2013).

[7] M.Kowalski et al. *Improved Cosmological Constraints from New, Old and Combined Supernova Datasets*, Astrophys.J.686:749-778, (2008).

[8] P. Coles, F. Lucchin. *Cosmology: The Origin and Evolution of Cosmic Structure*, John Wiley Sons, Ltd, (2002).

[9] D. Baumann, *Cosmology Part III Mathematical tripos.*

[10] L. Amendola, S. Tsujikawa, *Dark Energy: Theory and Observations*, Cambridge University Press, (2010).

[11] D. J. Eisenstein et al. *Detection of the Baryon Acoustic Peak in the Large-Scale Correlation Function of SDSS Luminous Red Galaxies*, Astrophys.J.633:560-574, (2005).

[12] J. Yoo, Y. Watanabe, *Theoretical models of dark energy*, Int. J. Mod. Phys. D 21, 1230002, (2012).

[13] S. Carrol, *Spacetime and Geometry*, Pearson Education limited, (2014).

[14] D. Huterer, *Weak lensing, dark matter and dark energy*, Gen. Rel. Grav. 42, 2177, (2010).

[15] E. V. Linder, *Exploring the Expansion History of the Universe*, Phys.Rev.Lett.90:091301, (2003).

[16] H. K. Jassal, J. S. Bagla, T. Padmanabhan, *WMAP constraints on low redshift evolution of dark energy*, Mon.Not.Roy.Astron.Soc. 356, (2005).

[17] Y. Hu, M. Li, X. D. Li, Z. Zhang, *Investigating the Possibility of a Turning Point in the Dark Energy Equation of State*, SCIENCE CHINA Physics, Mechanics Astronomy, (2014).

[18] B. Hu, M. Raveri, N. Frusciante, A. Silvestri, *EFTCAMB/EFTCosmoMC: Numerical Notes v3.0*, arXiv:1405.3590 [astro-ph.IM], (2017).

[19] T. Clifton, P. G. Ferreira, A. Padilla, C. Skordis, *Modified Gravity and Cosmology*, Physics Reports 513, 1, (2012).

[20] A. Joyce, B. Jain, J. Khoury, M. Trodden, *Beyond the Cosmological Standard Model*, Physics Reports 568, (2015).

[21] A. Silvestri, https://www.ictp-saifr.org/iii-joint-ictp-trieste-ictp-saifr-school-on-observational-cosmology/

[22] P. Brax, *The Cosmological constant problem*, Contemporary Physics, Taylor Francis, (2004).

[23] E.-A. Kontou, K. Sanders, *Energy conditions in general relativity and quantum field theory*, arXiv:2003.01815, (2020).

[24] R.R. Caldwell, *A Phantom Menace? Cosmological consequences of a dark energy component with super-negative equation of state*, Phys.Lett.B545:23-29, (2002).

[25] R. H. Brandenberger, *Back Reaction of Cosmological Perturbations and the Cosmological Constant Problem*, arXiv:hep-th/0210165, (2002).

[26] E. J. Copeland, M. Sami, S. Tsujikawa, *Dynamics of dark energy*, Int.J.Mod.Phys.D15:1753-1936, (2006).

[27] L. Pogosian, A. Silvestri, *What can cosmology tell us about gravity? Constraining horndeski gravity with* Σ *and* μ, Phys. Rev. D, 94:104014, (2016).

[28] T. Kobayashi, *Horndeski theory and beyond: a review*, Rept.Prog.Phys. 82, (2019).

[29] T. Kobayashi, M. Yamaguchi, J. Yokoyama, *Generalized G-inflation: Inflation with the most general second-order field equations*, Prog. Theor. Phys. 126, (2011).

[30] D. Langlois, K. Noui *Degenerate higher derivative theories beyond Horndeski: evading the Ostrogradski instability*, JCAP 1602, (2016).

[31] S. Peirone, G. Benevento, N. Frusciante, S. Tsujikawa *Cosmological constraints and phenomenology of a beyond-Horndeski model*, Phys. Rev. D 100, 063509, (2019).

[32] J. Gleyzes, D. Langlois, F. Piazza, F. Vernizzi, *Healthy theories beyond Horndeski*, Phys. Rev. Lett. 114, 211101, (2015).

[33] S. M. Carroll, V. Duvvuri, M. Trodden, M. S. Turner, *Is Cosmic Speed-Up Due to New Gravitational Physics?*, Phys.Rev.D70:043528, (2004).

[34] M. Blau, *Lecture Notes on General Relativity*, http://www.blau.itp.unibe.ch/GRLecturenotes.htm

[35] L. Pogosian, A. Silvestri, *The pattern of growth in viable f(R) cosmologies*, Phys.Rev.D77:023503,2008; Erratum-ibid.D81:049901, (2010).

[36] D. Blaschke, M. P. Dabrowski, *Conformal relativity versus Brans-Dicke and superstring theories*, Entropy 14, 1978-1996, (2012).

[37] S.W. Hawking, G.F.R. Ellis, *The large-scale structure of space-time*, Cambridge Univ. Press, (1999) .

[38] A. De Felice, S. Tsujikawa, *f(R) theories*, Living Rev. Rel. 13: 3, (2010).

[39] T. Chiba, *1/R gravity and Scalar-Tensor Gravity*, Phys.Lett.B575:1-3, (2003).

[40] I. Quiros, *Selected topics in scalar-tensor theories and beyond*, Int.J.Mod.Phys.D28,No 7, (2019).

[41] C. Brans, R. H. Dicke, *Mach's Principle and a Relativistic Theory of Gravitation*, Phys. Rev. 124, 925, (1961).

[42] J. Frieman, C. Hill, A. Stebbins, I. Waga, *Cosmology with Ultra-light Pseudo-Nambu-Goldstone Bosons*, Phys.Rev.Lett.75:2077-2080, (1995).

[43] S. Weinberg, *The Cosmological Constant Problems (Talk given at Dark Matter 2000, February, 2000)*, arXiv:astro-ph/0005265, (2000).

[44] J. Khoury, *Theories of Dark Energy with Screening Mechanisms*, arXiv:1011.5909 [astro-ph.CO], (2010).

[45] J. Khoury, A. Weltman, *Chameleon Fields: Awaiting Surprises for Tests of Gravity in Space*, Phys.Rev.Lett.93:171104, (2004).

[46] J. Khoury, A. Weltman, *Chameleon Cosmology*, Phys.Rev.D69:044026, (2004).

[47] C. M. Will, *The Confrontation between General Relativity and Experiment*, Living Rev. Relativity 17, (2014).

[48] A. Zanzi, *Chameleonic Theories: A Short Review*, Universe 2015, 1(3), 446-475, (2015).

[49] S. M. Carroll, M. Hoffman, M. Trodden, *Can the dark energy equation-of-state parameter w be less than -1?*, Phys.Rev.D68:023509, (2003).

[50] D. M. Scolnic et al., *The Complete Light-curve Sample of Spectroscopically Confirmed Type Ia Supernovae from Pan-STARRS1 and Cosmological Constraints from The Combined Pantheon Sample*, arXiv:1710.00845, (2018).

[51] M. Betoule et al., *Improved cosmological constraints from a joint analysis of the SDSS-II and SNLS supernova samples*, arXiv:1401.4064, (2014).

[52] DES Collaboration, *Dark Energy Survey year 1 results: Cosmological constraints from galaxy clustering and weak lensing*, Phys. Rev., D98,043526, (2018).

[53] H. Hildebrandt et al., *KiDS+VIKING-450: Cosmic shear tomography with optical+infrared data*, AA 633, A69, (2020).

[54] H. Hildebrandt et al., *KiDS-450: Cosmological parameter constraints from tomographic weak gravitational lensing*, arXiv:1606.05338, (2016).

[55] https://wwwmpa.mpa-garching.mpg.de/galform/virgo/millennium/

[56] S. Matarrese, S. Mollerach, M. Bruni, *Relativistic second-order perturbations of the Einstein-de Sitter Universe*, Phys.Rev. D58, (1998).

[57] A. Riotto, *Inflation and the Theory of Cosmological Perturbations*, arXiv:hep-ph/0210162, (2017).

[58] J. Carron, A. Lewis, *Maximum a posteriori CMB lensing reconstruction*, Phys. Rev. D 96, 063510, (2017).

[59] Planck Collaboration, *Planck 2018 results. VIII. Gravitational lensing*, arXiv:1807.06210, (2018).

[60] Planck Collaboration, *Planck 2018 results. I. Overview and the cosmological legacy of Planck*, arXiv:1807.06205, (2018).

[61] A. Lewis, A. Challinor, *Weak Gravitational Lensing of the CMB*, Phys.Rept. 429, (2006).

[62] C.-P. Ma, E. Bertschinger, *Cosmological Perturbation Theory in the Synchronous and Conformal Newtonian Gauges*, Astrophys.J. 455, (1995).

[63] S. Dodelson, *Modern Cosmology*, Academic Press, (2003).

[64] P. Cabella, M. Kamionkowski, *Theory of cosmic microwave background polarization*, arXiv:astro-ph/0403392, (2005).

[65] W. Hu, M. White, *CMB anisotropies: Total angular momentum method*, Physical Review D, (1997).

[66] A. Lewis and A. Challinor, *https://camb.info/*.

[67] A. Zucca, L. Pogosian, A. Silvestri, Y. Wang, G.-B. Zhao, *Generalized Brans-Dicke theories in light of evolving dark energy*, Phys. Rev. D 101, 043518, (2020).

[68] F. Perrotta, C. Baccigalupi, S. Matarrese, *Extended Quintessence*, Phys.Rev. D61 023507, (2000).

[69] C. Baccigalupi, S. Matarrese, F. Perrotta, *Tracking Extended Quintessence*, Phys.Rev. D62 123510, (2000).

[70] The LIGO Scientific Collaboration, The Virgo Collaboration, *GW170817: Observation of Gravitational Waves from a Binary Neutron Star Inspiral*, Phys. Rev. Lett. 119 161101, (2017).

[71] LIGO Scientific Collaboration, Virgo Collaboration, Fermi Gamma-Ray Burst Monitor, INTEGRAL, *Gravitational Waves and Gamma-Rays from a Binary Neutron Star Merger: GW170817 and GRB 170817A*, The Astrophysical Journal Letters, 848:L13, (2017).

[72] C. de Rham, S. Melville, *Gravitational Rainbows: LIGO and Dark Energy at its Cutoff*, Phys. Rev. Lett. 121, 221101, (2018).

[73] J. M. Ezquiaga, M. Zumalacárregui, *Dark Energy after GW170817: dead ends and the road ahead*, T Phys. Rev. Lett. 119, 251304, (2017).

[74] P. Creminelli, F. Vernizzi, *Dark Energy after GW170817 and GRB170817A*, Phys. Rev. Lett. 119, 251302, (2017).

[75] S. Weinberg, *Effective Field Theory for Inflation*, Phys.Rev.D77:123541, (2008).

[76] C. Cheung et al., (Harvard U.), *Effective Field Theory for Inflation*, JHEP 0803:014, (2008).

[77] P. Creminelli, G. D'Amico, J. Noreña, F. Vernizzi, *The Effective Theory of Quintessence: the w<-1 Side Unveiled*, JCAP 0902:018, (2009).

[78] N. Frusciante, G. Papadomanolakis, A. Silvestri, *An Extended action for the effective field theory of dark energy: a stability analysis and a complete guide to the mapping at the basis of EFTCAMB*, JCAP 1607 no.07, 018, (2016).

[79] P. Horava, *Membranes at Quantum Criticality*, JHEP 0903:020, (2009).

[80] N. Frusciante, L. Perenon, *Effective Field Theory of Dark Energy: a Review*, Phys.Rept. 857, (2020).

[81] G. Gubitosi, F. Piazza, F. Vernizzi, *The Effective Field Theory of Dark Energy*, arXiv:1210.0201 [hep-th], (2013).

[82] *https://camb.info/*

[83] B. Hu, M. Raveri, N. Frusciante, A. Silvestri, *Effective Field Theory of Cosmic Acceleration: an implementation in CAMB*, Phys. Rev. D 89, 103530, (2014).

[84] M. Zumalacarregui, E. Bellini, I. Sawicki, J. Lesgourgues, P. G. Ferreira, *hi class: Horndeski in the Cosmic Linear Anisotropy Solving System*, JCAP08 019, (2017).

[85] *https://www.cita.utoronto.ca/ zqhuang/coop/*

[86] E. Bellini et al., *A comparison of Einstein-Boltzmann solvers for testing General Relativity*, Phys. Rev. D 97, 023520, (2018).

[87] R. Kase, S. Tsujikawa, *Effective field theory approach to modified gravity including Horndeski theory and Hořava-Lifshitz gravity*, Int. J. Mod. Phys. D 23, 1443008, (2014).

[88] B. Hu, M. Raveri, M. Rizzato, A. Silvestri, *Testing Hu-Sawacki f(R) gravity with the Effective Field Theory approach*, arXiv:1601.07536 [astro-ph.CO], (2016).

[89] A. De Felice, S. Tsujikawa, *Generalized Brans-Dicke theories*, JCAP 1007:024, (2010).

[90] M. Newman, *Computational physics*, (2013).

[91] A. Barreira, B. Li, C. Baugh, S. Pascoli, *Linear perturbations in Galileon gravity models*, Phys.Rev. D86 124016, (2012).

[92] A. Barreira, B. Li, C. Baugh, S. Pascoli, *The observational status of Galileon gravity after Planck*, JCAP08 059, (2012).

[93] A. Heavens, *Statistical techniques in cosmology*, arXiv:0906.0664 [astro-ph.CO], (2010).

[94] *https://cosmologist.info/cosmomc/*

[95] A. Lewis, S. Bridle, *Cosmological parameters from CMB and other data: a Monte-Carlo approach*, Phys.Rev.D66:103511, (2002).

[96] M. Betoule et al., *Improved cosmological constraints from a joint analysis of the SDSS-II and SNLS supernova samples*, arXiv:1401.4064 [astro-ph.CO], (2014).

[97] A. G. Riess et al., *Milky Way Cepheid Standards for Measuring Cosmic Distances and Application to Gaia DR2: Implications for the Hubble Constant*, arXiv:1804.10655 [astro-ph.CO], (2018).

[98] M. Asgari et al., *KiDS+VIKING-450 and DES-Y1 combined: Mitigating baryon feedback uncertainty with COSEBIs*, AA 634, A127, (2020).

[99] *https://sci.esa.int/web/euclid*

[100] *https://www.desi.lbl.gov/*